UNIVERSITY OF CALIFORNIA SAN DIEGO

Control-Oriented Modeling and Model-Based Control of Gas Processing Facilities

A dissertation submitted in partial satisfaction of the
requirements for the degree Doctor of Philosophy

in

Engineering Sciences (Mechanical Engineering)

by

Sven Brüggemann

Committee in charge:

Professor Robert R. Bitmead, Chair
Professor Raymond De Callafon
Professor Maurício de Oliveira
Professor Philip Gill
Professor Behrouz Touri

2022

The Dissertation of Sven Brüggemann is approved, and it is acceptable in quality and form for publication on microfilm and electronically.

University of California San Diego

2022

TABLE OF CONTENTS

LIST OF FIGURES

LIST OF TABLES

ABBREVIATIONS

DAE Differential Algebraic Equation

GCTF Gas Compressor Test Facility

LPV Linear parameter-varying

LTI Linear time-invariant

MIMO Multiple-input multiple-output

ODE Ordinary Differential Equation

PDE Partial differential Equation

PREFACE

Control Theory is an interdisciplinary field with an expansive quantity of applications. While I have only explored a small subset of topics, my curiosity, academic freedom as well as guidance provided by my advisor, and the great contributions of collaborators have helped me to work on a relatively broad range of problems given the scope of my doctoral studies:

- adaptive nonlinear tracking model predictive control (MPC);
- parameter estimation algorithms for multiple output systems;
- learning control barrier function-based safety filters for autonomous vehicles;
- data-driven nonlinear tracking MPC using log-sum-exp neural networks;
- modeling and simulation of what-if scenarios of finite hospital resources used by COVID-19 patients; and
- control-oriented modeling and model-based control of gas processing facilities.

Including every work here would exceed the scope and likely lead to gibberish. The interested reader is referred to the corresponding publications. Instead, this dissertation focuses on the topic of control-oriented modeling and model-based control of gas processing facilities. Results have been developed as part of a close collaboration with my advisor Professor Robert R. Bitmead and Solar Turbines Incorporated, foremost Robert H. Moroto.

ACKNOWLEDGEMENTS

Suppose Acknowledgments Sections induce people to think sentimentally about their past. It has been shown that this nostalgia makes us focus on relationships with close others [51]. Though the small sample size and lack of statistical analysis on theses do not allow me to do any hypothesis testing (and a literature research does not meet my cost-benefit criterion), I have measurable (in the mathematical sense) confidence that this indeed holds. Why am I writing this? Firstly, this is an appropriate section in this document to write about something outside the narrow corset of control systems; it feels great to exercise my academic freedom! Secondly, while I will refer to my relationships and the support that came with them, I also wish to shine light on rationally irrelevant facts that enabled me to be where I am. This is consistent with the definition of *acknowledge* – "to accept or admit the existence or truth of (something)" [14].

Also, towards an open and honest relationship with the reader: often when I read a thesis the Acknowledgment Section interests me most. Assuming a similar behavior of my peers the upside is that my outreach here is exorbitant compared to that of, say the proofs in Appendix A. The fact that you are reading this underpins my point.

Consider the topic of relevant irrelevance. I have been able to conclude my doctoral studies also because I was born in Europe (there is much to unpack here, but I leave it as an exercise to the reader) and since my parents both have a college degree. They have not divorced and their income provided sufficient freedom and security to greatly care for me. The public school system I attended was of sufficient quality. I am white and identify myself as male. My name contains a German umlaut. Note that this list is incomplete.

Now back to nostalgia and my relationships that were crucial for the completion of my degree. I am truly grateful for the guidance and unfaltering support of my advisor Professor Bitmead. He has not only been crucial for my academic development, he has also shown by example how to act with true selflessness, humor and humbleness despite his enormous success for which I admire him. I have not only much appreciated his great advice on technical issues, but also his tremendous help on issues outside work. I am equally thankful to him for giving me

the space to collaborate with other scholars, e.g., Professor de Oliveira. I have also thoroughly enjoyed the collaboration with Profosser de Oliveira and his fantastic mentorship and great support for which I want to express my sincere gratitude. I have much appreciated the time and advice from the other members of my committee, too: Professor De Callafon, Professor Gill, and Professor Touri.

I believe that my admission to University of California San Diego, was greatly attributed to my work at University of California, Santa Barbara, which I visited before my doctoral studies. It was an incredibly fruitful time, on and off campus, to which Professor Teel, Professor Poveda (welcome back to California!) and Dr. Corrado Possieri as well as my community greatly contributed. They all did not only show me how to be incredibly successful academically, but also how to care for others and to how find my own path. Dr. Corrado Possieri's guidance and friendship has been invaluable since.

Although it is impossible to mention everyone here who deserves it, I give an incomplete list. Foremost, I am eternally grateful to my family who has shaped me and always supported my endeavors, irrespective of the implied costs for themselves. My partner Atzin Magdaleno has my deepest thanks for always listening, no matter how unimportant my thoughts were, for questioning me and helping me focusing on the important aspects of life, which I will always remember. I will never forget the inspiring friends I have made along the way with whom I have been able to share my disappointments and successes, and to enjoy life outside work: Drew Steeves who I cannot thank enough for his advice, companionship, and the adventures we have experienced together; Aamodh Suresh' teas and meals made it impossible not to be his friend, and I am very thankful for the talks, lunches, hikes, and his time; Cody Allen, Bharat Ramling, Behrooz Amini and Mohammad Ramadan who have always brightened my day in the lab; Sarah Manderville, Brian Loch, Arianna Garvin, Zuben Scott, Natalie Allen, Avaneesh and Melissa, Taryn Lucas, and Sarah Chang who have made La Jolla/Coast much better than it already was; Christopher Dambrosia as a reliable Sunday morning surf alarm.

Back to work, I greatly appreciate the support and funding provided by Solar Turbines

Incorporated, in particular the close collaboration with and guidance from Robert Moroto, and help from GB Singh Chauhan, Jenny Eyes, Vivek Khanna, Hiep Ly and Robert Mendoza. This dissertation contains published material and material currently prepared for submission for publication.

Chapter 1, in full, has been submitted for publication of the material as it may appear as Sven Brüggemann, Robert H. Moroto, and Robert R. Bitmead. "Control-oriented modeling of pipe flow in gas processing facilities." The dissertation author was the primary investigator and author of this paper.

Chapter 2, in full, has been submitted for publication of the material as it may appear as Sven Brüggemann, Robert H. Moroto, and Robert R. Bitmead. "Control-orientation, conservation and model-based network flow control." The dissertation author was the primary investigator and author of this paper.

Appendix B, in full, is a reprint of the material as it appears in: Sven Brüggemann, Robert H. Moroto, and Robert R. Bitmead. " Compendium of Control-Oriented Models of Gas Processing Equipment Components." ArXiv e-prints, November 2022.

VITA

2013 Bachelor of Science, University of Rostock, Germany

2016 Master of Science, RWTH Aachen University, Germany

2022 Doctor of Philosophy, University of California San Diego

PUBLICATIONS

- Sven Brüggemann and Robert R. Bitmead. "Forward-Looking Persistent Excitation in Model Predictive Control." Automatica, Vol. 136, 2022.
- Sven Brüggemann and Robert R. Bitmead. "Model Predictive Control with Forward-Looking Persistent Excitation." IFAC World Congress, Berlin, 2020.
- Sven Brüggemann and Robert R. Bitmead. "Surrogate problems for tractable excitation management in stochastic MPC" Proc. 58th IEEE Conference on Decision and Control, Nice, FR, Dec. 2018.
- S. Brüggemann, C. Possieri, J.I. Poveda, and A. R. Teel. "Robust Constrained Model Predictive Control with Persistent Model Adaptation." Proc. 55th IEEE Conference on Decision and Control, Las Vegas, NV , Dec. 2016.
- S. Brüggemann and R. R. Bitmead. "Exponential convergence of recursive least squares with forgetting factor for multiple-output systems", Automatica, 2021.
- Sven Brüggemann, Dominic Nightingale, Jack Silberman and Maurício de Oliveira. "Learning Robust Input Constrained Control Barrier Functions for Guaranteed Safety of Car-Like Robots." under review.
- Sven Brüggemann, Drew Steeves and Miroslav Krstic. "Simultaneous Lane-Keeping and Obstacle Avoidance by Combining Model Predictive Control and Control Barrier Functions." to appear in Proc. IEEE Conference on Decision and Control, Cancun, Mexico, 2022.
- S. Brüggemann and C. Possieri, "On the Use of Difference of Log-Sum-Exp Neural Networks to Solve Data-Driven Model Predictive Control Tracking Problems." in IEEE Control Systems Letters, vol. 5, no. 4, pp. 1267-1272, Oct. 2021, doi: 10.1109/LC-SYS.2020.3032083.
- S. Brüggemann, T. Chan, G. Wardi, J. Mandel, J. Fontanesi, and R. R. Bitmead. "Decision support tool for hospital resource allocation during the COVID-19 pandemic." Informatics in Medicine Unlocked, page 100618, 2021.

- Sven Brüggemann, Robert H. Moroto, and Robert R. Bitmead. "Control-orientation, conservation and model-based network flow control." under review.
- Sven Brüggemann, Robert H. Moroto, and Robert R. Bitmead. " Compendium of Control-Oriented Models of Gas Processing Equipment Components." ArXiv e-prints, November 2022.
- Sven Brüggemann, Robert H. Moroto, and Robert R. Bitmead. "Control-oriented modeling of pipe flow in gas processing facilities." under review.

ABSTRACT OF THE DISSERTATION

Control-Oriented Modeling and Model-Based Control of Gas Processing Facilities

by

Sven Brüggemann

Doctor of Philosophy in Engineering Sciences (Mechanical Engineering)

University of California San Diego, 2022

Professor Robert R. Bitmead, Chair

Gas processing facilities, where gas is received and treated, provide motivation and embodiment for the development of systematic *control-oriented* modeling tools suited to the design of process control solutions based on plant schematics and layouts. The control of these plants involves the interconnection of a number of elements including pipes, compressors, heat exchangers, valves and valve manifolds, and other process units and volumes. The goal of this work is to provide a systematic, scalable and reconfigurable modeling methodology eventually used for process control of such gas-handling facilities at nominal operation. We aim to simplify the control design so that it appeals to generalists without deep expertise in control of fluid flow, using software tools such as Simulink/MATLAB and Python. We provide control-oriented

component models of standard equipment incl. pipe intersections, compressors, valves and heat exchangers, which serve as modules for entire networks. By exploiting the index-1 property of systems of differential algebraic equations that naturally arise for interconnections our composite LTI state-space models *subsume* algebraic equations; hence, control-orientation. We also show that for networks conservation of mass is inherited by its components and leads to an integrator in the pressure channel with important implications for control design. The MATLAB code provided in the Appendix corroborates the suitability of our approach for software-based control design.

Introduction

Gas processing facilities, where gas is received, treated and compressed for onward transmission through a distribution pipeline network, provide motivation and embodiment for the development of systematic control-oriented modeling tools suited to the design of process control solutions based on plant schematics and layouts. Figure 1 shows the Gas Compressor Test Facility (GCTF) at Solar Turbines Incorporated as an example of such a facility. While currently the usual working medium is natural gas, often hydrogen and biogas can be processed, too, which is worth mentioning given the political agenda of a carbon-neutral economy.

The control of these plants involves the interconnection of a number of elements including pipes, compressors, heat exchangers, valves and valve manifolds, scrubbers and other process units and volumes. The control splits into two distinct aspects: process control for system-wide operational efficiency and accuracy, and safety systems to ensure unit and plant protection. The two control aspects differ in their timescales and in their scope, with the safety system acting

Figure 1. Gas Compressor Test Facility (GCTF) at Solar Turbines Incorporated [13].

across a wide range of operating points (rather than around a single operating point), being both faster, more highly nonlinear, and more localized to specific unit operation such as avoiding compressor surge.

The goal of this work is to provide a systematic, scalable and reconfigurable modeling methodology eventually used for process control of such gas-handling facilities. We aim to simplify the control synthesis so that it can be designed by a generalist without deep expertise in control of fluid flow, using software tools such as Simulink/MATLAB and Python. Correspondingly, we prioritize utility over high accuracy required for high-fidelity simulations.

The motivation for this research is that current control design in gas processing facilities is usually based on single channel PI control. Advantages include that no explicit models are required and the availability of heuristic tuning rules, e.g., the Ziegler–Nichols method [52]. For many scenarios the controller performance is not sufficient, though, particularly given the higher requirements for disturbance rejection, accuracy, and efficiency associated with microgrids and an increased share of renewable energies.

One disadvantage is that manual tuning of PI controller gains by operators is costly and required as soon as there is a change in the plant: modifications of facility components, change of nominal operating conditions, wear of tools, etc. Further, single channel controllers assume uncoupled dynamics: each control input only affects one specific signal output. This assumption does usually not hold in practice, so that rather ad hoc heuristic approaches such as selecting the minimum from multiple control inputs is used. Moreover, although high-resolution computer-aided simulations for single components are possible their extension to interconnected large-scale systems including diverse equipment such as valves, compressors and heat exchangers is not immediate. This complicates testing and validation of classical PI control in simulation.

To address these limitations, our ultimate aim is to replace single channel PI control by multiple-input-multiple-output (MIMO) control. We derive component models in form of MIMO state-space realizations which appeal to numerous methods from Linear Systems Theory and software tools such as MATLAB. We also present a matrix methodology for building networks

from component models, leading again to state-space descriptions. This allows the use of standard methods using commands such as `kalman`, `lqr` and `lqg` for entire networks, which dramatically increases the models' utility especially for engineers without a deep understanding of control systems. This *control-oriented* approach is one of the main features of our work and deviates substantially from the originally infinite-dimensional modeling based on partial differential equations (PDEs). Additionally to serving for control design, our models facilitate estimation, disturbance modeling, filtering and initial numerical validation, to name a few use cases.

Control-oriented captures the modeling focus on eventual model-based feedback controller design reflecting: plant operational objectives, the presence and capabilities of selected actuators and sensors, disturbance integration, and the possible reconfiguration of operations. More precisely, our models are designed to be used for the following conditions.

Plant: interconnected networks of pipes and processing elements located at one site on the order of tens of meters (rather than kilometers) in extent.

Objective: bulk flow estimation, bulk pressure regulation and disturbance flow rejection with flow as control input/manipulated variable.

Sensing/actuation: sampled at or below 1Hz in line with the plant's regulation objective. The focus is on widespread, reliable and accurate pressure sensing in particular, and on actuation using flow control valves. Sensing of flow with orifice plates is there for corroboration more than for control. Temperature sensing is slow and of limited presence in the plant.

Resonant and acoustic modes: while ever-present in compression systems, are at frequencies beyond the sensor and actuator bandwidth in plants of this size.

Models: should facilitate control design for this regime and be amenable to tuning by control-savvy plant engineers.

Although this is quite a specific scenario, it is fairly representative for gas processing facilities. We claim that our control-oriented models are well-suited for MIMO model-based control. Appealing to Popper's scientific theory of falsifiability [39], while it is impossible to prove that this is true in general, we present analysis and numerical experiments that unsuccessfully falsify and hence corroborate this hypothesis; methods from Linear Systems Theory facilitate these efforts. Further, as Laudan [28] writes "the aim of science is to secure theories with a high problem-solving effectiveness." Our control-oriented approach to lumped-parameter, linearized, spatially discretized, signal flow graph modeling operates with this recognition of the convenient fiction underpinning all modeling but reflective of the utility of the approach.

Related work

Fluid dynamics and, particularly, computational fluid dynamics, are well-established subjects centered on high-fidelity modeling of flows given design and boundary conditions; typically, they involve nonlinear PDEs and transport phenomena which are not amenable to finite-dimensional control design but instead are targeted and tested for simulation. Other pragmatic modeling for pipeline distribution systems [5, 26, 3] yields ordinary differential algebraic equations (DAEs), which again are not well suited to control design. Although, they can be used directly for controller synthesis in some circumstances [17] and, as noted in [5], if the DAE is of index 1. Theorem 4.1 [5] establishes that the DAEs are indeed of index 1 and so it is possible to rewrite the DAE as an ordinary differential equation (ODE) without the algebraic constraints. Effectively, we complete this conversion here.

For fluid or general mechanical systems we take a lead from Benner *et al.* [5] and Williams *et al.* [50] as examples where graph theoretic methods are applied to generate process models from component descriptions, with the latter paper specifically targeted at control design and the former at modeling for simulation. Williams *et al.* [50] is allied in its control objective with our work here and uses energy as the *lingua franca* to map states between subsystems. The edges of their graphs are energy preserving connections with the dynamics occurring at the nodes.

By contrast, Benner *et al.* [5] and we model the dynamics in the edges with the nodes applying the interaction constraints. For our target processes of gas processing plants, this latter structure accords better with the primary process control objective of pressure regulation and secondarily with flow estimation. Thermal energy is a byproduct and reflection of the inefficiency of the process. While of interest, temperature is not the central manipulated variable. However, it is noteworthy that the energy formulation of Williams *et al.* [50] for composite aircraft systems allows conservation laws to be absorbed into the component models, so that the aggregated state-space model can be directly applied for control design.

A recent comprehensive survey of modeling and feedback control design for HVAC systems is provided by Goyal *et al.* [21], which cites Rasmussen & Alleyne [40] who concentrate explicitly on control-oriented modeling in these vapor compression systems. However, because their pipes are short and well-insulated, the system structure again focuses on node dynamics rather than edge dynamics of our problem.

For large-scale domain-independent systems, works from Šiljak and colleagues [38, 45, 44] follow a top-down approach, decomposing large-scale networks into smaller subsystems, and analyze control-relevant notions such as (structural) stability, reachability and controllability. While their approach is generally applicable to the case of pipe flow, the logical direction differs: instead of decomposing, we *compose* interconnected systems from subsystems in a bottom-up approach under the assumption that structures are fixed (rendering structural stability [45] secondary). Further, the control actuator and, to a lesser extent, sensor locations are few when compared with the number of subsystems or network elements.

Contributions

Following [5], which deals with isothermal models of gas distribution networks, we commence by studying pipe flow in individual pipes before considering how these are connected into networks yielding automatable aggregation of subsystems. The authors of [5] propose a network DAE with the algebraic part being the conservation of mass flows at the connection

points. At this level of detail, this approach bears a strong resemblance to bond graph techniques [8], from which control design is problematic. However, since the resultant network DAE has index 1, the algebraic part can be solved locally to express some of the variables in terms of the others thereby eliminating them.

For our models, algebraic equations arise for intersecting pipes. In this case we create composite models which subsume algebraic equations while their state-space form satisfies our requirement of control orientation. These new elements preserve the linearity and other properties while also respecting the conservation laws. We extent this idea to other standard equipment and generate a compendium of control-oriented models, including compressors, valves, valve manifolds, heat exchangers and tanks.

We show how these components might be aggregated into network equations to compute the larger state-space system, which we show subsumes Mason's Gain Formula. That is, we are able to preserve the simplicity of the signal flow model of the pipe network as opposed to resorting to bond graphs or DAEs. Two examples in MATLAB corroborate the suitability of our models for control design. Additionally, signal filters allow us to isolate certain frequencies and hence efficiently simulate interconnected systems in closed loop, which would otherwise challenge even specialized solvers for stiff DAEs.

Other core aspects of our work are the inheritance of conservation of mass from the unit models to the network despite the absence of algebraic constraints and the consequences of this for the network model in the light of controller design; and, MIMO control design using these approximate models and cognizant of the role of the conservation of mass in these designs. To sum up, our main contributions are as follows.

- We develop control-oriented models of standard equipment in gas processing facilities subsuming algebraic constraints; this includes pipes, pipe intersections, compressors, valves, valve manifolds, heat exchangers and tanks.

- We experimentally validate pipe models using real-world data.

- We derive a matrix methodology for composing networks from modular components that can directly be implemented in software tools such as MATLAB.
- We show that conservation of mass as a component property is inherited by entire networks, and that this leads to an integrator in the system important for control design.
- We apply our developed methodology to a plant in simulation, similar to the GCTF at Solar Turbines Incorporated and show how to use our control-oriented interconnected models for digital control design including MATLAB code.
- The simplicity of our control-oriented models and their interconnection to complete networks provides access to MIMO feedback control design of complex systems for general engineers without a profound knowledge in control systems.

Thesis outline

The thesis is divided into two self-containing chapters and one self-containing appendix. Chapter 1 introduces the idea of control-oriented modeling and presents models for pipe flow with a focus on their eventual use for feedback control design at the process control level, as opposed to the unit level, in gas processing facilities. Accordingly, linearized facility-scale models are generated to describe pressures, mass flows and temperatures based on sets of nonlinear partial differential equations from fluid dynamics and thermodynamics together with constraints associated with their interconnection. As part of the treatment, the divergence of these simplified models from physics is assessed, since robustness to these errors will be an objective for the eventual control system. The approach commences with a thorough analysis of pipe flow models and then proceeds to study their automated interconnection into network models which subsume the algebraic constraints of bond graph or standard fluid modeling. The models are validated and their errors quantified by referring them to operational data from a commercial gas compressor test facility. For linear time-invariant models, the interconnection method to generate network models is shown to coincide with automation of Mason's Gain Formula. These

pipe network models based on engineering data are the first part of the development of general facility process control tools.

In Chapter 2 these models are then used for analysis and control design. More precisely, we study a gas network flow regulation control problem showing the closed-loop consequences of using interconnected component models which have been designed to preserve a variant of mass flow conservation without the inclusion of algebraic constraints into the dynamics. These are candidate control-oriented models because they are linear state-space systems. This leads to a study of mass conservation in flow models and the inheritance of conservation at the network level when present at each component. Conservation is expressed as a transfer function property at DC. This property then is shown to imply the existence of integrators and other DC structure of the network model, which has important consequences for the subsequent control design. An example based on an industrial system is used to explore the facility of moving from modeling to automated interconnection or components to model reduction to digital controller design and performance evaluation. Throughout, the focus is on the teasing out of control orientation in modeling. The example shows a strong connection between the modeling and the controller design.

Appendix B builds on the previous chapters and represents a compendium of control-oriented models of gas processing equipment components. Here we provide linear control-oriented state space models of gas flow through standard equipment such as tanks, valves and valve manifolds, compressors, heat exchangers and non-trivial pipe geometries. After presenting the catalog of components, using results from Chapter 2 we show a MATLAB example for a network in form of a gas loop. For the same example we also demonstrate an alternative approach using MATLAB's `connect` function.

Chapter 1

Control-oriented modeling of pipe flow in gas processing facilities

1.1 Introduction

Gas processing facilities, where natural gas is received, treated and compressed for onward transmission through a distribution pipeline network, provide motivation and embodiment for the development of systematic control-oriented modeling tools suited to the design of process control solutions based on plant schematics and layouts. The control of these plants involves the interconnection of a number of elements including pipes, compressors, heat exchangers, valves and valve manifolds, scrubbers and other process units and volumes. The control splits into two distinct aspects: process control for system-wide operational efficiency and accuracy, and safety systems to ensure unit and plant protection. The two control aspects differ in their timescales and in their scope, with the safety system acting across a wide range of operating points (rather than around a single operating point), being both faster, more highly nonlinear, and more localized to specific unit operation, such as avoiding compressor surge. Our focus will be the process control side with an emphasis on unified plant-wide operational effectiveness. The aim of this chapter is to develop interconnectable and reconfigurable unit system models, which are amenable to control design, with an objective of bringing multiinput-multioutput (MIMO) control into the picture for gas processing facilities; firstly from engineering design specifications and then augmented by data-based tuning.

Control-oriented captures the modeling focus on eventual model-based feedback controller design reflecting: plant operational objectives, the presence and capabilities of selected actuators and sensors, and the possible reconfiguration of operations. More precisely, our models are designed to be used for the following conditions.

Plant: interconnected networks of pipes and processing elements located at one site on the order of tens of meters (rather than kilometers) in extent.

Objective: bulk pressure regulation and disturbance flow rejection with flow as control input/-manipulated variable.

Sensing/actuation: sampled at or below 1Hz in line with the plant's regulation objective. The focus is on widespread, reliable and accurate pressure sensing in particular, and on actuation using flow control valves. Sensing of flow with orifice plates is there for corroboration more than for control. Temperature sensing is slow and of limited presence in the plant.

Resonant and acoustic modes: while ever-present in compression systems, are at frequencies beyond the sensor and actuator bandwidth in plants of this size.

Models: should facilitate control design for this regime and be amenable to tuning by control-savvy plant engineers.

Although this is quite a specific scenario, it is fairly representative for gas processing facilities.

The models we seek will be linear(ized), time-invariant (LTI) state-space systems, optionally parametrized by nominal operating point, and capable of systematic interconnection of unit models into facility models using computer-based MIMO control design tools. Models with time delay do not fall into this category and are therefore approximated by control-compliant dynamics if necessary. The *quid pro quo* for this utility is that these models are necessarily simplistic and approximate but that, by characterizing their nature, approximations might be addressed in control design. Inevitably, such modeling relies heavily on engineering knowledge of the specific application but admits fairly general applicability.

The subsystem models are based on simplified approximations to constituent equations from fluid dynamics, coupled partial differential equations (PDEs) plus algebraic equations, and are validated against plant data, including the assessment of model errors.

Fluid dynamics and, particularly, computational fluid dynamics, are well-established subjects centered on high-fidelity modeling of flows given design and boundary conditions; typically, they involve nonlinear PDEs and transport phenomena, which are not amenable to finite-dimensional control design but instead are targeted and tested for simulation. Other pragmatic modeling for pipeline distribution systems [5, 26, 3] yields ordinary differential algebraic equations (DAEs), which again are not well suited to control design. Although, they can be used directly for controller synthesis in some circumstances [17] and, as noted in [5], if the DAE is of index 1. Theorem 4.1 [5] establishes that the DAEs are indeed of index 1 and so it is possible to rewrite the DAE as an ordinary differential equation (ODE) without the algebraic constraints. Effectively, we complete this conversion here.

For fluid or general mechanical systems we take a lead from Benner *et al.* [5] and Williams *et al.* [50] as examples where graph theoretic methods are applied to generate process models from component descriptions, with the latter paper specifically targeted at control design and the former at modeling for simulation. Williams *et al.* [50] is allied in its control objective with our work here and uses energy as the *lingua franca* to map states between subsystems. The edges of their graphs are energy preserving connections with the dynamics occurring at the nodes. By contrast, Benner *et al.* [5] and we model the dynamics in the edges with the nodes applying the interaction constraints. For our target processes of gas processing plants, this latter structure accords better with the primary process control objective of pressure regulation and secondarily with flow estimation. Thermal energy is a byproduct and reflection of the inefficiency of the process. While of interest, temperature is not the central manipulated variable. However, it is noteworthy that the energy formulation of Williams *et al.* [50] for composite aircraft systems allows conservation laws to be absorbed into the component models, so that the aggregated state-space model can be directly applied for control design. A recent comprehensive survey

of modeling and feedback control design for HVAC systems is provided by Goyal *et al.* [21], which cites Rasmussen & Alleyne [40] who concentrate explicitly on control-oriented modeling in these vapor compression systems. However, because their pipes are short and well-insulated, the system structure again focuses on node dynamics rather than edge dynamics of our problem.

For large-scale domain-independent systems, works from Šiljak and colleagues [38, 45, 44] follow a top-down approach, decomposing large-scale networks into smaller subsystems, and analyze control-relevant notions, such as (structural) stability, reachability and controllability. While their approach is generally applicable to the case of pipe flow, the logical direction differs: instead of decomposing, we *compose* interconnected systems from subsystems in a bottom-up approach under the assumption that structures are fixed (rendering structural stability [45] secondary). Further, the control actuator and, to a lesser extent, sensor locations are few when compared with the number of subsystems or network elements.

Following [5], which deals with isothermal models of gas distribution networks, we commence by studying pipe flow in individual pipes before considering how these are connected into networks yielding automatable aggregation of subsystems. The authors of [5] propose a network DAE with the algebraic part being the conservation of mass flows at the connection points. At this level of detail, this approach bears a strong resemblance to bond graph techniques [8] from which control design is problematic. However, since the resultant network DAE has index 1, the algebraic part can be solved locally to express some of the variables in terms of the others thereby eliminating them. For our models, algebraic equations arise when pipes join but not when they branch. For joints a state variable is removed yielding a new network element subsuming the three joining pipes. These new elements preserve the linearity and other properties while also respecting the conservation laws. Further, we show how these components might be aggregated into network equations to compute the larger state-space system, which we show subsumes Mason's Gain Formula. That is, we are able to preserve the simplicity of the signal flow model of the pipe network as opposed to resorting to bond graphs or DAEs. Additionally, signal filters allow us to isolate certain frequencies and hence efficiently simulate interconnected

systems in closed loop, which would otherwise challenge even specialized solvers for stiff DAEs.

The pipe-flow models developed are validated against 1Hz operating data collected at the Solar Turbines Incorporated Gas Compressor Test Facility (GCTF) at Solar Turbines Incorporated in San Diego. This is a well instrumented site normally used to test compressor performance. We use engineering design values to derive the parametrized models and then experimental data from a number of recorded tests is used to compare the fit of the data and model outputs. The discrepancy between model and data is used to quantify and qualify the model performance. Specifically, we find that isothermal models, such as those used in [5], are subject to offsets and slow variations due to temperature gradients, which for this plant are measured but need not necessarily be. Accordingly, the control design needs to accommodate this known inaccuracy of the models. Indeed, the existing single-loop PI-controllers already give this clue and indicate that the principal plant objectives are the regulation of pressures and flows.

The design of network-ready models for pipe flow is the first stage of introducing model-based control design into these systems using engineering design information and data sheets. The project objective is to expand this to include other network elements, such as compressors, heat exchangers, vessels and valves, see Appendix B, and validate their use for MIMO control design in Chapter 2.

Part 1: Control-oriented pipe models

We start with a deep dive into: modeling of individual pipe segments as nonlinear PDEs and boundary conditions, spatial discretization to nonlinear ODEs with input signals, then linearized ODE models with inputs. These are then compared with experimental/operational data from the GCTF, yielding control-oriented finite-dimensional linear state-space models and an appreciation of their deviation from ideal behavior. We establish that these single pipe models inherently satisfy conservation of mass flow[1]. In Part 2, we explore how to move from pipe

[1]This central presence of mass conservation in flow models is more fully examined in our companion model-based control design Chapter 2. There, conservation is shown to connect to integrators and inherent model structure at $s = 0$, appreciation of which is critical for regulator design.

models to pipe network models.

1.2 PDE models

We formulate the pipe dynamics as a one-dimensional flow with standing assumptions common in the literature (e.g. [1, 3, 5, 25]). We assume these throughout this chapter.

Standing Assumption 1.1. *For the one-dimensional pipe flow,*

(i) the cross-sectional area of each pipe segment is constant;

(ii) average velocities across the cross section suffice for the computation of the mass flow;

(iii) there is no slip at the wall, i.e. the gas velocity at the inner pipe wall is zero;

(iv) friction along the pipe can be approximated by the Darcy-Weisbach equation, see e.g. [41];

(v) the compressibility factor is constant along the pipe;

(vi) capillary, magnetic and electrical forces on the fluid are negligible.

Item (ii) is a property of high Reynolds number turbulent flow. Under these assumptions, the constituent relations — Continuity, Momentum, Energy, Gas Equation, respectively — that serve as a basis for our model are

$$\frac{\partial \check{\rho}}{\partial t} = -\frac{\partial}{\partial x}(\check{\rho} v), \tag{1.1a}$$

$$\frac{\partial}{\partial t}(\check{\rho} v) + \frac{\partial}{\partial x}(\check{\rho} v^2 + p) = -\frac{\lambda}{2D}\check{\rho} v|v| - g\check{\rho}\frac{dh}{dx}, \tag{1.1b}$$

$$\not{q}\check{\rho} = \frac{\partial}{\partial x}\left[\check{\rho} v\left(c_v \check{T} + \frac{v^2}{2} + gh + \frac{\check{p}}{\check{\rho}}\right)\right] + \frac{\partial}{\partial t}\left[\check{\rho}\left(c_v \check{T} + \frac{v^2}{2} + gh\right)\right], \tag{1.1c}$$

$$\check{p} = \check{\rho} R_s T z_0, \tag{1.1d}$$

which are derived in e.g. [29] and whose parameters are defined in Table 1.1.

Table 1.1. Definitions of model variables and SI-units.

Symbol	Meaning	SI-unit
A	Cross-sectional area	$[\mathrm{m}^2]$
c	Speed of sound	$[\frac{\mathrm{m}}{\mathrm{s}}]$
c_v	Specific heat	$[\frac{\mathrm{J}}{\mathrm{kgK}}]$
D	Pipe inner diameter	[m]
D_o	Pipe outer diameter	[m]
g	Gravity constant	$[\frac{\mathrm{m}}{\mathrm{s}^2}]$
$h(x)$	Pipe elevation	[m]
k_{rad}	Lumped thermal conductivity pipe	$[\frac{\mathrm{W}}{\mathrm{m}^2\mathrm{K}}]$
$\bar{p}(x,t)$	Pressure nominal point	$[\frac{\mathrm{kg}}{\mathrm{s}^2\mathrm{m}}]$
$\check{p}(x,t)$	Pressure	$[\frac{\mathrm{kg}}{\mathrm{s}^2\mathrm{m}}]$
$p(x,t)$	Pressure deviation from nominal point	$[\frac{\mathrm{kg}}{\mathrm{s}^2\mathrm{m}}]$
$\bar{q}(x,t)$	Mass flow nominal point	$[\frac{\mathrm{kg}}{\mathrm{s}}]$
$\check{q}(x,t)$	Mass flow	$[\frac{\mathrm{kg}}{\mathrm{s}}]$
$q(x,t)$	Mass flow deviation from nominal point	$[\frac{\mathrm{kg}}{\mathrm{s}}]$
$\mathscr{q}$	Rate of heat flow per unit area	$[\frac{\mathrm{W}}{\mathrm{m}^2}]$
Re	Reynolds number	[1]
R_s	Specific gas constant	$[\frac{\mathrm{m}^2}{\mathrm{s}^2\mathrm{K}}]$
$\bar{T}(x,t)$	Temperature nominal point	[K]
$\check{T}(x,t)$	Temperature	[K]
$T(x,t)$	Temperature deviation from nominal point	[K]
T_0	Nominal temperature	[K]
T_{amb}	Ambient temperature	[K]
$v(x,t)$	Velocity	$[\frac{\mathrm{m}}{\mathrm{s}}]$
X	Pipe length	[m]
z	Compressibility factor	[1]
z_0	Constant compressibility factor	[1]
λ	Friction factor	[1]
$\check{\rho}(x,t)$	Density	$[\frac{\mathrm{kg}}{\mathrm{m}^3}]$

The boundary conditions

$$\check{p}(0,t), \quad \check{q}(X,t), \quad \check{T}(0,t),$$

are assumed to be known. Continuity Equation (1.1a) captures conservation of mass. Momentum Equation (1.1b) is obtained by a Newtonian approach considering forces acting on a fluid. Total

Energy Equation (1.1c) is the First Law of Thermodynamics in differential form, see e.g. [43]. The Gas Equation (1.1d) closely describes the behavior of natural gas at the conditions pertaining in the handling facility.

We develop a dynamic model for deviations, $p(X,t)$ and $q(0,t)$, and if required also for $T(X,t)$, from the nominal points, $\bar{p}(X,t)$, $\bar{q}(0,t)$, and $\bar{T}(X,t)$, and a related methodology that allows a systematic interconnection of pipe elements in a network. Towards this goal, in Section 1.3, from the constituent relations above we derive a nonisothermal, linear, 3D state-space model with the pressure, mass flow and temperature as state elements. Under the condition of a constant temperature, in Section 1.4 we revisit (1.1) and introduce a simplified isothermal 2D model. In the next section we validate both models against operating data from the GCTF and compare them to the numerical solution of the PDEs in (1.1). This analysis suggests using the isothermal model parametrized by spatially varying nominal temperature and managing small offsets and slow drifts with the controller design. Section 1.7 treats the removal of algebraic constraints stemming from the DAEs and proposes a catalog of common network units in state-space form, including a new pipe joint element. To interconnect these unit models to pipe networks, Section 1.8 contains a matrix methodology, which we prove subsumes and automates Mason's Gain Formula in the MIMO context. The properties of interconnected components are then illustrated by a numerical experiment in Section 1.9[2]. We finish this chapter with a brief conclusion and directions for future research.

1.3 Nonlinear and linear nonisothermal 3D ODE models

Towards a nonisothermal 3D model with pressure, mass flow and temperature as state elements, consider constituent relations (1.1). Notice that "3D" refers to the number of states and not the spatial dimension. For the corresponding total energy equation, (1.1c), the heat flux, $\dot{q}$, is assumed to be limited to radial conduction through the pipe, so that similar to [37] and

[2] A compendium of linear state-space models for a variety of elements is provided, with derivations, in Appendix B. The latter also includes examples and MATLAB code for interconnected networks and establishes the mass conservation property of each model.

neglecting conduction through the gas,

$$\cancel{q}\rho A dx = k_{\text{rad}}\pi D_o dx(T_{\text{amb}} - \check{T}). \tag{1.2}$$

This characterization enables the formulation of PDEs that isolate the time derivatives of the desired state variables.

Proposition 1.1. *Let $|v| \ll c = \sqrt{z_0 R_s T_0}$, i.e., the gas velocity is much smaller than speed of sound. Then, constituent equations* (1.1) *and the heat flux described in* (1.2) *yield*

$$\frac{\partial \check{p}}{\partial t} = \frac{R_s z_0}{A c_v}\left[k_{rad}\pi D_o(T_{amb} - \check{T}) - \frac{\partial \check{q}}{\partial x}\check{T}(c_v + R_s z_0) + \frac{\partial \check{p}}{\partial x}\frac{R_s z_0 \check{T}\check{q}}{\check{p}} - \frac{\partial \check{T}}{\partial x}\check{q}(c_v + R_s z_0) + \frac{\lambda R_s^2 z_0^2 \check{T}^2 \check{q}^2 |\check{q}|}{2DA^2\check{p}^2}\right], \tag{1.3a}$$

$$\frac{\partial \check{q}}{\partial t} = -A\frac{\partial \check{p}}{\partial x} - \frac{\lambda R_s \check{T} z_0}{2DA}\frac{\check{q}|\check{q}|}{\check{p}} - \frac{Ag}{R_s \check{T} z_0}\frac{dh}{dx}\check{p}, \tag{1.3b}$$

$$\frac{\partial \check{T}}{\partial t} = \frac{R_s z_0 \check{T}}{A c_v \check{p}}\left[k_{rad}\pi D_o(T_{amb} - \check{T}) - \frac{\partial \check{q}}{\partial x}\check{T} R_s z_0 + \frac{\partial \check{p}}{\partial x}\frac{R_s z_0 \check{T}\check{q}}{\check{p}} - \frac{\partial \check{T}}{\partial x}\check{q}(c_v + R_s z_0) + \frac{\lambda R_s^2 z_0^2 \check{T}^2 \check{q}^2 |\check{q}|}{2DA^2\check{p}^2}\right]. \tag{1.3c}$$

The proof is provided in the Appendix. Proposition 1.1 enables us to obtain a linear 3D state-space realization, through spatial discretization and subsequent linearization of these PDEs.

We commence with the spatial discretization using simple differences. Subscripts $\cdot_\ell$ and $\cdot_r$ connote variables at left (entry) and right (exit) sides of the pipe. Input variables are identified with the pipe PDE boundary conditions, $\check{p}_\ell$, $\check{q}_r$ and $\check{T}_\ell$, and the state variables with the ODE solution, $\check{p}_r$, $\check{q}_\ell$ and $\check{T}_r$, where,

$$\begin{aligned} \check{p}_\ell &= \check{p}(0,t), & \check{q}_\ell &= \check{q}(0,t), & \check{T}_\ell &= \check{T}(0,t), \\ \check{p}_r &= \check{p}(X,t), & \check{q}_r &= \check{q}(X,t), & \check{T}_r &= \check{T}(X,t). \end{aligned}$$

The subscripts are motivated by the definition of a positive x-direction from left to right, but do

not imply any specific flow direction, only that one is not free to prescribe both the pressure and flow at a single point. This yields the nonlinear nonisothermal 3D model:

$$\begin{aligned}\dot{\check{p}}_r &= \frac{R_s z_0}{A c_v}\left[k_{\text{rad}}\pi D_o(T_{\text{amb}}-\check{T}_r) - \frac{\check{q}_r-\check{q}_\ell}{X}\check{T}_r\,(c_v+R_s z_0) + \frac{\check{p}_r-\check{p}_\ell}{X}\frac{R_s z_0 \check{T}_r \check{q}_r}{\check{p}_r}\right. \\ &\qquad \left. -\frac{\check{T}_r-\check{T}_\ell}{X}\check{q}_r\,(c_v+R_s z_0) + \frac{\lambda R_s^2 z_0^2 \check{T}_r^2 \check{q}_r^2|\check{q}_r|}{2DA^2\check{p}_r^2}\right] \qquad (1.4a)\\ &\doteq f_p(\check{p}_\ell,\check{p}_r,\check{q}_\ell,\check{q}_r,\check{T}_\ell,\check{T}_r),\end{aligned}$$

$$\begin{aligned}\dot{\check{q}}_\ell &= -A\frac{\check{p}_r-\check{p}_\ell}{X} - \frac{\lambda R_s \check{T}_\ell z_0}{2DA}\frac{\check{q}_\ell|\check{q}_\ell|}{\check{p}_\ell} - \frac{Ag}{R_s\check{T}_\ell z_0}\frac{dh}{dx}\check{p}_\ell \qquad (1.4b)\\ &\doteq f_q(\check{p}_\ell,\check{p}_r,\check{q}_\ell,\check{T}_\ell),\end{aligned}$$

$$\begin{aligned}\dot{\check{T}}_r &= \frac{R_s z_0 \check{T}_r}{A c_v \check{p}_r}\left[k_{\text{rad}}\pi D_o(T_{\text{amb}}-\check{T}_r) - \frac{\check{q}_r-\check{q}_\ell}{X}\check{T}_r R_s z_0 + \frac{\check{p}_r-\check{p}_\ell}{X}\frac{R_s z_0 \check{T}_r \check{q}_r}{\check{p}_r}\right. \\ &\qquad \left. -\frac{\check{T}_r-\check{T}_\ell}{X}\check{q}_r\,(c_v+R_s z_0) + \frac{\lambda R_s^2 z_0^2 \check{T}_r^2 \check{q}_r^2|\check{q}_r|}{2DA^2\check{p}_r^2}\right] \qquad (1.4c)\\ &\doteq f_T(\check{p}_\ell,\check{p}_r,\check{q}_\ell,\check{q}_r,\check{T}_\ell,\check{T}_r),\end{aligned}$$

We propose the discretization from (1.3) to (B.44) as it approximates reasonable well the original infinite-dimensional at low frequencies relevant for our control problem, as discussed below.

Linearizing (B.44) results in the MIMO LTI 3D state-space realization, with some abuse of notation,

$$\dot{x}_t = Ax_t + Bu_t, \qquad (1.5a)$$

$$y_t = x_t, \qquad (1.5b)$$

where $A = \frac{\partial f}{\partial x}\Big|_{\bar{x},\bar{u}}, B = \frac{\partial f}{\partial u}\Big|_{\bar{x},\bar{u}}$, with $f \doteq \begin{bmatrix} f_p & f_q & f_T \end{bmatrix}^\top$ and $\frac{\partial(\cdot)}{\partial x}\Big|_{\bar{x},\bar{u}}$ indicating the Jacobian with respect to x evaluated at nominal point $\bar{x}$ and $\bar{u}$, and B denoted accordingly. Further, letting

$$p(x,t) = \check{p}(x,t) - \bar{p}(x,t), \quad q(x,t) = \check{q}(x,t) - \bar{q}(x,t), \quad T(x,t) = \check{T}(x,t) - \bar{T}(x,t),$$

the state and input vectors are given by the following deviations from nominal/steady-state values,

$$x_t = \begin{bmatrix} p_r & q_\ell & T_r \end{bmatrix}^\top, \quad u_t = \begin{bmatrix} p_\ell & q_r & T_\ell \end{bmatrix}^\top.$$

We stress that for such a state-space realization, which is the basis for modern model-based control design, the preponderance of existing tools in linear systems theory is directly applicable, such as the determination of stability, DC gains, observability and controllability. To assess sufficiency for control-oriented design, we will use this nonisothermal 3D model as a benchmark for the reduced isothermal 2D model introduced next. Where appropriate, we also compare the solution of the linear system to both the nonlinear 3D model, (B.44), and the original PDEs, (1.3).

1.4 Isothermal 2D linear ODE model

Assume that the temperature is constant, i.e. $T(x,t) = T_0$ for all $x \in [0,X]$ and $t \geq 0$. The Continuity, Momentum and Gas Equations in (1.1) suffice to obtain

$$\frac{\partial \check{p}}{\partial t} = -\frac{R_s T_0 z_0}{A} \frac{\partial \check{q}}{\partial x}, \tag{1.6a}$$

$$\frac{\partial \check{q}}{\partial t} = -A \frac{\partial \check{p}}{\partial x} - \frac{\lambda R_s T_0 z_0}{2DA} \frac{\check{q}|\check{q}|}{\check{p}} - \frac{Ag}{R_s T_0 z_0} \frac{dh}{dx} \check{p}, \tag{1.6b}$$

where for the mass flow, $\check{q}$, we additionally used the relation $\check{q} = \check{\rho} A v$. We also neglect the partial derivative of the inertia (or kinematic) term, $\check{\rho} v^2$, justified by the fact that the speed of sound, c, usually greatly exceeds the velocity of the fluid [5, pp. 174]. This is also consistent with Proposition 1.1.

Following [5], a spatial discretization of (1.6) yields

$$\dot{\check{p}}_r = -\frac{R_s T_0 z_0}{AX}(\check{q}_r - \check{q}_\ell), \tag{1.7a}$$

$$\dot{\check{q}}_\ell = -\frac{A}{X}(\check{p}_r - \check{p}_\ell) - \frac{\lambda R_s T_0 z_0}{2DA}\frac{\check{q}_\ell|\check{q}_\ell|}{\check{p}_\ell} - \frac{Ag}{R_s T_0 z_0}\frac{h}{X}\check{p}_\ell. \tag{1.7b}$$

Linearizing around nominal points denoted by subscript *ss* and using tildes to denote perturbation variables, we obtain

$$\dot{p}_r = \alpha(q_r - q_l) \tag{1.8a}$$

$$\dot{q}_\ell = \beta p_r + \kappa p_\ell + \gamma q_\ell, \tag{1.8b}$$

with

$$\begin{aligned}
\alpha &= -\frac{R_s T_0 z_0}{AX}, \quad \beta = -\frac{A}{X}, \\
\kappa &= \frac{A}{X} + \frac{\lambda R_s T_0 z_0}{2DA}\frac{\bar{q}_\ell|\bar{q}_\ell|}{\bar{p}_\ell^2} - \frac{Agh}{R_s T_0 z_0 X}, \\
\gamma &= -\frac{\lambda R_s T_0 z_0}{DA}\frac{|\bar{q}_\ell|}{\bar{p}_\ell}.
\end{aligned}$$

The LTI ODEs (B.2) represent a system that can be equivalently realized by

$$\dot{x}_t = \begin{bmatrix} 0 & -\alpha \\ \beta & \gamma \end{bmatrix} x_t + \begin{bmatrix} 0 & \alpha \\ \kappa & 0 \end{bmatrix} u_t, \tag{1.9a}$$

$$y_t = x_t \tag{1.9b}$$

with $x_t = \begin{bmatrix} p_r & q_\ell \end{bmatrix}^\top$ as the state vector and $u_t = \begin{bmatrix} p_\ell & q_r \end{bmatrix}^\top$ as the input vector.

We note immediately several properties revealed by the linear model. The elements (α, β, γ) of the system matrix are all negative and the matrix possesses two eigenvalues at $\frac{\gamma}{2} \pm \sqrt{\frac{\gamma^2}{4} - \alpha\beta}$. As γ is related to the friction (factor), it is smaller than $\alpha\beta = R_s z_0 T_0 / X^2$ for

typical pipe lengths; thus the eigenvalues are complex. The quantity $R_s z_0 T_0/X^2$ is the square of the resonant frequency of a pipe of length X, since $c = \sqrt{z_0 R_s T_0}$ is the speed of sound. So the linearized state-space model is that of a lightly damped resonant system.

In addition to stability, the control-oriented nature of the model allows us to deduce important properties, such as controllability. Input matrix B is full row rank, so (A, B) is reachable. If pressure p_r is measured then the system is also observable. Pressure is the simplest and most reliably measured process variable.

The DC gain from u_t to x_t can be readily extracted,

$$G_{\mathrm{DC}} = -A^{-1}B = -\frac{1}{\alpha\beta}\begin{bmatrix} \alpha\kappa & \alpha\gamma \\ 0 & -\alpha\beta \end{bmatrix} = \begin{bmatrix} -\frac{\kappa}{\beta} & -\frac{\gamma}{\beta} \\ 0 & 1 \end{bmatrix},$$

and reveals the following. In steady state:

- p_r is equal to p_ℓ with appropriately signed corrections due to non-zero flow and elevation;
- regardless of the pressure, q_ℓ is equal to q_r in steady state, as demanded by conservation of mass;

A more detailed analysis will be provided for the 3D state model in Section 1.9.

Spatial discretization

The spatial discretization of the PDEs using p_ℓ and q_r as the input signals is neither capricious nor refractory but reflects two central matters: the boundary conditions required to specify the solution for pipe flow and the requirement for reachability of the resultant state-space model. The two are not disjoint. Assuming horizontal pipes, the two PDEs (2.8)-(2.9) may be

combined to yield the damped wave equation.

$$\frac{\partial^2 \check{p}}{\partial x^2} - \frac{\lambda c^2}{2DA^2}\frac{\check{q}|\check{q}|}{\check{p}^2}\frac{\partial \check{p}}{\partial x} = \frac{1}{c^2}\frac{\partial^2 \check{p}}{\partial t^2} + \frac{\lambda}{DA}\frac{\check{q}}{\check{p}}\frac{\partial \check{p}}{\partial t},$$
$$\frac{\partial^2 \check{q}}{\partial x^2} - \frac{\lambda c^2}{2DA^2}\frac{\check{q}|\check{q}|}{\check{p}^2}\frac{\partial \check{q}}{\partial x} = \frac{1}{c^2}\frac{\partial^2 \check{q}}{\partial t^2} + \frac{\lambda}{DA}\frac{\check{q}}{\check{p}}\frac{\partial \check{q}}{\partial t},$$

with distinct boundary conditions. This PDE is hyperbolic and requires Dirichlet, Neumann or mixed boundary conditions at both ends to define the solutions [19]. Pressure $\check{p}_\ell(t)$ provides the left Dirichlet boundary condition and, via (2.9), $\check{q}_r(t)$ provides the right mixed boundary condition.

An alternative view of this spatial discretization is that, drawing on the electrical transmission line analogue of the pipe, the voltage/pressure and current/flow at one end of the line/pipe may not be independently prescribed, since they are constrained by the driving-point impedance. From the control system perspective of this dissertation, the selection of $\check{p}_\ell$ and $\check{q}_\ell$ as input signals would not yield the requisite system model reachability mentioned above.

Cascaded pipe models

As discussed in the introduction, it is our primary concern to provide sufficiently accurate models for frequencies below one Hertz well-suited for process control for facilities with pipes of length of around tens of meters (rather than kilometers). Towards this goal, in Figure 1.1 below we compare the frequency response of the a single pipe of 30m with those of two 15m pipes and three 10m pipes using the composite model for pipes in series from Section 1.7.3, which in fact represents a finer discretization. We observe that the behaviors for relevant low frequencies indeed coincide; changes for high frequencies are outside the relevant range and account for acoustical modes associated with the configurations and boundaries. Per the control objective, the bulk flow modes are preserved while the resonances fall outside the sensor and actuator bandwidths.

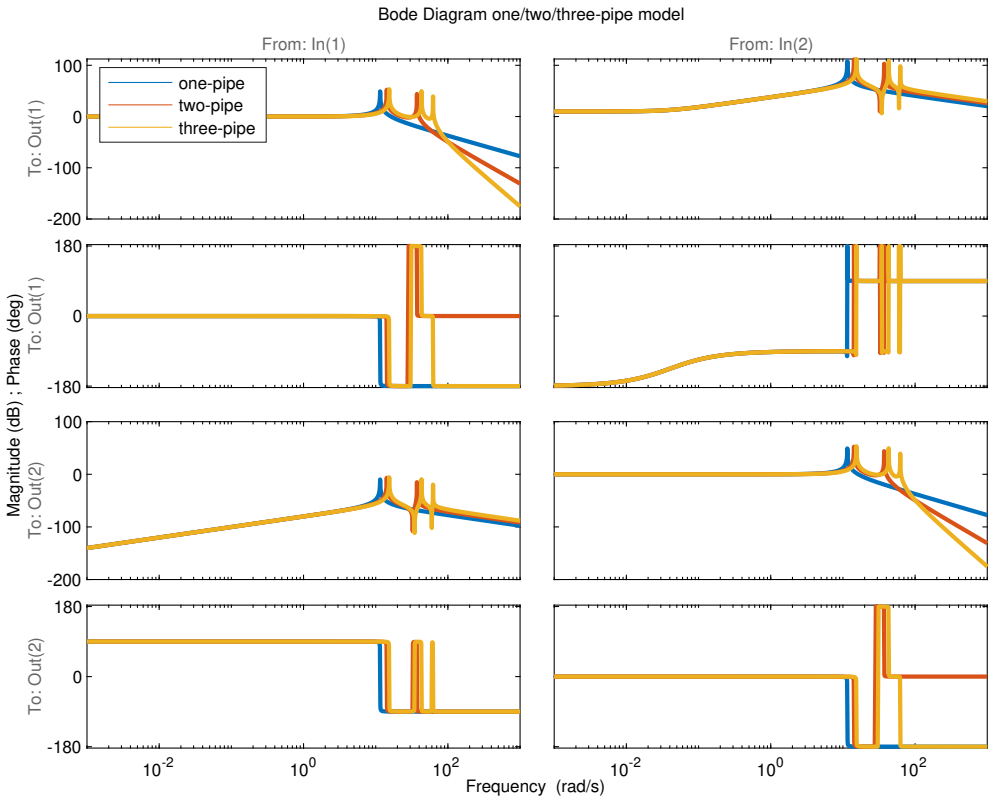

Figure 1.1. Comparison of the frequency responses from $\{p_{0,\ell}, q_{n-1,r}\} \to \{p_{n-1,r}, q_{0,\ell}\}$ with $n = \{1,2,3\}$ between one pipe $(n = 1)$, two pipes $(n = 2)$ and three pipes $(n = 3)$ in series with overall identical length.

1.4.1 Nonisothermal modeling and Bernoulli

To ensure sufficient accuracy of linear models it is important around which nominal point they are applied. Although one may use (1.7) to generate the corresponding values, we do so by solving the constituent equations in (1.1) directly for steady-state values. In this fashion, firstly, we are able to accommodate spatially varying temperatures and secondly, we reveal the error inherent to the isothermal assumption and avoid its propagation.

Proposition 1.2. *Suppose at steady state the change in density along the pipe is negligible. Then,*

the constituent equations in (1.1) *yield*

$$\bar{q}_r = \bar{q}_\ell, \tag{1.10a}$$

$$\bar{p}_r = \bar{p}_\ell^{\bar{T}_\ell/\bar{T}_r} \exp\left(\frac{\lambda X z_0 R_s \bar{T}_r}{2DA^2\bar{p}_r^2}\bar{q}_r|\bar{q}_r| - \frac{gh}{R_s z_0 \bar{T}_r}\right). \tag{1.10b}$$

If further $|v|, |h| \ll c$, $D \geq \frac{\lambda}{2}$, *and* $X|v| \ll c$, *then*

$$\bar{p}_r \approx \bar{p}_\ell^{\bar{T}_\ell/\bar{T}_r}\left(1 - \frac{\lambda X z_0 R_s \bar{T}_r}{2DA^2\bar{p}_r^2}\bar{q}_r|\bar{q}_r| - \frac{gh}{R_s z_0 \bar{T}_r}\right). \tag{1.10c}$$

Proof. For brevity, we drop subscript *ss* in this proof. The nominal mass flow in (1.10a) follows directly from the continuity equation (1.1a) by setting the time derivative to zero.

For the nominal pressure in (1.1b), for the left-hand side, Lurie shows in [29] that

$$\frac{\partial}{\partial t}(\breve{\rho}v) + \frac{\partial}{\partial x}(\breve{\rho}v^2) = \breve{\rho}\left(\frac{\partial v}{\partial t} + v\frac{\partial v}{\partial x}\right).$$

Now assume we are at steady state, so that for $\frac{\partial v}{\partial t} = 0$ and (1.1b),

$$\begin{aligned} v\frac{\partial v}{\partial x}dx &= -\frac{1}{\bar{\rho}}\frac{\partial \bar{p}}{\partial x}dx - \frac{\lambda}{2D}v|v|dx - gdh, \\ \frac{1}{g}vdv &= -\frac{1}{g\bar{\rho}}d\bar{p} - \frac{\lambda}{2Dg}v|v|dx - dh, \end{aligned} \tag{1.11}$$

with length dx. We used the fact that the change in velocity, dv, and pressure, $d\bar{p}$, along a control volume at steady state is exactly $\frac{\partial(\cdot)}{\partial x}dx$. Without loss of generality we now assume that the height at $x = 0$ is zero. Additionally, under the hypothesis and (1.10a), we can treat the velocity as a constant so that integrating (1.11) along the pipe using (1.1d) yields

$$\frac{v_r^2 - v_\ell^2}{2g} = -\frac{R_s z_0}{g}\left(\bar{T}_r \ln \bar{p}_r - \bar{T}_\ell \ln \bar{p}_\ell\right) - \frac{\lambda X}{2Dg}v|v| - h. \tag{1.12}$$

As $v_r = v_\ell$ and towards an expression for $\bar{p}_r$,

$$0 = -\ln\left(\frac{\bar{p}_r^{\bar{T}_r}}{\bar{p}_\ell^{\bar{T}_\ell}}\right) - \frac{\lambda X}{2DR_s z_0} v_r|v_r| - \frac{gh}{R_s z_0},$$
$$\bar{p}_r = \bar{p}_\ell^{\bar{T}_\ell/\bar{T}_r} \exp\left(-\frac{\lambda X}{2DR_s z_0 \bar{T}_r} v_r|v_r| - \frac{gh}{R_s z_0 \bar{T}_r}\right),$$

which with (1.1d) gives (1.10b). By the additional hypothesis,

$$|hg| \ll c^2 = RsT_r z_0,$$
$$\lambda \frac{X}{2D} v_r^2 \leq X v_r^2 \ll c^2 = RsT_r z_0,$$

so that

$$\begin{aligned}\bar{p}_r &\approx \bar{p}_\ell^{\bar{T}_\ell/\bar{T}_r}\left(1 - \frac{\lambda X}{2DR_s z_0 \bar{T}_r} v_r|v_r| - \frac{gh}{R_s z_0 \bar{T}_r}\right) \\ &= \bar{p}_\ell^{\bar{T}_\ell/\bar{T}_r}\left(1 - \frac{\lambda X z_0 R_s \bar{T}_r}{2DA^2 \bar{p}_r^2} \bar{q}_r|\bar{q}_r| - \frac{gh}{R_s z_0 \bar{T}_r}\right),\end{aligned}$$

using again the Gas Equation, (1.1d). □

On the assumptions

For better understanding of conditions under which the assumptions hold and to underline the model's suitability for control, consider Methane with $R_s = 518.28 \frac{\mathrm{J}}{^\circ\mathrm{K\ mol}}$, a low temperature of $\check{T}_r = 300^\circ$K and a constant compressibility factor $z_0 = 0.95$. The related speed of sound within the medium is $c = 14.77 \times 10^4 \frac{\mathrm{m}}{\mathrm{s}}$. Hence, the assumptions on the gas velocity, v, height, h, and length, X, conform to typical values in our control domain of gas processing facilities. Also, given a usual friction factor $\lambda \ll 1$, the lower bound on the diameter, D, renders our formula applicable to many industrial scenarios.

Relation to Bernoulli's Equation and isothermal model

The proof of Proposition 1.2 is of interest in itself since it delineates the relation between the dynamic Momentum Equation, (1.1b), and static Bernoulli's Equation, (1.12), commonly used for computing static variables, including a term for head loss, $h_l \doteq \frac{\lambda X}{2Dg} v|v|$, often referred to as the Darcy-Weissbach Equation [41]. Furthermore, observe that the approximated nominal point, (1.10c), coincides with the nominal point derived by the discretized model, (1.7), under the isothermal assumption and negligible change in density. In other words, Proposition 1.2 also quantifies the error induced through the isothermal assumption.

1.5 Model validation

We now wish to assess both the isothermal and nonisothermal models in light of their suitability for control-oriented design, using operational industrial process data from the GCTF. The data fits the problem formulation: it is sampled at 1Hz and describes pressure, mass flow and temperature variations for pipes on the order of tens of meters. Accordingly, it is appropriate for model validation and tuning for this application. Our conclusion is that, for pipe component modeling, the isothermal 2D model is sufficient for model-based control because: temperature variations in these elements are modest, temperature sensing devices can be both limited in number and variable in dynamic response, and variations with temperature can be accommodated by an appropriate controller.

Figure 1.2 shows the facility at Solar Turbines Incorporated. This is a well-instrumented site used for compressor testing and from which comprehensive data sets are available. The particular pipe section under consideration is sketched in Figure 1.3. Notice that we simplify the stepped pipe geometry by neglecting the stub at the end of the vertical middle section, assuming instead a constant slope and an accordingly adjusted friction factor[3]. The relevant data is plotted in Figure 1.4, with behavior in the relevant time scale for our goal of relatively slow process

[3]We use Haaland's formula [23] to estimate the friction factor for the straight pipes and empirical formulas in [41, Ch. 15] to approximate the friction losses induced by the bends and stub.

control. We observe that the output pressure, p_r, closely follows the input pressure, p_ℓ, and is higher despite head losses through friction. This is due to the vertical middle section and heat flux causing changes in temperature. As Figure 1.4 shows, the temperature is relatively constant, but varies with changes in pressure and mass flow. We notice that T_ℓ is measured by a more accurate sensor, given its lower quantization error, which can be observed in the middle zoom. We additionally note that T_r is lower than T_ℓ for most of the time, as is also apparent in the zoom on the right, and it seems to be dynamically faster than T_ℓ, as shown in the left zoom, which may partly be caused by different thermal inertias and processing of the sensors. Given the speed, accuracy and prevalence of pressure sensors, it is apparent that they will provide the primary signals used for feedback control and the quality of capturing the pressure state behavior should be the main model objective. We shall return to this shortly in Subsection 1.5.3.

1.5.1 Linear nonisothermal 3D model

We begin by validating the nonisothermal 3D model from Section 1.4 linearized around the nonisothermal nominal point developed in Proposition 1.2. In particular, let $\bar{q}_r = \text{mean}(q_r(t))$, $\bar{p}_\ell = \text{mean}(p_\ell(t))$, $\bar{T}_\ell = \text{mean}(T_\ell(t))$ and $\bar{T}_r = \text{mean}(T_r(t))$ so that Proposition 1.2 yields the corresponding nominal values $\bar{p}_r$ and $\bar{q}_\ell$. We then use p_ℓ and q_r from the data set as model inputs and compare our modeled pressure p_r against the related pressure in the data, recalling that data

Figure 1.2. Gas compressor test facility (GCTF) at Solar Turbines Incorporated. [13]

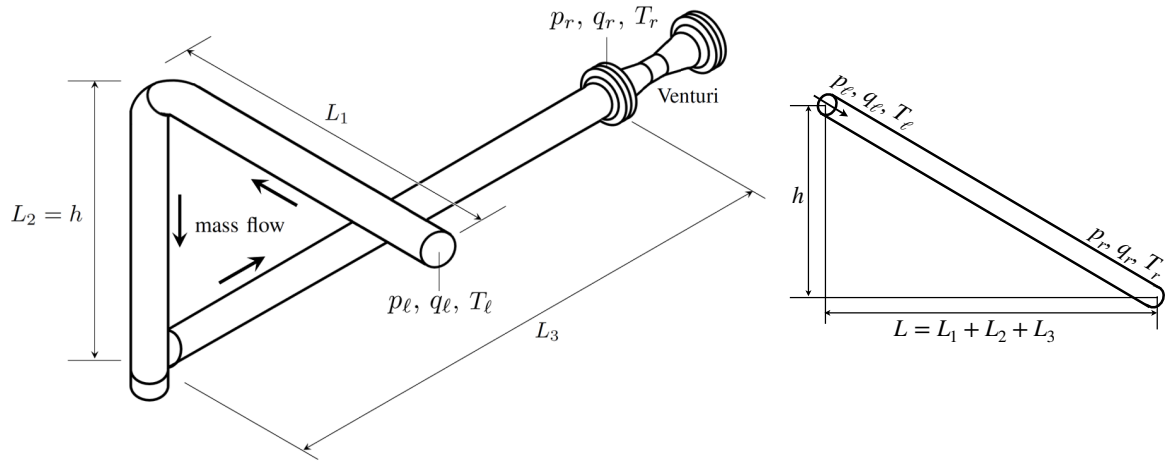

(a) Candidate geometry

(b) Modeled geometry

Figure 1.3. GCTF pipe section considered for model validation.

of q_ℓ for comparison with our model output is not available. Additionally, we study the linear model against the PDEs in (1.1) solved numerically as a two-point boundary value problem, and to which we refer as the *PDE model*. The lumped thermal conductivity, k_{rad}, is approximated at quasi steady state following [37, Section 3], using $\bar{T}_\ell$ and $\bar{T}_r$. The simulation results are shown in Figure 1.5.

For the nonisothermal 3D linear model, we see that the simulated output p_r is in a small neighborhood of the measured pressure, but has a small offset. Additionally, we observe that the modeled mass flow q_ℓ is close to the data input, q_r. This is expected for the short length of the pipe $X \approx 30$m and sampling rate of once per second. The zoom reveals that when the pressure increases at around 800s, the model output q_ℓ first increases before the signal input q_r follows suit. This is consistent with a positive mass flow that increases first at the gas entry side of the pipe.

The temperature calculations from the successive models, while close (within 0.64K), exhibit more variability than those of pressure and mass flow. The computed T_r values also

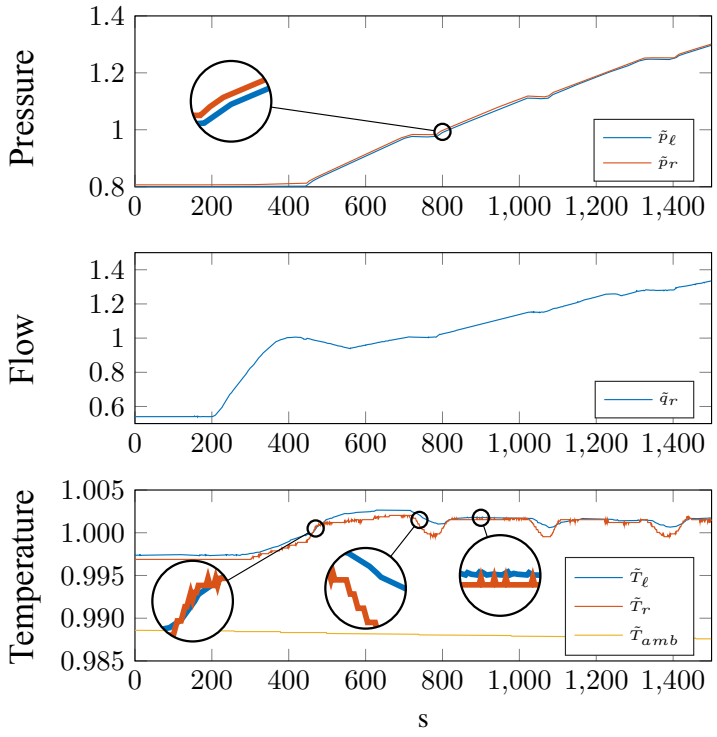

Figure 1.4. Normalized data from GCTF. The variables p_ℓ, q_r and T_ℓ will be used as model inputs, whereas p_r and T_r will be used to validate the corresponding model outputs. We observe quantization errors and measurement noise.

exceed the T_ℓ data at times, especially for the linear model. Further, there are times, around 500s for example, where the T_r data also exceeds T_ℓ data. These discrepancies indicate two types of problem: the entry and exit temperature sensors have differing response times and accuracies, as is common in application; and the heat flux model in (1.2) is too simplistic to capture the dependence of heat flux on velocity and geometry. (See [24] for more detailed analysis of these phenomena.) From a control-oriented perspective, this adds further weight to accommodating these slow variations – we quantify time constants shortly in Subsection 1.5.3 via eigenvalue analysis – through the design of the controller and to preserve the parsimony of the linear model, which captures the salient dynamics.

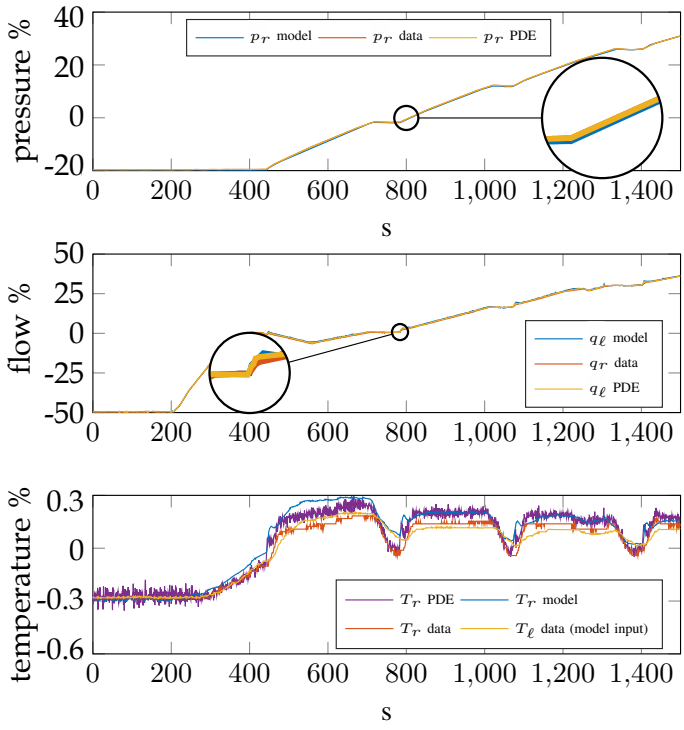

Figure 1.5. Percentage deviations from the nominal point (determined as described above) of the nonisothermal 3D linear model with data as model inputs, compared against GCTF data and PDE model (1.1).

1.5.2 Linear isothermal 2D model

Consider now the isothermal 2D model for which the model parameters and nominal point are equal to those of the nonisothermal 3D model above, except the temperature, which we set to $T_0 = (T_{\ell,ss} + T_{r,ss})/2$. As before, p_ℓ and q_r from the data set are model inputs, and we compare the modeled pressure p_r against p_r from the data. The result is shown in Figure 1.6. Notice that the modeled responses for pressure and mass flow seem congruent with those of the nonisothermal 3D model, i.e., the modeled pressure is close to the measured pressure, but displays a small static offset. The mass flows at both ends of the pipe are close, consistent with

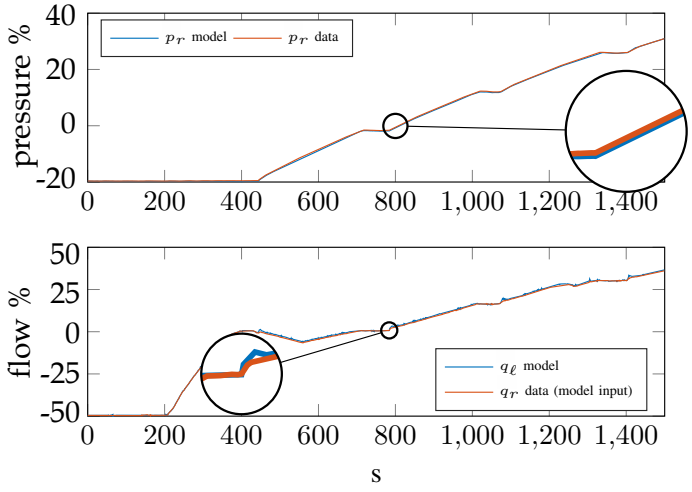

Figure 1.6. Isothermal 2D model with percentage deviations from the nominal point, compared against GCTF data and driven by the respective data inputs.

conservation of mass at steady state.

1.5.3 Isothermal 2D vs. nonisothermal 3D model

The results above are now evaluated in view of the control-oriented aspect of our approach. The similarity of both the isothermal and nonisothermal model and their accuracy characterize Figure 1.7, which shows the relative error between the modeled and measured pressure. The errors of the respective models are closely aligned, rather constant and at most at a rate of 4×10^{-3}. Both the isothermal 2D and the nonisothermal 3D linear models exhibit almost

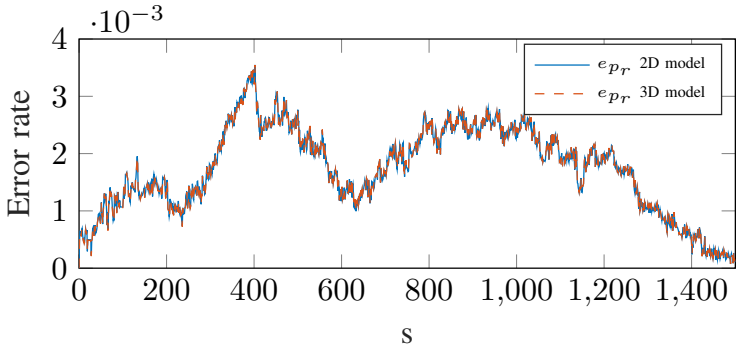

Figure 1.7. Respective p_r pressure percentage errors of the isothermal 2D and nonisothermal 3D models.

identical small offsets in simulated pressure and both capture the pressure dynamics accurately. From a control design perspective, the controller can be constructed to accommodate this modeling error.

Computing the eigenvalues of the system matrices of the related isothermal 2D and nonisothermal 3D linear models, respectively A_{iso} and A_{niso}, and of the truncation of A_{niso} to its first two rows and columns, $[A_{niso}]_{1:2}$, we have

$$\begin{aligned}
\text{eig}(A_{iso}) &= (-3.90 \pm 12.47i), \\
\text{eig}(A_{niso}) &= (-3.90 \pm 14.31i, -0.12), \\
\text{eig}\left([A_{niso}]_{1:2}\right) &= (-3.88 \pm 14.31i) \\
&\approx \text{eig}(A_{iso}).
\end{aligned}$$

From this, we conclude that the temperature state is both effectively decoupled from the pressure and mass flow states and, further, governed by a time constant approximately thirty times that of the reduced-order 2D system, which preserves the dominant lightly damped oscillatory dynamics. Consequently, for moderate temperature gradients, it is reasonable to take the temperature as a constant and employ the isothermal 2D model.

Pressing on with this control-oriented analysis, we note the respective DC gains,

$$\begin{aligned}
\lim_{t\to\infty} x_t^{\text{2D}} &= -A_{iso}^{-1} B_{iso} = \begin{bmatrix} 1.004 & -600.19 \\ 0 & 1 \end{bmatrix}, \\
\lim_{t\to\infty} x_t^{\text{3D}} &= -A_{niso}^{-1} B_{niso} = \begin{bmatrix} 1.004 & -600.33 & -25.35 \\ 0 & 1 & 0 \\ 0 & 0.03 & 0.92 \end{bmatrix}.
\end{aligned}$$

Continuing the discussion in Section 1.4, steady-state conservation of mass flow follows for both models as the DC gains from $(p_\ell, T_\ell) \to q_\ell$ are zero and $q_r \to q_\ell$ is precisely one. For the

steady-state pressure, there is (to two decimal places) a unity gain from $p_\ell \to p_r$, indicating that changes due to friction and height differences are marginal (cf. κ in Section 1.4), and a drop of similar size for both models from $q_r \to p_r$ due to additional friction (cf. γ in Section 1.4) for this example. The negative gain from $T_\ell \to p_r$ for the nonisothermal model may be due to larger heat losses to the environment; a characteristic not captured by the isothermal model. Yet, given the magnitude of the SI units used here and low temperature variations in pipe elements, the consequential discrepancy is small, as corroborated by the simulations.

The isothermal 2D model, which relies only on mass flow and pressure measurements, dovetails with the fact that especially pressure sensors (in contrast to temperature sensors) are usually well-distributed in gas processing facilities, fast and reliable. The 2D isothermal model will be used for pipe segments and the control design will be expected to accommodate the small offsets and slow variation of dynamics with changing temperatures. The experimental results and customary practice of sparse temperature measurements (also due to slow temperature sensing responses) suggest that temperatures in typical pipes need not directly be modeled using the 3D model; exceptions are heat exchangers, compressors and other strongly temperature-affecting devices. Driven by this evaluation, we continue the exposition with a focus on this isothermal model.

Part 2: Control-oriented models of pipe networks

1.6 DAEs, signal flow graphs and bond graphs

Bond graphs [8] provide a systematic method for deriving dynamic equations for interconnected electro-mechanical-hydraulic systems. They combine *effort* variables and *flow* variables, with component properties linking the two types and conservation laws and continuity governing the flows at interconnection. In the framework of fluid flow in pipe networks [29, 5], this leads to a set of PDEs for the dynamics combined with algebraic equations for the constraints. Discretizing the spatial derivative yields DAE system models, which are problematic

for direct control design for these interconnected systems. By contrast, Signal Flow Graphs (SFGs) correspond to systems described exclusively by ODEs; transfer functions in the linear case. Interconnected systems are directly managed by methods such as Mason's Gain Formula for the linear case, or by writing the composite state variable ODEs without algebraic constraints. It is these latter model forms, which are amenable to control design tools.

We consider three fundamental interconnections of pipe elements: series connection, branching and joining. Using the isothermal 2D model above, we develop a catalog of composite models that describe common units in the form of interconnections of pipes. In this way, algebraic constraints and DAEs will be avoided, as exemplified through the component of joining pipes introduced first. For clarity, 1. we limit this section to the 2D model, but the methodology is equivalently applicable to the 3D model; and 2. without loss of generality, we assume that the steady state mass flow, q_{ss}, is positive. That is, $\cdot_\ell$ denotes the side where the steady state mass flow enters the pipe and $\cdot_r$ the side with an outgoing mass flow; hence the denomination *joint* and *branch* to come.

The reduced state vector demonstrates that an interconnection of single pipes into more complex components, with corresponding algebraic constraints, cannot immediately be translated to a SFG using only single pipe models. We also point out that on the contrary, bond graphs [8] are able to represent more complex components including algebraic constraints. However, constraints, such as those in (1.13), would lead to a causal conflict of type 1 and degree 1 [8, Definition 4.19], which in turn implies the existence of DAEs and therefore disaccords with our objective of control-oriented modeling.

1.7 From DAEs of index 1 to composite models

1.7.1 Joint

Consider the joint shown in Figure 1.8(a) and let $p_{i,\ell}$ ($p_{i,r}$) be the pressure p_ℓ (p_r) of pipe P_i. The mass flow is denoted accordingly, so that the interconnection dictates the simplified

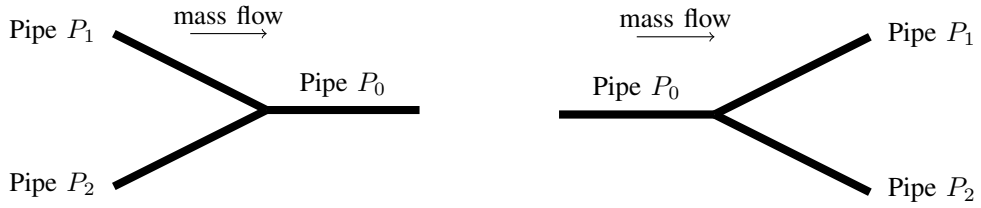

(a) Joint **(b)** Branch

Figure 1.8. Pipe junctions

algebraic constraints,

$$p_{1,r} = p_{2,r} = p_{0,\ell}, \tag{1.13a}$$

$$q_{0,\ell} = q_{1,r} + q_{2,r}. \tag{1.13b}$$

The first equation is related to continuity and the second represents conservation of mass at the junction. This composite joint model would have a state of dimension six:

$$\begin{bmatrix} p_{0,r} & p_{1,r} & p_{2,r} & q_{0,\ell} & q_{1,\ell} & q_{2,\ell} \end{bmatrix}^\top,$$

in lexicographic ordering, plus the algebraic constraints, (1.13). However, due to (1.13a) we can omit $p_{2,r}$ as a state (which would naturally arise in three pipe models).

Define α_1 and α_2 to be the parameters in (1.9) for pipes 1 and 2, and

$$\delta = \frac{\alpha_1}{\alpha_1 + \alpha_2}. \tag{1.14}$$

Then, the six-state composite joint system plus constraint (1.13) may be rewritten as an unconstrained five-state system

$$\dot{x}_t = A_j x_t + B_j u_t,$$

$$y_t = C_j x_t + D_j u_t,$$

with

$$A_j = \begin{bmatrix} 0 & 0 & -\alpha_0 & 0 & 0 \\ 0 & 0 & \alpha_1(1-\delta) & -\alpha_1(1-\delta) & -\alpha_1(1-\delta) \\ \beta_0 & \kappa_0 & \gamma_0 & 0 & 0 \\ 0 & \beta_1 & 0 & \gamma_1 & 0 \\ 0 & \beta_2 & 0 & 0 & \gamma_2 \end{bmatrix}, \tag{1.15a}$$

$$B_j = \begin{bmatrix} 0 & 0 & \alpha_0 \\ 0 & 0 & 0 \\ 0 & 0 & 0 \\ \kappa_1 & 0 & 0 \\ 0 & \kappa_2 & 0 \end{bmatrix}, C_j = \begin{bmatrix} 1 & 0 & 0 & 0 & 0 \\ 0 & 0 & 0 & 1 & 0 \\ 0 & 0 & 0 & 0 & 1 \end{bmatrix}, \tag{1.15b}$$

$$D_j = 0_{3\times 3}. \tag{1.15c}$$

The state, input and output vectors are now

$$\begin{aligned} x_t &= \begin{bmatrix} p_{0,r} & p_{1,r} & q_{0,\ell} & q_{1,\ell} & q_{2,\ell} \end{bmatrix}^\top, \\ u_t &= \begin{bmatrix} p_{1,\ell} & p_{2,\ell} & q_{0,r} \end{bmatrix}^\top, \\ y_t &= \begin{bmatrix} p_{0,r} & q_{1,\ell} & q_{2,\ell} \end{bmatrix}^\top. \end{aligned}$$

Calculation of the steady-state gain from input three, $q_{0,r}$, to outputs two, $q_{1,\ell}$, and three, $q_{2,\ell}$, shows that, in steady state,

$$\begin{aligned} q_{1,\ell} + q_{2,\ell} &= \frac{\beta_1\gamma_2}{\beta_1\gamma_2 + \beta_2\gamma_1} q_{0,r} + \frac{\beta_2\gamma_1}{\beta_1\gamma_2 + \beta_2\gamma_1} q_{0,r}, \\ &= q_{0,r}. \end{aligned}$$

That is, this five-state composite joint model satisfies the conservation of mass flow, (1.13b). Constraint (1.13a) is redundant, since the variables $p_{2,r}$ and $p_{0,\ell}$ have been removed; they can be computed from (1.13a). The new model parameter δ, defined in (1.14), describes the nominal proportion of flow $q_{0,\ell}$ attributed to each of the feeding pipes. This is the formal process of removing the constraint from the DAE of index 1.

1.7.2 Branch

Differently from the joint, for the branch in Figure B.1 the equality constraint on the pressures relates the state variable, $p_{0,r}$, to input signals of the single pipe model of the branching pipes, $p_{1,\ell}$ and $p_{2,\ell}$, i.e.,

$$p_{0,r} = p_{1,\ell} = p_{2,\ell}, \tag{1.16a}$$

$$q_{0,r} = q_{1,\ell} + q_{2,\ell}, \tag{1.16b}$$

so that the dimension of the composite model does not reduce, but is equal to the direct sum of those of the single pipe models of the individual pipes. Similarly, constraint (1.16b) on the mass flows does not prescribe any interdependence of any input variables, but rather sets the input signal of the single pipe model of pipe P_0 as the sum of two other state variables. Hence, an additional parameter, such as δ for the joint is absent. The related matrices for a branch model

are

$$A_b = \begin{bmatrix} 0 & 0 & 0 & -\alpha_0 & \alpha_0 & \alpha_0 \\ 0 & 0 & 0 & 0 & -\alpha_1 & 0 \\ 0 & 0 & 0 & 0 & 0 & -\alpha_2 \\ \beta_0 & 0 & 0 & \gamma_0 & 0 & 0 \\ \kappa_1 & \beta_1 & 0 & 0 & \gamma_1 & 0 \\ \kappa_2 & 0 & \beta_2 & 0 & 0 & \gamma_2 \end{bmatrix}, \tag{1.17a}$$

$$B_b = \begin{bmatrix} 0 & 0 & 0 \\ 0 & \alpha_1 & 0 \\ 0 & 0 & \alpha_2 \\ \kappa_0 & 0 & 0 \\ 0 & 0 & 0 \\ 0 & 0 & 0 \end{bmatrix}, C_b = \begin{bmatrix} 0 & 1 & 0 & 0 & 0 & 0 \\ 0 & 0 & 1 & 0 & 0 & 0 \\ 0 & 0 & 0 & 1 & 0 & 0 \end{bmatrix}, \tag{1.17b}$$

with state $x_t = \begin{bmatrix} p_{0,r} & p_{1,r} & p_{2,r} & q_{0,\ell} & q_{1,\ell} & q_{2,\ell} \end{bmatrix}^\top$, input $u_t = \begin{bmatrix} p_{0,\ell} & q_{1,r} & q_{2,r} \end{bmatrix}^\top$ and output $y_t = \begin{bmatrix} p_{1,r} & p_{2,r} & q_{0,\ell} \end{bmatrix}^\top$. The feedthrough matrix D_b is zero.

Remark 1.7.1. *It is straightforward to expand these ideas to intersections comprising m-input pipes and n-output pipes. This construction is available in Appendix B and generalizes the systematic reduction of index-1 DAEs to systems of ODEs.*

1.7.3 Pipes in series

N pipes in series are depicted in Figure 1.9, and are of particular interest if pipe parameters (see Table 1.1) change along the dimension of x or the discretization error grows too large for a given length. For conciseness we only state the relevant matrices here that result from the

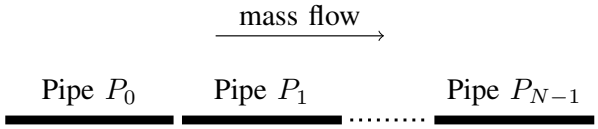

Figure 1.9. Pipe series

continuity conditions and conservation of mass, i.e.,

$$p_{i,r} = p_{i+1,\ell}, \quad q_{i,r} = q_{i+1,\ell}, \tag{1.18}$$

with $i \in \{0,1,\ldots,N-2\}$. The state, input and output elements $p_{i,r}$ and $q_{i,\ell}$ in lexicographical order, i.e., $x_t = \begin{bmatrix} p_{0,r} & \ldots & p_{N-1,r} & q_{0,\ell} & \ldots & q_{N-1,\ell} \end{bmatrix}^\top$, $u_t = \begin{bmatrix} p_{0,\ell} & q_{N-1,r} \end{bmatrix}^\top$ and $y_t = \begin{bmatrix} p_{N-1,r} & q_{0,\ell} \end{bmatrix}^\top$, yield

$$A_s = \begin{bmatrix} \mathbf{0} & A_{s,12} \\ A_{s,21} & A_{s,22} \end{bmatrix}, B_s = \begin{bmatrix} B_{s,1}^\top & B_{s,2}^\top \end{bmatrix}^\top,$$
$$C_s = \begin{bmatrix} \mathbf{0}_{2,2(N-1)} & I_2 & \mathbf{0}_{2,2(N-1)} \end{bmatrix},$$

and $D_s = \mathbf{0}$, where the subscripts for $\mathbf{0}$ and I describe the dimension and

$$A_{s,12} = \begin{bmatrix} -\alpha_0 & \alpha_0 & & \mathbf{0} \\ & \ddots & \ddots & \\ & & \ddots & \alpha_{N-2} \\ \mathbf{0} & & & -\alpha_{N-1} \end{bmatrix},$$

$$A_{s,21} = \begin{bmatrix} \beta_0 & & & \mathbf{0} \\ \kappa_1 & \ddots & & \\ & \ddots & \ddots & \\ \mathbf{0} & & \kappa_{N-1} & \beta_{N-1} \end{bmatrix},$$

$$A_{s,22} = \mathrm{diag}(\gamma_0, \gamma_1, \ldots, \gamma_{N-1}),$$

$$B_{s,1} = \begin{bmatrix} \mathbf{0}_{2(N-1),2} \\ 0 \quad \alpha_{N-1} \end{bmatrix}, B_{s,2} = \begin{bmatrix} \kappa_0 \quad 0 \\ \mathbf{0}_{2(N-1),2} \end{bmatrix}.$$

Since each pipe conforms to steady-state conservation of mass flow, the interconnection automatically does as well. Bode diagrams are provided in [9] for 2i2o models of a 30-meter pipe section as: a single 30m pipe, two 15m pipes in series, three 10m pipes in series; low-frequency responses coincide.

1.8 Systematic model interconnection

Building on the composite models above, we introduce a matrix formulation that enables the construction of state-space models for interconnected components of pipes, joints and branches.

1.8.1 Matrix methodology

Towards this goal, with N interconnected components, let $\mathscr{U}_i \subset \mathbb{R}^{n_{u,i}}$ and $\mathscr{Y}_i \subset \mathbb{R}^{n_{y,i}}$ be the set of inputs and outputs for component i, respectively, with state $x_t^{(i)} \in \mathbb{R}^{n_{x,i}}$, input $u_t^{(i)} \in \mathbb{R}^{n_{u,i}}$

and output $y_t^{(i)} \in \mathbb{R}^{n_{y,i}}$. The model matrices are denoted accordingly. Further, $\overline{\mathscr{U}}$ and $\overline{\mathscr{Y}}$ are the respective sets of external inputs and outputs. We assume that the input of every component is either connected to the output of another component or represents an external input.

Assumption 1.1 (connectedness)**.** *Let $i \in \{1,2,\ldots,N\}$. For any $u \in \mathscr{U}_i$ there exists a $j \in \{1,2,\ldots,N\}, j \neq i$, such that $u \in \mathscr{Y}_j \cup \overline{\mathscr{U}}$.*

Internal interconnections are governed by the continuity of pressure and mass flow per (1.18). We begin by stacking the state-space models of the individual network components. With some abuse of notation,

$$\dot{x}_t = Ax_t + Bw_t, \quad y_t = Cx_t + Dw_t \tag{1.19}$$

where

$$A = \text{blkdiag}(A^{(1)}, A^{(2)}, \ldots, A^{(N)}), \tag{1.20a}$$

$$B = \text{blkdiag}(B^{(1)}, B^{(2)}, \ldots, B^{(N)}), \tag{1.20b}$$

$$C = \text{blkdiag}(C^{(1)}, C^{(2)}, \ldots, C^{(N)}), \tag{1.20c}$$

$$D = \text{blkdiag}(D^{(1)}, D^{(2)}, \ldots, D^{(N)}). \tag{1.20d}$$

The total state vector, $x_t \in \mathbb{R}^{n_{x,1}+n_{x,2}+\cdots+n_{x,N}}$, total output vector, $y_t \in \mathbb{R}^{n_{y,1}+n_{y,2}+\cdots+n_{y,N}}$, and *component* input vector, $w_t \in \mathbb{R}^{n_{u,1}+n_{u,2}+\cdots+n_{u,N}}$ are composed correspondingly of direct sums. Assumption 1.1 yields

$$w_t = Fy_t + Gu_t, \tag{1.21}$$

where u_t denotes the total input vector of external signals feeding into the total system. The matrix F describes connections between component inputs and outputs, and G is related to the connection between external inputs and internal components. Hence, both matrices are sparse

and constructed as follows,

$$[F]_{i,j} = \begin{cases} 1, & \text{if } [y_t]_j = [w_t]_i, \\ 0, & \text{otherwise,} \end{cases} \tag{1.22a}$$

$$[G]_{i,j} = \begin{cases} 1, & \text{if } [u_t]_j = [w_t]_i, \\ 0, & \text{otherwise,} \end{cases} \tag{1.22b}$$

with $[\cdot]_{i,j}$ denoting the matrix element in row i and column j, and vectors written accordingly. This formulation is applied to a numerical example in Section 1.9. It allows us to define a state model of the total system.

Proposition 1.3. *A (perhaps non-minimal) state-space realization of* (B.45) *and* (1.21) *is given by*

$$x_t = \bar{A}x_t + \bar{B}u_t, \quad y_t = \bar{C}x_t + \bar{D}u_t, \tag{1.23}$$

where

$$\bar{A} = A + BF(I - DF)^{-1}C, \quad \bar{C} = (I - DF)^{-1}C,$$
$$\bar{B} = B\left[I + F(I - DF)^{-1}D\right]G, \quad \bar{D} = (I - DF)^{-1}DG.$$

Proof. Substituting w from (1.21) into (B.45) for y_t yields

$$y_t = (I - DF)^{-1}Cx_t + (I - DF)^{-1}DGu_t,$$
$$w_t = F(I - DF)^{-1}Cx_t + \left[I + F(I - DF)^{-1}D\right]Gu_t. \tag{1.24}$$

Now substituting from (1.24) into (B.45) for $\dot{x}_t$ produces the closed-loop state-space connected

system.

$$\dot{x}_t = \left[A + BF(I - DF)^{-1}C\right] x_t + B\left[I + F(I - DF)^{-1}D\right] Gu_t,$$
$$y_t = (I - DF)^{-1}Cx_t + (I - DF)^{-1}DGu_t.$$

□

Here, the total output, y_t, is set to be the outputs of all components. However, if only some variables constitute to the total output modifying y_t is a simple exercise through the multiplication of $\bar{C}$ and $\bar{D}$ by an appropriate selection matrix.

1.8.2 Subsuming Mason

Next, we show that the state-space realization above subsumes Mason's Gain Formula [30]. The latter is a method to find transfer functions of SFGs with multiple inputs and multiple outputs and has also been established in a simple matrix form in e.g. [11]. The interest in this equivalence result lies in its generality for linear systems and advantage over Mason's Gain Formula via simple matrix manipulation without relying on symbolic matrix inversions with transfer functions as matrix elements. Further, the calculation in Proposition 1.3 yields all the closed-loop transfer functions between each input and each output, versus Mason, which computes SISO transfer functions using Cramer's Rule.

Mason's Gain Formula formulation in [11] starts by writing the vector of output signals, $\bar{y}$, as the interconnection of $y_t^{(i)}$ and $\bar{u}_t$ with transfer function matrices,

$$y_t = \mathcal{Q}y_t + \mathcal{P}u_t. \tag{1.25}$$

Mason's Gain Formula is then that the solution is given by

$$y_t = (I - \mathcal{Q})^{-1}\mathcal{P}u_t. \tag{1.26}$$

Proposition 1.4. *A state-variable realization of Mason's Gain Formula transfer function,* $(I - \mathcal{Q})^{-1}\mathcal{P}$*, is given in* (B.49).

This is proven in the Appendix.

1.9 Numerical experiment

We apply our modeling methodology to the loop illustrated in Figure B.7, which represents a hypothetical pipe loop at the GCTF. Such a feedback system creates problems for DAE methods, such as those in [5] because of the algebraic constraints. Here we use it as a proof-of-concept test case and rely, rather unrealistically but similarly to [5] for distribution networks, on isothermal models and treatment of the compressor and valve as static gains. Clearly, the thermal properties of compressors, heat exchangers and valves play an important role on the spatial scales of gas processing facilities and these will form the focus for ongoing modeling.

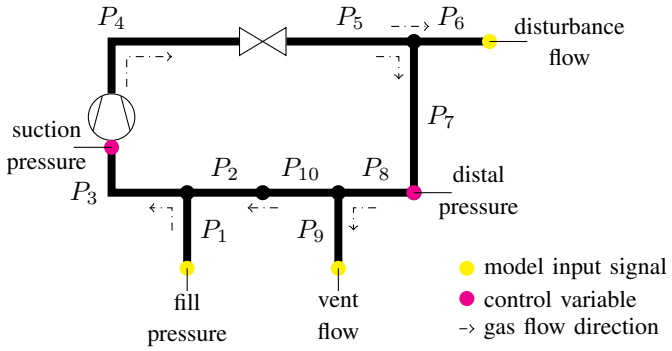

Figure 1.10. Pipe network with compressor and valve ⋈. In process control parlance, the fill pressure and vent flow are manipulated variables, the suction and distal pressures are controlled variables, and the flow from P_6 is a disturbance signal.

The gas is methane and flows clockwise, entering through pipe P_1 and exiting through pipes P_6 and P_9. The aim is to regulate the pressures $p_{3,r}$ and $p_{7,r}$ in the face of leakage via P_6. The Haaland formula [41] and assumed parameters[4] yield a friction factor for each pipe of $\lambda = 0.0111$.

[4] All pipes are assumed to have the same geometry, i.e., $X = 10\text{m}, D = 0.7\text{m}, \text{roughness} = 4.57 \times 10^{-5}\text{m}$. Further, we assume that $Re \approx 1.168 \times 10^8, T_0 = 300\text{K}, z_0 = 0.95, R_s = 518.28\text{J/(Kmol)}$, $\tilde{p}_{ss,\ell} = 25 \times 10^5\text{Pa}$ and $\tilde{q}_{ss} = 21\text{m/s}^2$.

1.9.1 Network model

The compressor and valve, whose corresponding variables are respectively labeled by subscripts c and v, are modeled as static gains

$$D_c = \begin{bmatrix} k_c & 0 \\ 0 & 1 \end{bmatrix}, \quad D_v = \begin{bmatrix} k_v & 0 \\ 0 & 1 \end{bmatrix},$$

where $k_c = 4$ and $k_v = 0.8$. Further, pipes (P_1, P_2, P_3) are modeled as a joint, as in (1.15), and (P_5, P_6, P_7) and (P_8, P_9, P_{10}) as branches, as in (B.4). Composing the system according to (B.46), results in the component input vector,

$$w_t = \begin{bmatrix} p_{1,\ell} & p_{2,\ell} & q_{3,r} & p_{c,\ell} & q_{c,r} & p_{4,\ell} & q_{4,r} \\ p_{v,\ell} & q_{v,r} & p_{5,\ell} & q_{6,r} & q_{7,r} & p_{8,\ell} & q_{9,r} & q_{10,r} \end{bmatrix}^\top,$$

and the total output vector,

$$y_t = \begin{bmatrix} p_{3,r} & q_{1,\ell} & q_{2,\ell} & p_{c,r} & q_{c,\ell} & p_{4,r} & q_{4,\ell} \\ p_{v,r} & q_{v,\ell} & p_{6,r} & p_{7,r} & q_{5,\ell} & p_{9,r} & p_{10,r} & q_{8,\ell} \end{bmatrix}^\top.$$

The inputs of the total system are

$$u_t = \begin{bmatrix} p_{1,\ell} & q_{6,r} & q_{9,r} \end{bmatrix}^\top.$$

With (B.48), the total input and output vector, u_t and y_t, as well as the component input vector, w_t, are the basis for the construction of F and G. For example, $[w_t]_1 = p_{1,\ell}$ is an input of the total system and the first element of u_t. Hence $[G]_{1,1} = 1$. Further, $[w_t]_2 = p_{2,\ell}$ connects to $p_{10,r} = [y_t]_{14}$, so that $[F]_{2,14} = 1$. Similarly, $[w_t]_{11} = q_{6,r}$ is another total input, i.e., $q_{6,r} = [u_t]_2$,

so that $[G]_{11,2} = 1$. In this way, by passing through $_t$ and following (B.48), we can fill the matrices with ones at the appropriate location and zeros otherwise. The eigenvalues of the resulting interconnected system all have negative real part; hence stability is demonstrated. Some eigenvalues have large imaginary parts pointing to the high-oscillatory resonant modes, which we ignore in the control design, which will recognize the presence of anti-aliasing filters in the sensors, see Chapter 2.

1.9.2 Steady state: conservation of mass

The isothermal LTI closed-loop system is stable with the overall pressure static gains from $p_{1,\ell}$ to all but $p_{2,r}$ greater than one. Increasing the compressor and/or valve gains can bring about instability, as might be expected. Further, since the frequency response of each component is available, standard stability tests may be performed. Indeed, the control design is to construct a stabilizing 2-input/2-output regulator to reject the effect of the disturbance flow.

To evaluate the model in terms of conservation of mass, we also analyze the steady-state gains from the three loop inputs, $p_{1,\ell}$, $q_{6,r}$ and $q_{9,r}$, to each pipe's mass flow. The corresponding DC-gain values are shown in Table 1.2. Each column represents one model input and each row shows the corresponding steady-state change in mass flow from nominal due to a unit step change of the respective input and zero inputs otherwise.

Table 1.2. DC (steady-state) gains from inputs to mass flows.

to\from	fill: $p_{1,\ell}$	vent: $q_{9,r}$	dist: $q_{6,r}$
$q_{1,\ell}$	0	1	1
$q_{2,\ell}$	0.184	-1.022	-0.8
$q_{3,\ell}$	0.184	-0.022	0.2
$q_{4,\ell}$	0.184	-0.022	0.2
$q_{5,\ell}$	0.184	-0.022	0.2
$q_{6,\ell}$	0	0	1
$q_{7,\ell}$	0.184	-0.022	-0.8
$q_{8,\ell}$	0.184	-0.022	-0.8
$q_{9,\ell}$	0	1	0
$q_{10,\ell}$	0.184	-1.022	-0.8

Step response fill pressure change

Evaluating the first column with input $p_{1,\ell}$, a zero change in mass flows $q_{6,\ell}, q_{9,\ell}$ is consistent the other zero inputs, $q_{9,r} = q_{6,r} = 0$. As a result, the steady-state mass flow $q_{1,\ell} = 0$. A higher fill pressure leads to a larger mass flow around the loop, uniformly through all pipes, as evident by the numerical values of the other rows of the same column.

Step responses vent and disturbance flow changes

Evaluating the second column with input $q_{9,r} = 1$ and zero disturbance flow, i.e. $q_{6,r} = 0$ (and hence $q_{6,\ell} = 0$), 1kg/s^2 enters the loop through $q_{9,r}$ so that $q_{9,\ell} = 1$. We further note that mass flow around the loop uniformly dropped by -0.022 excluding pipes P_{10} and P_2. The flow through Pipe P_{10} and P_2 reduces by -1.022 as a result of the reduced overall flow and unit flow exiting through pipe P_9. Then, the additional flow $q_{1,\ell} = 1$ through pipe P_1 brings the flow back to -0.022. The same reasoning can be applied to the last column related to the disturbance input $q_{6,r}$.

Our analysis shows that conservation of mass around the loop is captured through the use of composite models and the matrix methodology presented above, without imposing additional algebraic constraints. Further, the linear time-invariant model is amenable to direct feedback controller design and stability analysis.

1.10 Conclusion and further directions

In this chapter, we present control-oriented models in the form of LTI state-space realizations that capture the dominant dynamics for the pressure, mass flow and temperature in pipes at a scale appropriate for gas processing facilities. Validation against real-world data and simulation of the initial constituent equations illustrate their suitability for model-based controller design, which will incorporate requirements for robustness to minor static offsets and slow variations. Building on these models, we elaborate on the need for composite elements for

interconnections to absorb DAEs, and provide a corresponding catalog of composite models for common units. To increase practical relevance of the proposed model, we also introduce a matrix methodology that enables a simple creation of pipe networks and illustrate its behavior with a numerical experiment. The analysis of costs and benefits of nonisothermal models indicates and quantifies inaccuracies of the models and distinguishes between models parametrized by nominal temperature versus those parametrized by measured temperatures. Here, we focus on process control; additional (nonlinear) control systems across multiple operating points may be employed for safety, start-up and shutdown and these could be local to specific units, and rapid in their action. Our methods are not targeted towards these controllers.

The control-oriented modeling developed here draws guidance at the formulation stage from the control objective specification in the introduction. The next chapters take these methods further. In Appendix B, the modeling methods are applied to a generate linear state-space models for a wider variety of network elements. We provide a compendium of modeled elements together with their derivation and proof of internal satisfaction of conservation rules. The compendium also provides example MATLAB code illustrating the connection process for models. Chapter 2 on the other hand marries the control-oriented modeling with model-based control and provides strong evidence of the role played by model features here in subsequent controller development. Particularly, we explore in detail the regulation control effect of the mass-conserving models.

This chapter, in full, has been submitted for publication of the material as it may appear as Sven Brüggemann, Robert H. Moroto, and Robert R. Bitmead. “Control-oriented modeling of pipe flow in gas processing facilities.” The dissertation author was the primary investigator and author of this paper.

Chapter 2

Control-orientation, conservation of mass and model-based control of compressible fluid networks

2.1 Introduction

Our purpose is to analyze more fully network modeling and controller design based on the control-oriented models of Chapters 1 and Appendix B, where standard fluid models, such as [6], which incorporate algebraic constraints associated with conservation of mass and pressure continuity at junctions, are replaced by linear state-space models adapted to effect these properties inherently, i.e. without the inclusion of explicit constraints. These unit models may be aggregated to yield more complicated network models, which in turn may be used for multi-input multi-output (MIMO) control design with standard tools. We put to the test the validity of whether these units models from Chapter 1 and Appendix B truly are control-oriented and actually capture conservation and continuity when combined into full network models. This is examined in detail, notably to establish the presence of integrators or DC structure in the composite models. The subsequent controller design using these models is conducted and shown to reflect the requirements of conservation in the plant.

Our concern is to blend targeted but reusable control-oriented modeling methods with subsequent standard model-based control via the specific objective of designing controllers for

compressible fluid regulation in a gas processing facility. The particular example process is the Gas Compressor Test Facility (GCTF) of Solar Turbines Incorporated, sponsor of this work. The corresponding model is developed and presented in Chapter 1 and Appendix B and consists of linear state-space unit models interconnectable to yield a plant-wide or network composite model. The focus here is on two core aspects: the inheritance of conservation of mass from the units to the network despite the absence of algebraic constraints and the consequences of this for the network model in the light of controller design; and, MIMO control design using these approximate models and cognizant of the role of the conservation of mass in these designs. Throughout, the emphasis lies on the utility of the methodology for MIMO control design in gas processing facilities.

In the first part of the body of this chapter, we establish: explicit interconnection rules; mass conservation properties of the composite network model inferred from those of the components; consequences for the low-frequency dynamics of the network systems, such as the presence of integrators and differentiators, which have a strong bearing on regulator design [12, 4, 33]. The second part of this chapter is devoted to controller design for a prototype control-oriented model from Chapter 1 and Appendix B for the GCTF. We endeavor to come to grips with what it means for a model to be control-oriented by referring to philosophers of science and the specifics of the GCTF target example.

The gas facility control problem is characterized as follows:

(i) A MIMO digital controller is sought to regulate the measured bulk pressures to nominal values in the face of disturbances.

(ii) There is no intention to control turbulent or resonant acoustic modes in the system. Accordingly, the sampling rate for the digital controller is one sample per second or below and anti-aliasing filters with cut-off frequency 0.4 Hz are included into sensor channels.

(iii) The flow and pressure actuation is effected with control valves responding to the command signals, perhaps via a local controller, which is not part of our analysis.

(iv) The loop is subject to disturbance flows and pressures, which are roughly constant at this sampling rate.

(v) Because temperature sensing is slower than the sampling rate, we treat temperatures as known parameters in the models, as we do for compressor speed.

The development of our control design and analysis will be mindful of these objectives, particularly the emphasis on regulation of bulk pressure aspects with this sample rate. The loop model of the GCTF will provide the basis for the design study.

This chapter is structured as follows. Section 2.2 provides a brief treatment of models described by hyperbolic partial differential equations (PDEs) and their spatial discretization to yield linear lumped-parameter state-space models. To facilitate understanding, this is conducted for current and voltage in a linear electrical transmission line and analogously for the flow and pressure in our mildly nonlinear pipe model. This leads to an analysis of conservation of current in the line and conservation of mass flow in the pipe as consequences and artful generalizations of conservation of charge and mass. Section 2.3 compares the features captured by the discretized and linearized models: resonant modes, bulk behavior and conservation. Section 2.4 presents the interconnection rules for the unit models and develops consequences for the transfer functions of the interconnected systems. Conservation of mass is explicitly defined for linear systems as a transfer function property in Section 2.5. Sections 2.6 and 2.7 show that mass conservation of a network model is inherited from conservation of every component model and that this property affects the DC plant dynamics. For networks with flow input signals only, it leads to the presence of an integrator in the system. The latter sections of this chapter, Sections 2.8-2.9 provide an example of MIMO LQG control design for the GCTF loop model, which possesses an integrator.

As we stated above, the objective is to trace through the control design possibilities engendered by the replacement of algebraic constraints, leading to differential algebraic equations (DAEs), or bond graph models by state-space or signal flow graph models, which preserve the mass conservation properties. An interesting feature is how the conservation properties appear in

network models and in turn affect the control design using standard MATLAB tools. Hopefully, we tease out some answers to the question of what it means to be control-oriented.

2.2 PDE element models

To help fix ideas, we present the parallel derivation of two lumped-parameter linear state-space models from discretization and (where needed) linearization of their constituent PDEs. The transmission line model is included because it is well known, linear and exhibits conservation of electrical charge. It is an adjunct to the main fluid flow model and its manifestation of conservation of mass.

2.2.1 Transmission lines

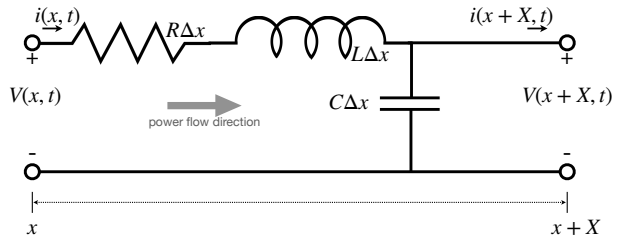

Figure 2.1. Lumped-parameter transmission line model with zero shunt conductance.

A lumped-parameter transmission line segment of length Δx with zero shunt conductance is depicted in Figure 2.1. The partial differential equation (PDE) *Telegraph Equations* describing this system are

$$\frac{\partial i}{\partial x}(x,t) = -C\frac{\partial v}{\partial t}(x,t), \tag{2.1}$$

$$\frac{\partial v}{\partial x}(x,t) = -Ri(x,t) - L\frac{\partial i}{\partial t}(x,t). \tag{2.2}$$

Direct calculations yield

$$\frac{\partial^2 i}{\partial x^2} = RC\frac{\partial i}{\partial t} + LC\frac{\partial^2 i}{\partial t^2}, \tag{2.3}$$

$$\frac{\partial^2 v}{\partial x^2} = RC\frac{\partial v}{\partial t} + LC\frac{\partial^2 v}{\partial t^2}, \tag{2.4}$$

$$\frac{\partial (iv)}{\partial x} = -Ri^2 - \frac{\partial \left[\frac{1}{2}Li^2\right]}{\partial t} - \frac{\partial \left[\frac{1}{2}Cv^2\right]}{\partial t}. \tag{2.5}$$

Equations (2.3) and (2.4) are damped wave equations and (2.5) captures the propagation, dissipation and storage of power along the line. The properties of the solutions, including energy and mass flow, are determined by the boundary conditions.

2.2.2 One-dimensional pipe flow

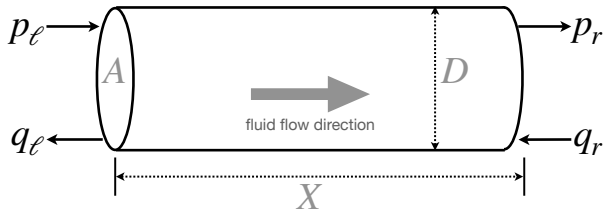

Figure 2.2. Pipe diagram defining: flow and signal directions; length, diameter, and cross-sectional area.

One-dimensional isothermal compressible gas flow in horizontal pipes may be described by the following partial differential equations, which combine: the Euler equations, Ideal Gas Equation, and the assumption that the transport velocity is significantly lower than the speed of sound, $c = \sqrt{R_s T_0 z_0}$. (See [10, 6].)

$$\frac{\partial \check{p}}{\partial t} = -\frac{c^2}{A}\frac{\partial \check{q}}{\partial x}, \tag{2.6}$$

$$\frac{\partial \check{q}}{\partial t} = -A\frac{\partial \check{p}}{\partial x} - \lambda \frac{c^2}{2DA}\frac{\check{q}|\check{q}|}{\check{p}}. \tag{2.7}$$

The solution of these equations defines pressure, $\check{p}(x,t)$, and mass flow, $\check{q}(x,t)$, as functions of space, $x \in [0,X]$ with length X, and time, $t \in (0,\infty)$. Define the nominal values of pressure and

flow to be $\bar{p}(x,t)$ and $\bar{q}(x,t)$. Further, define variations about these nominal values:

$$p(x,t) = \breve{p}(x,t) - \bar{p}(x,t), \quad q(x,t) = \breve{q}(x,t) - \bar{q}(x,t).$$

Then the linearization of the pipe flow PDEs, assuming flow $\breve{q}$ is positive, is

$$\frac{\partial p}{\partial t} = -\frac{c^2}{A}\frac{\partial q}{\partial x}, \tag{2.8}$$

$$\frac{\partial q}{\partial t} = -A\frac{\partial p}{\partial x} - \frac{\lambda c^2}{DA}\frac{\bar{q}}{\bar{p}}q + \frac{\lambda c^2}{2DA}\frac{\bar{q}^2}{\bar{p}^2}p. \tag{2.9}$$

In turn, this yields damped wave equations for q and for p, *cf.* (2.3), (2.4).

$$\frac{\partial^2 q}{\partial x^2} - \frac{\lambda c^2}{2DA^2}\frac{\bar{q}^2}{\bar{p}^2}\frac{\partial q}{\partial x} = \frac{1}{c^2}\frac{\partial^2 q}{\partial t^2} + \frac{\lambda}{DA}\frac{\bar{q}}{\bar{p}}\frac{\partial q}{\partial t}, \tag{2.10}$$

$$\frac{\partial^2 p}{\partial x^2} - \frac{\lambda c^2}{2DA^2}\frac{\bar{q}^2}{\bar{p}^2}\frac{\partial p}{\partial x} = \frac{1}{c^2}\frac{\partial^2 p}{\partial t^2} + \frac{\lambda}{DA}\frac{\bar{q}}{\bar{p}}\frac{\partial p}{\partial t}. \tag{2.11}$$

2.2.3 Spatial discretization and state-space models

Regarding the transmission line as a two-port network, we recognize that circuit variables, i and v, cannot both be independently prescribed at a single port. Accordingly, we treat $v_\ell(t)V(x,t)$ and $i_r(t) \doteq i(x+X,t)$ as the input variables and $v_r(t) \doteq V(x+X,t)$ and $i_\ell(t) \doteq i(x,t)$ as output or response variables. This choice of (v_ℓ, i_r) as the free input signals coincides with the (mixed Dirichlet, Neumann) boundary condition specification required for the hyperbolic damped wave equation, (2.3) or (2.4). This is explained in more detail for the pipe model in Chapter 1. Spatial discretization of (2.1-2.2) yields a linear state-space description.

$$\begin{bmatrix} \dot{v}_r \\ \dot{i}_\ell \end{bmatrix} = \begin{bmatrix} 0 & \frac{1}{CX} \\ -\frac{1}{LX} & -\frac{R}{L} \end{bmatrix} \begin{bmatrix} v_r \\ i_\ell \end{bmatrix} + \begin{bmatrix} 0 & -\frac{1}{CX} \\ \frac{1}{LX} & 0 \end{bmatrix} \begin{bmatrix} v_\ell \\ i_r \end{bmatrix}. \tag{2.12}$$

Similarly, since for the pipe model pressure and flow behave analogously to voltage and

current in the transmission line and cannot be separately prescribed functions of time at the same point in space and (2.10) and (2.11) are also a damped wave equations, define

$$p_\ell = p(x,t), \qquad p_r = p(x+X,t),$$
$$q_\ell = q(x,t), \qquad q_r = q(x+X,t).$$

The discretized and linearized state-space equations are[1]

$$\begin{bmatrix} \dot{p}_r \\ \dot{q}_\ell \end{bmatrix} = \begin{bmatrix} 0 & \frac{c^2}{AX} \\ -\frac{A}{X} & -\frac{\lambda c^2}{DA}\frac{\bar{q}_r}{\bar{p}_\ell} \end{bmatrix} \begin{bmatrix} p_r \\ q_\ell \end{bmatrix} + \begin{bmatrix} 0 & -\frac{c^2}{AX} \\ \frac{A}{X} + \frac{\lambda c^2}{2DA}\frac{\bar{q}_r^2}{\bar{p}_\ell^2} & 0 \end{bmatrix} \begin{bmatrix} p_\ell \\ q_r \end{bmatrix}. \tag{2.13}$$

2.3 Model properties for pipe and transmission line

The damped wave equations, (2.3-2.4) for the transmission line and (2.10-2.11) for the pipe, and the spatially discretized and linearized state-space variants, (2.12) and (2.13) respectively, exhibit wave resonance and damping due to resistance or friction. For the transmission line model, the eigenvalues are at $-\frac{R}{2L} \pm \sqrt{\frac{R^2}{4L^2} - \frac{1}{(LCX^2)}}$, while for the pipe they are at $-\frac{\lambda c^2}{2DA}\frac{\bar{q}_r}{\bar{p}_\ell} \pm \sqrt{\frac{(\lambda c^2)^2}{4(DA)^2}\frac{\bar{q}_r^2}{\bar{p}_\ell^2} - \frac{c^2}{X^2}}$. Since the R and λ terms are small, the surds yield imaginary numbers, whose physical interpretation as oscillations is immediate, even though one refers to transverse electromagnetic propagation and the other to acoustic compression waves. The negative real parts, likewise, are simply interpreted. Figure 2.3 shows the four frequency response magnitudes for a representative 10m steel gas pipe.

The acoustic resonant mode, here at 6.25Hz, falls well above the Nyquist sampling

[1]The friction correction term to $\frac{A}{X}$, $\frac{\lambda c^2}{2DA}\frac{\bar{q}_r^2}{\bar{p}_\ell^2}$ may be taken into account in the system or input matrix and appears because $\bar{p}_r = \left(1 - \frac{\lambda c^2 X}{2DA^2}\frac{\bar{q}_r^2}{\bar{p}_\ell^2}\right)\bar{p}_\ell$. It is a small term compared to $\frac{A}{X}$.

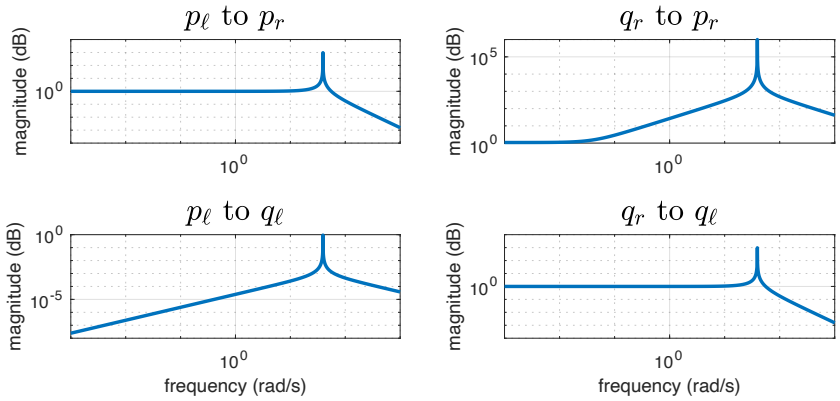

Figure 2.3. Pipe Bode magnitude plots: (p_ℓ, q_r) to (p_r, q_ℓ).

frequency of 0.25-0.5Hz. The DC gains of (2.12) and (2.13) are given symbolically by

$$\mathrm{G}_{(2.12)} = \begin{bmatrix} 1 & -RX \\ 0 & 1 \end{bmatrix}, \; \mathrm{G}_{(2.13)} = \begin{bmatrix} 1 + \frac{\lambda c^2 X}{2DA^2} \frac{\bar{q}^2}{\bar{p}^2} & -\frac{X\lambda c^2}{DA^2} \frac{\bar{q}}{\bar{p}} \\ 0 & 1 \end{bmatrix}. \tag{2.14}$$

2.4 Signal Flow Graph models

2.4.1 Philosophy of signal flow graph modeling

The input-output representations implicit in (2.12) and (2.13) conform to viewing the transmission line or pipe segments as signal-flow graphs with directed connections. This is in keeping with their eventual application as part of a feedback control system. These ideas date back to Claude Shannon [42] and Samuel Mason [31] and may be contrasted with the undirected graph methods of Jan Willems' *Behavioral Theory* [46, 47], including electrical and mechanical analogs [48, 49], and directed DAE methods associated with *Bond Graphs* [6, 20]. The critical aspect of signal-flow graph representations is their conformity with control design tools, such as those in MATLAB. The price of directed graph methods is that they entail an implied (and somewhat arbitrary) causality of the interconnection, which in electrical networks would imply buffering at junctions. However, as remarked above, there is direct relation to the requisite

boundary conditions and this choice of signals and state.

As Laudan [28] states "the aim of science is to secure theories with a high problem-solving effectiveness." And this approach to lumped-parameter, linearized, spatially discretized, signal flow graph modeling operates with this recognition of the convenient fiction underpinning all modeling but reflective of the utility of the approach. Indeed, Harold Black's original analysis of the analog negative feedback amplifier [7] adopts this approach. Newcomb [35] and Anderson & Vongpanitlerd [2] identify ports and driving-point impedances for this purpose. Enough name dropping. For us, it permits access to MATLAB's design and analysis tools and network modeling from component subsystems; very utile indeed.

2.4.2 Directed pipe connections and 'ports'

The signal flow graph models derived above have directions associated with each signal. Thus, p_ℓ and q_r are input signals, indicating that they are specified from outside the pipe, and p_r and q_ℓ are output signals, meaning that they are determined by the pipe system and the input signals. The spatially localized connection sites, however, possess one input signal and one output signal, namely (p_ℓ, q_ℓ) at the left end and (p_r, q_r) at the right. We further appropriate circuit terminology and identify two distinct location types, which we term *ports*. As in [6], every element in our interconnected system presents pipe signal interfaces to other elements and to the outside world.

Definition 2.1 (Ports)**.**

***p*-port** *of a component possesses two signals: an input pressure signal p_ℓ and an output flow signal q_ℓ.*

***q*-port** *of a component possesses two signals: an input flow signal q_r and an output pressure signal p_r.*

Internal series connection of two components, 1 and 2, will involve the cascading of signals $p_{2,\ell} = p_{1,r}$ and $q_{1,r} = q_{2,\ell}$ at the junction point. This describes a p-port to q-port

connection. Likewise, connection to the outside of the network must respect the type and causality of the signals. These rules are specified below.

Interconnection Rules

I. Connections are permitted only between:

   i. a p-port and a q-port, or

   ii. a p-port and an external pressure source/input signal plus an external flow sink/output signal, or

   iii. a q-port and an external flow source/input signal plus an external pressure sink/output signal.

II. Pressure input signals must connect to pressure output signals and flow input signals must connect to flow output signals.

III. Connection of one variable of a port requires connection of the other.

IV. All ports must be connected and algebraic loops avoided.

These rules conform to the connections examined in Chapter 1 to formulate the systematic interconnection of state-space models. Each component model possesses input and output signals and, in Proposition 1.3, it is shown how a (possibly non-minimal) state-space realization of the interconnection of gas system elements can be directly constructed with the above rules. This construction replaces and extends the graph-theoretic DAE methods of [6] and yields a new input-output transfer function satisfying Mason's Gain Formula, 1.4.

Per Chapter 1 the fluid-flow network model commences with an aggregate (direct sum) model of all elements in state-space form, with some abuse of notation,

$$\dot{x}_t = Ax_t + Bw_t, \quad y_t = Cx_t + Dw_t, \tag{2.15}$$

with $x_t \in \mathbb{R}^{n_x}, w_t \in \mathbb{R}^{n_w}$ and $y_t \in \mathbb{R}^{n_y}$. Interconnections and external sources $u_t \in \mathbb{R}^{n_u}$ and sinks $z_t \in \mathbb{R}^{n_z}$ are described by

$$w_t = Fy_t + Gu_t, \quad z_t = Hx_t + Ju_t, \tag{2.16}$$

with structured matrices $[F, G, H, J]$ with 0-1 elements.

The Interconnection Rules allow us to group outputs by their type, pressure or flow, and connection, internal or external. Denote the (row-organized) collection of input and output signals as

$$y_t = \begin{bmatrix} z_p \\ z_q \\ \tilde{y}_p \\ \tilde{y}_q \end{bmatrix}, \quad w_t = \begin{bmatrix} u_p \\ u_q \\ \tilde{w}_p \\ \tilde{w}_q \end{bmatrix}, \tag{2.17}$$

where, for the connected network: $z_p \in \mathbb{R}^{n_{zp}}$ and $z_q \in \mathbb{R}^{n_{zq}}$ are external pressure and mass flow output signals; $u_p \in \mathbb{R}^{n_{uq}}$ and $u_q \in \mathbb{R}^{n_{uq}}$ are external pressure and mass flow input sources; $\tilde{y}_p \in \mathbb{R}^{n_{\tilde{y}p}}$ and $\tilde{y}_q \in \mathbb{R}^{n_{\tilde{y}q}}$ are internal pressure and mass flow output signals; $\tilde{w}_p \in \mathbb{R}^{n_{\tilde{w}p}}$ and $\tilde{w}_q \in \mathbb{R}^{n_{\tilde{w}q}}$ are internal pressure and mass flow input signals.

Lemma 2.1. *The connection rules imply the following.*

(i) $\tilde{w}_q = \tilde{y}_q$ *whence* $n_{\tilde{w}q} = n_{\tilde{y}q}$.

(ii) $\tilde{w}_p = \tilde{y}_p$ *whence* $n_{\tilde{w}p} = n_{\tilde{y}p}$.

(iii) The number of external pressure input signals equals the number of external flow output signals: $n_{up} = n_{zq}$.

(iv) The number of external pressure output signals equals the number of external flow input signals: $n_{zp} = n_{uq}$.

We denote the unconnected network by the transfer function matrix, suppressing the s-dependence,

$$\begin{bmatrix} Z_p \\ Z_q \\ \tilde{Y}_p \\ \tilde{Y}_q \end{bmatrix} = \begin{bmatrix} T_{zp,up} & T_{zp,uq} & T_{zp,\tilde{w}p} & T_{zp,\tilde{w}q} \\ T_{zq,up} & T_{zq,uq} & T_{zq,\tilde{w}p} & T_{zq,\tilde{w}q} \\ T_{\tilde{y}p,up} & T_{\tilde{y}p,uq} & T_{\tilde{y}p,\tilde{w}p} & T_{\tilde{y}p,\tilde{w}q} \\ T_{\tilde{y}q,up} & T_{\tilde{y}q,uq} & T_{\tilde{y}q,\tilde{w}p} & T_{\tilde{y}q,\tilde{w}q} \end{bmatrix} \begin{bmatrix} U_p \\ U_q \\ \tilde{W}_p \\ \tilde{W}_q \end{bmatrix}, \tag{2.18}$$

and the connected transfer function matrix, formed by connecting $\tilde{w}_p = \tilde{y}_p$ and $\tilde{w}_q = \tilde{y}_q$, by

$$\begin{bmatrix} Z_p(s) \\ Z_q(s) \end{bmatrix} = \begin{bmatrix} T_{pp}(s) & T_{pq}(s) \\ T_{qp}(s) & T_{qq}(s) \end{bmatrix} \begin{bmatrix} U_p(s) \\ U_q(s) \end{bmatrix}. \tag{2.19}$$

2.5 Conservation properties of state-space models

In (2.14) above, the algebraic unity DC-gain in $[\mathrm{G}_{(2.13)}]_{2,2}$ together with zero DC-gain in $[\mathrm{G}_{(2.13)}]_{2,1}$ suggest conservation rules at play. However, while charge and mass are conserved, instantaneous current and mass flow need not be because of the circuit capacitance and the gas compressibility. Integrating (2.1) and (2.8) spatially from left to right, we see that

$$\begin{aligned} i_r &= i_\ell - C\int_\ell^r \frac{\partial v}{\partial t}\,dx, \\ q_r &= q_\ell - \frac{A}{c^2}\int_\ell^r \frac{\partial p}{\partial t}\,dx. \end{aligned} \tag{2.20}$$

That is, the deficit in current conservation is attributed to the time derivative of the voltage along the line, and that in mass flow conservation to the pressure time-variation along the pipe. Conservation in flow variables occurs when these time-derivatives are zero. That is, at steady state. From this point on, we drop the parallel references to the transmission line problem and concentrate solely on fluid flow systems.

For the connected fluid network (2.19), and with a slight abuse of language – *mass* for *mass flow* – we make the following definition.

Definition 2.2. *For a linear fluid system with transfer function matrix as in* (2.19)*, we say the system conserves mass if*

$$\lim_{s\to 0} \mathbf{1}_{n_{zq}} T_{qq}(s) = \mathbf{1}_{n_{uq}} \text{ and } \lim_{s\to 0} T_{qp}(s) = \mathbf{0},$$

where $\mathbf{1}_n$ *is a row vector of ones in* $\mathbb{R}_n$ *and* $\mathbf{0}$ *is the zero matrix of appropriate dimensions.*

The upshot from this definition is that, if the system (2.19) possesses a steady-state (and Definition 2.2 does not require stability), then

$$\lim_{t\to\infty} \mathbf{1}_{n_{zq}} z_q(t) = \lim_{t\to\infty} \mathbf{1}_{n_{uq}} u_q(t),$$

for the associated steady-state time-domain flow variables. As we see from (2.14), our linearized models of pipe elements satisfy conservation of mass flow. Other system elements, such as branches, joints, compressors, valves, heat exchangers, tanks, manifolds derived in Chapter 1 and Appendix B, also are seen to possess this property.

Lemma 2.1 has the following consequence.

Corollary 2.1. *If the connection rules apply, then the matrices in* (2.19) *have the following dimensions*

$$\begin{aligned}
\dim T_{pp} &= n_{zp} \times n_{up} = n_{uq} \times n_{up}, \\
\dim T_{pq} &= n_{zp} \times n_{uq} = n_{uq} \times n_{uq}, \\
\dim T_{qp} &= n_{zq} \times n_{up} = n_{up} \times n_{up}, \\
\dim T_{qq} &= n_{zq} \times n_{uq} = n_{up} \times n_{uq}.
\end{aligned}$$

2.6 Interconnection of conservative gas flow elements

Assumption 2.1. *For each network component, conservation of mass is satisfied and the interconnection rules between components are satisfied.*

This assumption is satisfied for all component models from Chapter 1 and Appendix B. We have the following property of interconnected networks.

Theorem 2.1 (Mass-conserving network)**.** *Subject to Assumption 2.1, the network also satisfies conservation of mass.*

Proof: We have $y_q^\top = \begin{bmatrix} z_q^\top & \tilde{y}_q^\top \end{bmatrix} \in \mathbb{R}^{n_{yq}}$, with $n_{yq} = n_{zq} + n_{\tilde{y}q}$, and conformably for w_q. Allowing signals to reach steady state (which we denote by subscript $(\cdot)_{,ss}$), by hypothesis of mass-conserving elements we have,

$$\mathbf{1}_{n_{yq}} y_{q,ss} = \mathbf{1}_{n_{wq}} w_{q,ss},$$

$$\begin{bmatrix} \mathbf{1}_{n_{zq}} & \mathbf{1}_{n_{\tilde{y}q}} \end{bmatrix} \begin{bmatrix} z_{q,ss} \\ \tilde{y}_{q,ss} \end{bmatrix} = \begin{bmatrix} \mathbf{1}_{n_{uq}} & \mathbf{1}_{n_{\tilde{w}q}} \end{bmatrix} \begin{bmatrix} u_{q,ss} \\ \tilde{w}_{q,ss} \end{bmatrix},$$

From Lemma 2.1, $\tilde{y}_q = \tilde{w}_q$, so

$$\begin{bmatrix} \mathbf{1}_{n_{zq}} & \mathbf{1}_{n_{\tilde{y}q}} \end{bmatrix} \begin{bmatrix} z_{q,ss} \\ \tilde{y}_{q,ss} \end{bmatrix} = \begin{bmatrix} \mathbf{1}_{n_{uq}} & \mathbf{1}_{n_{\tilde{y}q}} \end{bmatrix} \begin{bmatrix} u_{q,ss} \\ \tilde{y}_{q,ss} \end{bmatrix},$$

$$\mathbf{1}_{n_{\tilde{y}q}} z_{q,ss} = \mathbf{1}_{n_{uq}} u_{q,ss}.$$

This is conservation of mass of the connected system. □

2.7 Integrators in mass-conserving networks

The presence of integrators in transfer functions is important for the design of feedback regulator control systems. We next establish that mass-conserving fluid networks implicitly

possess integrators in the mass-flow to pressure path. Since the pressure signal is most easily measured, admitting rapid and accurate sampling versus, say, the mass flow or temperature signals, pressure provides the most common signal for disturbance rejection feedback, target control specification and output sensing. By contrast, mass flow is frequently the dominant input variable effected by valves. These integrators, in the fluid system and in the network models here, are central to the design of effective feedback controls and hence the control relevance of these models and methodology for their construction.

The fluid dynamics Continuity Equation (2.8) applied to a single pipe exhibits the integration property.

$$\frac{\partial p}{\partial t} = -\frac{c^2}{A}\frac{\partial q}{\partial x}.$$

This may be spatially discretized and then integrated with respect to time to yield

$$p(\bar{x},t) - p(\bar{x},t_0) = -\frac{c^2}{AL}\int_{t_0}^{t} [q_r(\tau) - q_\ell(\tau)]\, d\tau. \tag{2.21}$$

Here from the Mean Value Theorem, $\bar{x}$ is a point inside the $(x, x+L)$ interval. In physical terms, (2.21) reflects the property that a steady-state mismatch between the flows into and out from the pipe results in an unbounded change in pressure.

This analysis may be extended to the network behavior.

Theorem 2.2. *For a fluid network satisfying Assumption 2.1 and possessing pressure input signals, the transfer function $T_{qp}(s)$ in* (2.19) *possesses a blocking zero at $s = 0$. So, a steady-state difference between inflows and outflows can only be achieved by unbounded pressure inputs.*

Proof: From Definition 2.2, conservation of mass entails $T_{qp}(0) = \mathbf{0}$; hence the first part of the statement. Now, from the Laplace transform Final Value Theorem, the steady-state

difference between net flow out and net flow in is given by

$$\begin{aligned} d &= \lim_{s\to 0} s\left[\mathbf{1}_{n_{zq}} Z_q(s) - \mathbf{1}_{n_{uq}} U_q(s)\right] \\ &= \lim_{s\to 0} s\mathbf{1}_{n_{zp}} T_{qp}(s), \end{aligned} \tag{2.22}$$

where we have used

$$Z_q(s) = T_{qp}(s)U_p(s) + T_{qq}(s)U_q(s),$$

from (2.19) rewritten as

$$T_{qp}(s)U_p(s) = Z_q(s) - T_{qq}(s)U_q(s), \tag{2.23}$$

and first equality for conservation of mass from Definition 2.2. Now if d in (2.22) is non-zero, then

$$\mathbf{1}_{n_{zp}} T_{qp}(s)U_p(s) = \frac{d}{s} + \text{terms with no poles at } s = 0.$$

Since $T_{qp}(0) = 0$, if $d \neq 0$ then $U_p(s)$ must have a double pole at $s = 0$. □

For connected networks with only flow input signals and only pressure output signals, that is from Lemma 2.1, $n_{zq} = n_{up} = 0$ and $n_{zp} = n_{uq} > 0$, we make the following assumption.

Assumption 2.2. *The unconnected network satisfies $n_{\tilde{w}q} > 0$ and has $T_{zp,\tilde{w}q}(s)$ full rank at $s = 0$.*

This assumption is evidently an observability or, as we shall see, detectability condition. It ensures that the externally measured pressure signals suffice to reveal static mismatches in internal flows. Inspecting the steady-state gains, (2.14), of the fundamental pipe equation, (2.13), or its transmission line precursor, (2.12), the satisfaction of Assumption 2.2 is assured provided that the pipe friction is non-zero or the line resistance is non-zero. It is a testable condition for

the network and is evidently satisfied by the pipe element in the upper right figure of Figure 2.3.

With this new assumption, we can now state the central result.

Theorem 2.3 (Network with integrator)**.** *Consider the fluid network with external input signals, which are mass flows alone and satisfying Assumptions 2.1 and 2.2. Then the output pressure signals contain a term proportional to the integral of* $\mathbf{1}_{n_{uq}} u_q(t)$*, the mass flow mismatch into the network.*

Proof: We have $n_{zq} = n_{up} = 0$ and $n_{zp} = n_{uq} \neq 0$. From (2.18), identify the non-zero-dimension submatrices of the unconnected system's transfer function and extract the component output flow signals.

$$\tilde{Y}_q(s) = T_{\tilde{y}q,uq} U_q(s) + T_{\tilde{y}q,\tilde{w}p} \tilde{W}_p(s) + T_{\tilde{y}q,\tilde{w}q} \tilde{W}_q(s). \tag{2.24}$$

From conservation of mass of the individual network components and $n_{zq} = 0$, we have that $n_{yq} = n_{\tilde{y}q}$ and

$$\mathbf{1}_{n_{\tilde{y}q}} \begin{bmatrix} T_{\tilde{y}q,uq}(0) & T_{\tilde{y}q,\tilde{w}q}(0) \end{bmatrix} = \begin{bmatrix} \mathbf{1}_{n_{uq}} & \mathbf{1}_{n_{\tilde{w}q}} \end{bmatrix},$$

or since $n_{\tilde{y}q} = n_{\tilde{w}q}$,

$$\mathbf{1}_{n_{\tilde{y}q}} T_{\tilde{y}q,\tilde{w}q}(0) = \mathbf{1}_{n_{\tilde{y}q}}.$$

That is $T_{\tilde{y}q,\tilde{w}q}(0)$ has an eigenvalue at 1 with left eigenvector $\mathbf{1}_{n_{\tilde{y}q}}$. Additionally, we have

$$\lim_{s \to 0} T_{\tilde{y}q,\tilde{w}p} = 0.$$

Returning to (2.24) and substituting for the connection $\tilde{W}_q(s) = \tilde{Y}_q(s)$,

$$\lim_{s\to 0} \mathbf{1}_{n_{yq}} \tilde{Y}_q = \lim_{s\to 0} \mathbf{1}_{n_{uq}} U_q + \lim_{s\to 0} \mathbf{1}_{n_{yq}} \tilde{Y}_q.$$

Thus, to first order in s,

$$s\mathbf{1}_{n_{yq}} \tilde{Y}_q(s) = \mathbf{1}_{n_{uq}} U_q(s).$$

That is, the internal flow signal vector, $\tilde{y}_q(t)$, contains the integral of $\mathbf{1}_{n_{uq}} u_q(t)$, the integral of the network flow mismatch.

The (output) pressure signals satisfy, after substituting for the connection $\tilde{W}_p(s) = \tilde{Z}_p(s)$,

$$Z_p(s) = (I - T_{zp,\tilde{w}p})^{-1} \left[T_{zp,uq} U_q(s) + T_{zp,\tilde{w}q} \tilde{Y}_q(s) \right].$$

Assumption 2.2 ensures that integral of $\mathbf{1}_{n_{uq}} u_q(t)$ appears in the output pressure. □

The presence of integrators in the pressure measurements of gas flow networks with only external flow signals appearing as inputs, is a manifestation of the physical property that, if the net mass flow into a network is unbalanced, i.e. sums to a non-zero number, in steady state, then this is reflected in the output pressures becoming unbounded. Of course, this is a manifestation of conservation of mass. But, from a control systems perspective, it is important to demonstrate that this is (i) a property captured by the approximate models and their aggregation into network models, and (ii) manifested through the appearance of an integrator, whose role in feedback control design is to ensure mass flow balance without the imposition of a constraint to achieve this.

2.8 Control-oriented component and network models

Linearized MIMO state-space component models have been developed in Chapter 1 and Appendix B based on extensions of the pipe models (2.13) to include branch and join combinations, tanks, valves, manifolds, etc. As explained earlier, these models themselves replace DAE constructions from [6] for distribution systems and make the conceptual leap from physical models to directed signal flow graphs. Compressor models have been adapted from [15]; see Appendix B. These component models each possess the following features.

(i) They are finite-dimensional linear state-space models with flows, pressures and temperatures as signals and states. Isothermal variants are possible with gas temperatures appearing as parameters.

(ii) They conserve mass per Definition 2.2.

(iii) They satisfy Assumption 2.2.

(iv) They are continuous-time and capture both bulk modes and resonant behaviors.

The component models may be connected using the MATLAB methods described in Chapter 1 or MATLAB's `connect` function, see Appendix B, which comply with the Interconnection Rules of Section 2.4 and the analyses above. Therefore, the predicates of Theorems 2.1, 2.2 and 2.3 abide.

But what makes them *control-oriented?* This requires the specification of a control problem and the application of the network models for control design. This gas processing facility regulation problem was presented in the Introduction and has guided the analysis so far. It is worth stating that the price paid for control-orientation is a departure from verisimilitude in high-frequency fluid flow modeling and adoption of directed graph models, which ignore back flows and pressures. The benefit is simplicity and amenability to the tools of controller design. Ultimately, however, it is the utility of these models for the construction of MIMO feedback control, which is the only meaningful metric of performance or acceptability.

2.9 MIMO control loop

The control objective is to regulate the pressures in the gas loop depicted in Figure 2.4. This is a representation of the Solar Turbines Incorporated GCTF in San Diego, California, which is used to evaluate compressor performance in operation. The GCTF is: well-instrumented; of a scale appropriate to gas handling facilities; equipped with safety control systems over and above regulation and process control objectives, which are presently handled by local SISO PI controllers and which we seek eventually to replace via the systematic introduction of MIMO control based on our aggregated models. At this stage, proof of concept MIMO design is the objective prior to in-situ testing of regulation performance.

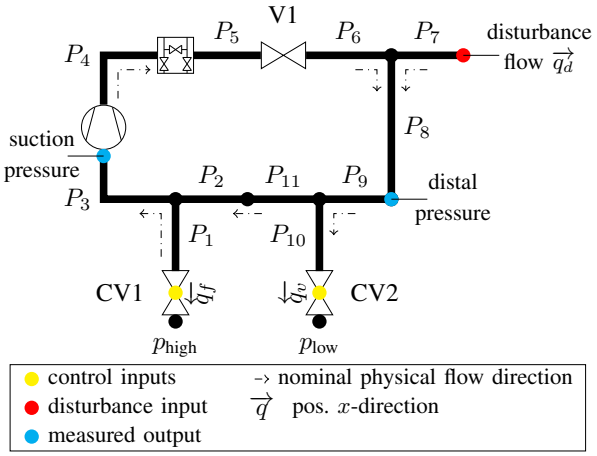

Figure 2.4. Pipe network with compressor, valves and valve manifold.

The general problem statement in the Introduction is qualified as follows.

- A two-input/two-output digital MIMO controller is sought to regulate the two measured pressures: compressor suction pressure, p_{suc}, and distal pressure, p_{dstl}, shown as blue dots in Figure 2.4. There is particular emphasis on managing p_{suc}, the inlet pressure to the compressor.

- The two control inputs, i.e. manipulated variables, shown as yellow dots in the figure, are the mass fill flow, q_f, through valve CV1 and the mass vent flow, q_v, through valve CV2.

- The loop is subject to a disturbance flow, q_d, indicated by a red dot in the figure. This disturbance flow is roughly constant at this sampling rate.

- Isothermal models are used with temperature as a parameter.

Accordingly, by *controller inputs* we refer to signals input to the controller, p_{suc} and p_{dstl}; *controller outputs* describe signals output by the controller, q_f and q_v.

Network modeling

For modeling we proceeded as follows:

(I) Individual pipe, branch, valve, compressor, and manifold mass-conserving component models from Chapter 1 and Appendix B are combined using MATLAB, abiding by the Interconnection Rules. This yields a three-input (q_f, q_v, q_d) and two-output (p_{suc}, p_{dstl}) continuous-time linear state-space model of dimension 30. This model has the following poles:

  – a single integrator, pole at $s = 0$, per Theorem 2.3;

  – all the other poles are stable;

  – some pairs of stable poles have strong oscillatory response, from the resonant behavior, with the natural frequencies of these poles lying above the anti-aliasing filter bandwidth.

(II) A 46th-order system is constructed by concatenating the continuous-time model (I) with two eighth-order Butterworth low-pass antialiasing filters at 0.4Hz on each of the measured signals, p_{suc} and p_{dstl};

(III) Balanced truncation is applied to Model (II) to reduce the order to eleven. The integrator mode from Model (I) is unstable and therefore is left invariant by balanced truncation. For model reduction via `modred` we use the `Truncate` option to ensure that the strictly

proper original model yields a strictly proper reduced model. This, in turn, allows discrete delay-free LQG design with a Kalman filter in place of the default predictor without causing an algebraic loop in MATLAB. Obviously, in the real world no algebraic loop would occur.

(IV) The model is discretized at 1 Hz sampling rate using MATLAB's function `c2d`.

Figure 2.5 shows the Hankel singular values of the stable part of the anti-alias-filtered system. There are 45 values associated with the stable modes plus the integrator, which is excluded from the reduction. For the control design, ten modes were chosen plus the integrator.

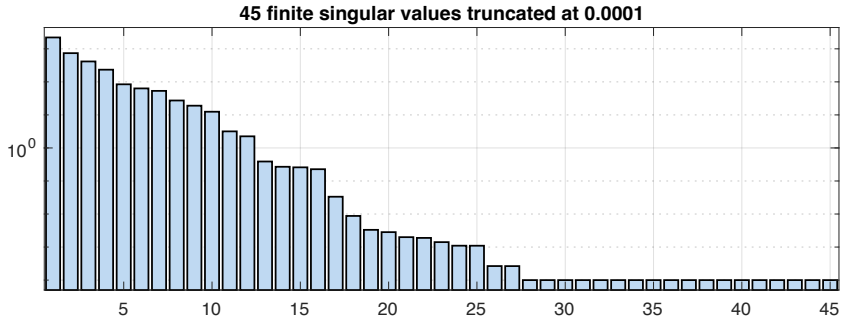

Figure 2.5. Hankel singular values of stable part of filtered system.

Figure 2.6 displays the four impulse responses of continuous-time Model (I) (thin blue lines) and reduced-order filtered Model (III) (think red lines) from control inputs to measured outputs.

Open-loop dynamics

All four plots reveal stable low-frequency behavior and fast oscillations in the unfiltered signals related to the resonant modes of the components comprised by the loop. The non-vanishing offsets show the integrator from mass flow to pressure conservation of mass (Theorem 2.3). The large pressure amplitudes are due to the unit conversion. There is no obvious pairing of any input and output signals, which is problematic for SISO PID controllers assuming decoupled dynamics.

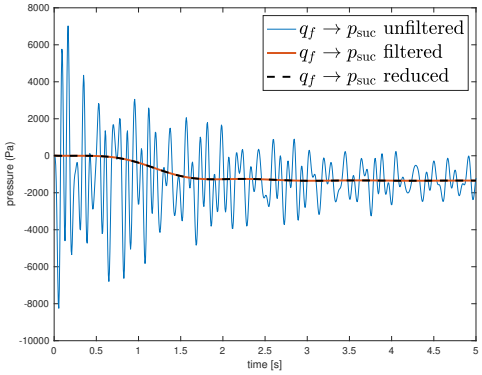

(a) Fill flow to suction pressure.

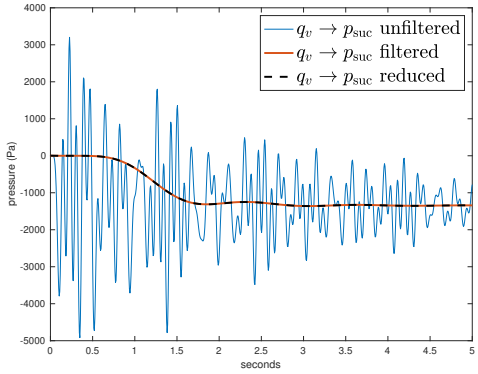

(b) Vent flow to suction pressure.

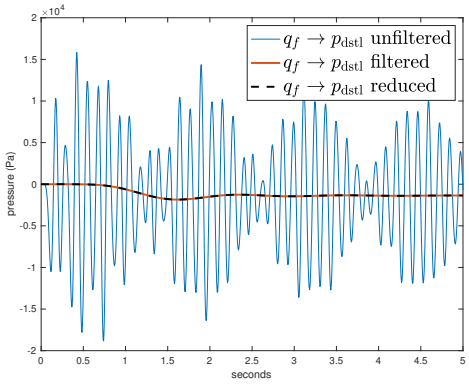

(c) Fill flow to distal pressure.

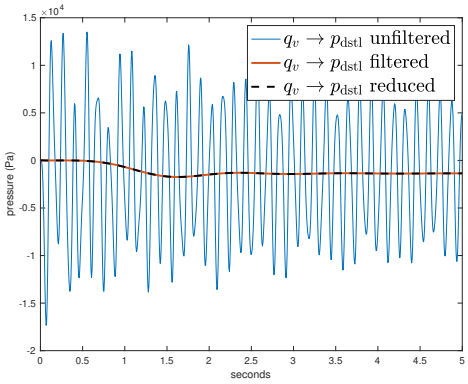

(d) Vent flow to distal pressure.

Figure 2.6. Loop impulse responses from fill and vent flow to suction and distal pressure for Model (I) (thin blue lines) and anti-aliased Model (III) (thicker red lines)

LQG control design

Since the aim of the project is to facilitate MIMO control design, the standard MATLAB function `lqg` is used, firstly without a disturbance model and secondly with integral action, since the control objective is to regulate suction and distal pressures in the face of the step-like disturbance flow.

Figure 2.7 shows closed-loop responses to a step at time $t = 0.5$s in the flow out of the loop. The upper plot shows the closed-loop responses of the suction pressures for the three plant models – the full 30th-order continuous-time network model, the anti-aliased 46th-order model, and the reduced 11th-order model used for the design – in feedback with the 11th-order LQG

digital controller. The center plot shows the corresponding fill flow control input and the lower plot the sum of fill and vent flow inputs. These latter two plots are the outputs of the controller for the closed loops with the full-order plant with antialiasing filters and for the reduced -order plant. Evidently, each closed-loop is stable and there is a steady-state offset to the pressure. The fast unfiltered pressure signal exhibits the underlying resonant system behavior and the absence of anti-aliasing filter group delay. There are very little differences between the anti-aliased full-order responses and the reduced-order. By imposing larger LQ penalty on the vent flow relative to the fill flow, the controller empahsises the latter.

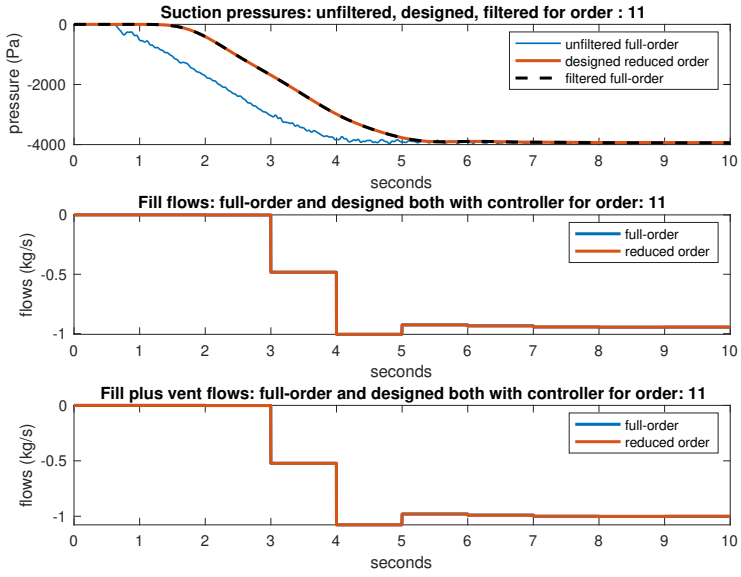

Figure 2.7. Disturbance flow to suction pressure closed-loop step responses; step at 0.5s.

Per Theorem 2.2, since the pressure is finite, the sum of the control inflows exactly matches the disturbance outflow. The LQG design is straightforward and yields static offset of 4kPa (0.6 psi) in the suction pressure for a 1kg/s disturbance flow.

LQG control with integral action

We next include a modified LQG design with integral action again using MATLAB's `lqg` function, but with this augmentation for the regulation objective. The responses are shown in

Figure 2.8. Several features are evident.

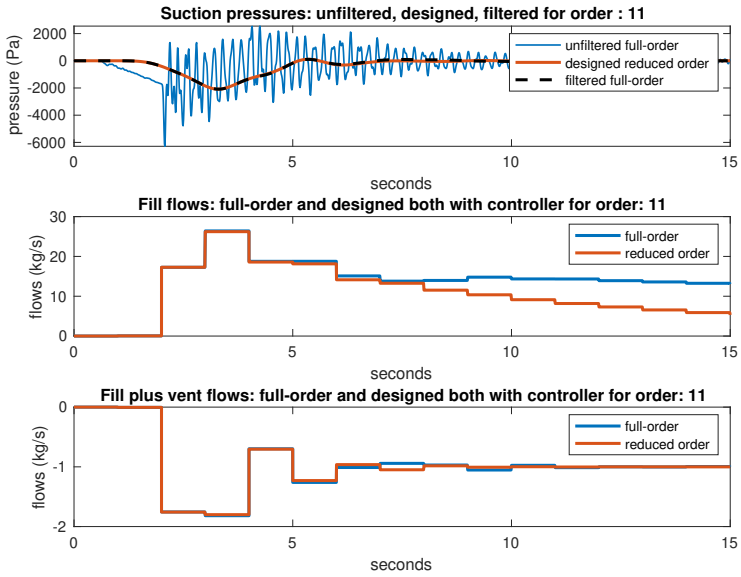

Figure 2.8. Disturbance closed-loop step responses with integral action LQG; step at 0.5s.

1. Regulation of the suction pressure to zero, i.e. its nominal value, is achieved.

2. Because of the integral action, the closed-loop response is slower than LQG for the same weighting matrices.

3. The 2i2o controller order is now 13 rather than 11 for the LQG case because of the two channels of integral action.

4. The total flows again balance exactly the disturbance in steady state.

5. The regulation objective on both suction and distal pressure forces the vent flow to be applied in spite of its heavier weighting than fill flow.

6. The unfiltered full-order closed-system exhibits resonances and the absence of the anti-aliasing filter group delay.

The conclusion from this example is that the approach of control-oriented modeling and model-based control has led to a MIMO digital controller preserving the well-appreciated aspects of LQG control design with and without integral action. Further, the role of the integrators present in the system model and ultimately traceable to conservation of mass led to an easily comprehended control design schema for the simplified models and standard control design tools. The complexity of the composite models and their many resonant modes is suppressed by anti-alias filtering then model reduction. This admits feedback control design focused on managing low frequency bulk behavior unencumbered by acoustic properties of these systems.

2.10 Future direction

This chapter explores the chain of ideas stemming from replacing DAEs in these fluid models by signal flow graph models more amenable to control design but preserving the algebraic mass conservation properties. These conservation ideas are unraveled in some detail and identified with component transfer function properties. This is shown to be a feature preserved by network interconnections subject to logical connection rules. This, in turn, led to DC gain properties and the presence of integrators, which affect the subsequent control design. This is then examined using a nominal industrial model and standard LQG design packages from MATLAB. The important feature of preserving the design aspects is exhibited in this example, thereby validating the claim that these models are *control-oriented,* since the target regulation controller appeared in choices made at each stage of modeling and control design.

While we examined the performance of the designed digital controllers on the resonant continuous-time full-order system, clearly the acid test is to implement and test these controllers on a real plant (a) to ascertain their performance in practice and (b) to appreciate what amenable design flexibility is garnered by MIMO control in this arena.

Extension of these ideas of modeling for control, where the control problem is stated prior to the modeling phase, to other areas, such as thermal systems, minerals processing, materials

handling etc would also be of interest. Equally, the methodology explored here might be more thoroughly developed by including ideas from [36] where the control objective plays a central role in modifying the model reduction phase. This permits replacement of balanced truncation by a more control-oriented approach, yielding the modeling, model reduction and control design each to reflect the overarching closed-loop objectives.

This chapter, in full, has been submitted for publication of the material as it may appear as Sven Brüggemann, Robert H. Moroto, and Robert R. Bitmead. "Control-orientation, conservation and model-based network flow control." The dissertation author was the primary investigator and author of this paper.

Appendix A

Proofs Chapter 1

A.1 Proposition 1.1

By hypothesis and with $\check{q} = \check{\rho} A v$, equation (1.3b) results directly from the momentum and ideal gas equation, (1.1b) and (1.1d), see e.g. [5].

For the pressure-related PDE, let $a_1 \doteq \frac{c_v}{R_s z_0} - \frac{R_s z_0}{2A^2}\frac{\check{q}^2\check{T}}{\check{p}^2} + \frac{gh}{R_s \check{T} z_0}$. Then, solving energy equation (1.1c) for $\frac{\partial \check{p}}{\partial t}$ yields

$$\frac{\partial \check{p}}{\partial t} = a_1^{-1}\left(\cancel{q}\check{\rho} + \frac{\partial \check{T}}{\partial t}\underbrace{\left(\frac{gh\check{p}}{R_s\check{T}^2 z_0} - \frac{R_s z_0 \check{q}^2}{2A^2\check{p}}\right)}_{\doteq -a_2} - \frac{R_s z_0 \check{T}\check{q}}{A^2\check{p}}\frac{\partial \check{q}}{\partial t}\right.$$
$$\left. - \frac{\partial}{\partial x}\left[\frac{\check{q}}{A}\left(c_v\check{T} + gh\right) + \frac{\check{q}^3 R_s^2 \check{T}^2 z_0^2}{2\check{p}^2 A^3} + \frac{\check{q} R_s \check{T} z_0}{A}\right]\right).$$

From continuity and ideal gas equations, resp. (1.1a) and (1.1d),

$$\frac{\partial \check{T}}{\partial t} = \frac{z_0 R_s \check{T}^2}{\check{p} A}\frac{\partial \check{q}}{\partial x} + \frac{\check{T}}{\check{p}}\dot{\check{p}}, \tag{A.1}$$

since $(a_1 + \frac{\check{T}}{\check{p}} a_2)^{-1} = \frac{R_s z_0}{c_v}$ and, using (1.3b), yields

$$\begin{aligned}\frac{\partial \check{p}}{\partial t} = \frac{R_s z_0}{c_v} \Bigg(& \not{q}\check{\rho} + \frac{\partial \check{q}}{\partial x}\left(\frac{gh}{A} + \frac{3R_s^2 z_0^2 \check{q}^2}{2A^3\check{p}^2}\right) + \frac{R_s z_0 \check{T}\check{q}}{A^2\check{p}}\Bigg[A\frac{\partial \check{p}}{\partial x} \\ & + A\left(\frac{z_0 R_s \check{q}^2}{A^2\check{p}}\frac{\partial \check{T}}{\partial x} - \frac{z_0 R_s \check{T}\check{q}^2}{A^2\check{p}^2}\frac{\partial \check{p}}{\partial x}\right) + \frac{\lambda z_0 R_s \check{T}}{2DA\check{p}}\check{q}|\check{q}| \\ & + gA\frac{\check{p}}{z_0 R_s \check{T}}\frac{dh}{dx}\Bigg] \\ & - \frac{\partial}{\partial x}\left[\frac{\check{q}}{A}\left(c_v\check{T} + gh\right) + \frac{\check{q}^3 R_s^2 \check{T}^2 z_0^2}{2\check{p}^2 A^3} + \frac{\check{q} R_s \check{T} z_0}{A}\right]\Bigg).\end{aligned}$$

Computing the spatial derivative leads to

$$\begin{aligned}\frac{\partial \check{p}}{\partial t} = \frac{R_s z_0}{c_v A}\Bigg[& \not{q}\rho A - \frac{\partial \check{q}}{\partial x}\check{T}\left(c_v + R_s z_0\right) + \frac{\partial \check{p}}{\partial x}\frac{R_s z_0 \check{T}\check{q}}{\check{p}} \\ & - \frac{\partial \check{T}}{\partial x}\check{q}\left(c_v + R_s z_0\right) + \frac{\lambda R_s^2 z_0^2 \check{T}^2 \check{q}^2 |\check{q}|}{2DA^2\check{p}^2}\Bigg],\end{aligned}$$

which with (1.2) results in (1.3a).

For the temperature, we use the result above and (A.1) to obtain

$$\begin{aligned}\frac{\partial \check{T}}{\partial t} = \frac{R_s z_0 \check{T}}{c_v A\check{p}}\Bigg[& \not{q}\rho A - \frac{\partial \check{q}}{\partial x}\check{T} R_s z_0 + \frac{\partial \check{p}}{\partial x}\frac{R_s z_0 \check{T}\check{q}}{\check{p}} \\ & - \frac{\partial \check{T}}{\partial x}\check{q}\left(c_v + R_s z_0\right) + \frac{\lambda R_s^2 z_0^2 \check{T}^2 \check{q}^2 |\check{q}|}{2DA^2\check{p}^2}\Bigg],\end{aligned}$$

which with (1.2) results in (1.3c).

A.2 Proposition 1.4

For readability we exclude the subscript t in this proof. From (B.45), state-variable realizations of the transfer functions $\mathcal{Q}$ and $\mathcal{P}$ are given by the following:

$$\mathcal{Q} = [D + C(sI - A)^{-1}B]F, \tag{A.2}$$

$$\mathcal{P} = [D + C(sI - A)^{-1}B]G. \tag{A.3}$$

Firstly, use the matrix inversion formula to write

$$\begin{aligned}(I - \mathcal{Q})^{-1} &= \{I - [D + C(sI - A)^{-1}B]F\}^{-1}, \\ &= (I - DF)^{-1} + \\ &\quad (I - DF)^{-1}C[sI - A - BF(I - DF)^{-1}C]^{-1} \\ &\quad BF(I - DF)^{-1}. \end{aligned} \tag{A.4}$$

Define the u_t-component of w_t as $w_t^{u_t} = [I + F(I - DF)^{-1}D]Gu_t = w_{t,1}^{u_t} + Fw_{t,2}^{u_t}$ with $w_{t,1}^{u_t} = Gu_t$ and $w_{t,2}^{u_t} = (I - DF)^{-1}DGu_t$ and appeal to linearity to define

$$\begin{aligned}\dot{x}_{t,1} &= [A + BF(I - DF)^{-1}C]x_{t,1} + Bw_{t,1}^{u_t}, \\ \dot{x}_{t,2} &= [A + BF(I - DF)^{-1}C]x_{t,2} + BFw_{t,2}^{u_t}, \\ y_t &= (I - DF)^{-1}C(x_{t,1} + x_{t,2}) + w_{t,2}^{u_t}. \end{aligned}$$

From here and the definitions of $w_1^{\bar{u}}$ and $w_2^{\bar{u}}$, it is apparent that $\bar{y} = \bar{y}_1 + \bar{y}_2$ where,

$$\dot{x}_{t,1} = [A + BF(I - DF)^{-1}C]x_{t,1} + BGu_t, \tag{A.5}$$

$$y_{t,1} = (I - DF)^{-1}Cx_{t,1}, \tag{A.6}$$

and

$$\dot{x}_{t,2} = [A + BF(I - DF)^{-1}C]x_{t,2} + BF(I - DF)^{-1}DGu_t, \tag{A.7}$$

$$y_{t,2} = (I - DF)^{-1}Cx_{t,2} + (I - DF)^{-1}DGu_t, \tag{A.8}$$

System 1 (A.5)-(A.6): Denote the system transfer function $\mathscr{K} = (I - DF)^{-1}C(sI - A)^{-1}B$ and rewrite (A.5) as output feedback around $\mathscr{K}$.

$$\dot{x}_{t,1} = Ax_{t,1} + B(Fy_{t,1} + Gu_t).$$

In turn, writing this in terms of $\mathscr{K}$ and using (A.4) for $(I - \mathscr{Q})^{-1}$, we have

$$\begin{aligned}
y_{t,1} &= \mathscr{K}(Fy_{t,1} + Gu_t) \\
&= (I - \mathscr{K}F)^{-1}\mathscr{K}Gu_t \\
&= [I - (I - DF)^{-1}C(sI - A)^{-1}BF]^{-1}(I - DF)^{-1}C(sI - A)^{-1}BGu_t \\
&= \{I + (I - DF)^{-1}C[sI - A - BF(I - DF)^{-1}C]^{-1}BF\}(I - DF)^{-1}C(sI - A)^{-1}BGu_t \\
&= \{(I - DF)^{-1} + (I - DF)^{-1}C[sI - A - BF(I - DF)^{-1}C]^{-1}BF(I - DF)^{-1}\} \\
&\qquad\qquad C(sI - A)^{-1}BGu_t, \\
&= (I - \mathscr{Q})^{-1}C(sI - A)^{-1}BGu_t.
\end{aligned} \tag{A.9}$$

System 2 (A.7)-(A.8): Directly comparing (A.4) to (A.7)-(A.8), we see that

$$\bar{y}_{t,2} = (I - \mathscr{Q})^{-1}DGu_t. \tag{A.10}$$

Combining (A.9) and (A.10) we have

$$\begin{aligned} y_t &= y_{t,1} + y_{t,2}, \\ &= (I - \mathcal{Q})^{-1} C(sI - A)^{-1} BGu_t + (I - \mathcal{Q})^{-1} DGu_t, \\ &= (I - \mathcal{Q})^{-1} \mathcal{P} u_t. \end{aligned}$$

■

Appendix B

A compendium of control-oriented models of gas processing equipment components

Introduction

For transient modeling of gas flow through pipe networks, fluid dynamics and computational fluid dynamics, are well-established subjects focused on high-fidelity modeling given design and boundary conditions. They involve nonlinear partial differential equations (PDEs) and transport phenomena, which are not amenable to finite-dimensional control design but instead are targeted and tested for simulation.

Other more pragmatic modeling for gas pipeline distribution systems [5, 26, 3] is usually based on discretization and yields a system of ordinary differential algebraic equations (DAEs), which again is not well-suited to control design. Although, it can be used directly for controller synthesis in some circumstances [17] and, as noted in [5], if the DAE is of index 1. Theorem 4.1 in Benner et al. [5] establishes that the DAEs describing the gas flow through interconnected pipes are indeed of index 1 and so it is possible to rewrite the DAE as an ordinary differential equation (ODE) without the algebraic constraints.

This fact is used in the previous chapter to rewrite the system of DAEs as a (state-space) system of linear ordinary differential equations (ODEs) *subsuming* the algebraic constraints. Thus, to synthesize model-based controllers the rich literature on Linear Systems Theory can be exploited such as Mason's Gain Formula for modeling interconnections. An equivalent approach

for interconnections adapted to state-space realizations is presented in Chapter 1.

Here we build on Chapter 1 and provide linear control-oriented state-space models of gas flow through standard equipment such as valves, compressors, manifolds and non-trivial pipe geometries. After presenting the catalog of components, we show how to interconnect them: we briefly recall the matrix methodology derived in Chapter 1, accompanied by a MATLAB example for a gas loop; secondly for the same example we provide an alternative approach using MATLAB's `connect` function.

All the aforementioned models are suited to model-based MIMO control design tools as they are in state-space form and they can be physically parametrized. Conservation of mass is the source of the algebraic constraints in [5, 26, 3] and is a property subsumed in these new models. This is characterized in by model transfer function properties at frequency zero, see Chapter 2. Each of the component models is shown to posses this property

This chapter is meant to serve as an accompaniment to the material in Chapters 1 and 2. Details of assumptions are provided there, along with motivations and derivations from PDEs. Accordingly, it is organized by component type for the first eight sections with Section 9 devoted to the presentation of the approach to interconnection of the components into systems amenable to use with MATLAB's control system design tools.

Notation

We denote pressures by $\check{p}(x,t)$ and mass flows by $\check{q}(x,t)$, where x is the spatial dimension and t the time. For the nominal values we write $\bar{p}(x)$ and $\bar{q}(x)$, whereas deviations are described by $p(x,t) = \check{p}(x,t) - \bar{p}(x)$ and $q(x,t) = \check{q}(x,t) - \bar{q}(x)$. Assume $x \in [0,X]$ for some $X > 0$. We define $p_\ell \doteq p(0,t)$ and $p_r \doteq p(X,t)$, and accordingly for the mass flow. The same convention holds for the temperature $T(x,t)$ where applicable. Signals related to component i for some $i \in \mathbb{N}$ are denoted by the additional subscript i. By $\mathbf{0}$ we denote the zero matrix of appropriate size; $\mathbf{0}_n$ is the related *row vector*, and $\mathbf{0}_{n,m}$ is the related matrix of dimension $n \times m$. The same

notation is used for the matrix of ones, $\mathbf{1}$. For matrix A, we write $[A]_{i,j}$ for the matrix element in row i and column j, and similarly for vectors. The following table lists the meaning of common parameters.

Table B.1. Definitions of variables and their SI-units.

Symbol	Meaning	SI-unit
A	Cross-sectional area	[m^2]
c_v, c_p	Specific heat capacities	[J/(kg K)]
D	Pipe inner diameter	[m]
g	Gravity constant	$[\frac{\text{m}}{\text{s}^2}]$
$h(x)$	Pipe elevation from $x = 0$ to $x = X$	[m]
P_i	Pipe i	
R_s	Specific gas constant	$\left[\frac{\text{m}^2}{\text{s}^2\text{K}}\right]$
T_0	Constant temperature	[K]
V	Volume	[m^3]
X	Pipe length	[m]
z_0	Constant compressibility factor	[1]
λ	Friction factor	[1]
α	Pipe coefficient pressure dynamics	
β	Pipe coefficient mass flow dynamics	
γ	Pipe coefficient mass flow dynamics	
κ	Pipe coefficient mass flow dynamics	

B.1 Single pipe

State-space model single pipe model

Under the assumptions below the one-dimensional pipe flow can be described by the following state-space model:

$$\dot{x}_t = \begin{bmatrix} 0 & -\alpha \\ \beta & \gamma \end{bmatrix} x + \begin{bmatrix} 0 & \alpha \\ \kappa & 0 \end{bmatrix} u,$$

$$y_t = x_t,$$

with $x_t = \begin{bmatrix} p_r & q_\ell \end{bmatrix}^\top$ as the state and output vector, and $u_t = \begin{bmatrix} p_\ell & q_r \end{bmatrix}^\top$ as the input vector. The coefficients are

$$\alpha = -\frac{R_s T_0 z_0}{AX}, \quad \beta = -\frac{A}{X}, \tag{B.1a}$$

$$\kappa = \frac{A}{X} + \frac{\lambda R_s T_0 z_0}{2DA} \frac{\bar{q}|\bar{q}|}{\bar{p}_\ell^2} - \frac{Agh}{R_s T_0 z_0 X}, \tag{B.1b}$$

$$\gamma = -\frac{\lambda R_s T_0 z_0}{DA} \frac{|\bar{q}|}{\bar{p}_\ell}. \tag{B.1c}$$

B.1.1 Assumptions

Assumption B.1. *The change in temperature along the pipe is negligible.*

Assumption B.2. *For the one-dimensional pipe flow,*

(i) the cross-sectional area of each pipe segment is constant;

(ii) at each point in x-dimension averaged velocities suffice;

(iii) friction along the pipe can be approximated by the Darcy-Weisbach equation, see e.g. [41];

(iv) the compressibility factor is constant along the pipe;

(v) capillary, magnetic and electrical forces on the fluid are negligible;

(vi) the gas velocity is much smaller than the speed of sound.

B.1.2 Derivation

Under the assumptions above Benner *et al.* [5] derive a nonlinear model for an isothermal one-dimensional pipe flow. Towards a discretization and linearization of the related nonlinear

dynamics, let the boundary conditions p_ℓ and q_r be given, whereas p_r and q are to be determined through the model. Spatial discretization and linearization of [5, Eq. 3.2] yields

$$\dot{p}_r = \alpha(q_r - q_l) \tag{B.2a}$$

$$\dot{q}_\ell = \beta p_r + \kappa p_\ell + \gamma q_\ell, \tag{B.2b}$$

or equivalently,

$$\dot{x}_t = \begin{bmatrix} 0 & -\alpha \\ \beta & \gamma \end{bmatrix} x_t + \begin{bmatrix} 0 & \alpha \\ \kappa & 0 \end{bmatrix} u_t,$$

with terms as described above.

B.1.3 Conservation of mass

The DC gain from u to x can be readily extracted,

$$-A^{-1}B = -\frac{1}{\alpha\beta}\begin{bmatrix} \alpha\kappa & \alpha\gamma \\ 0 & -\alpha\beta \end{bmatrix} = \begin{bmatrix} -\frac{\kappa}{\beta} & -\frac{\gamma}{\beta} \\ 0 & 1 \end{bmatrix},$$

which shows that $T_{qp}(0) = 0$ and $\mathbf{1}T_{qq}(0) = 1$, where

$$X(s) = T(s)U(s) = \begin{bmatrix} T_{pp}(s) & T_{pq}(s) \\ T_{qp}(s) & T_{qq}(s) \end{bmatrix} U(s).$$

By Definition 2.2 this is conservation of mass.

B.2 Branch

Consider a branching pipe geometry as shown in Figure B.1.

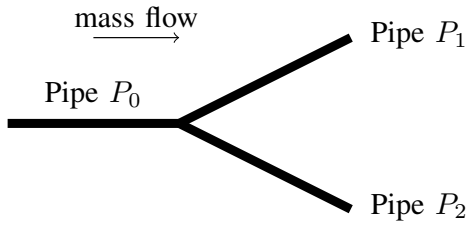

Figure B.1. Branch

State-space model simple branch

Under the assumptions from Section B.1.1 and matching conditions at the junction

$$p_{0,r} = p_{1,\ell} = p_{2,\ell},$$

$$q_{0,r} = q_{1,\ell} + q_{2,\ell},$$

the state-space realization of the one-dimensional pipe flow through the branch depicted above is as follows:

$$\dot{x}_t = \begin{bmatrix} 0 & 0 & 0 & -\alpha_0 & \alpha_0 & \alpha_0 \\ 0 & 0 & 0 & 0 & -\alpha_1 & 0 \\ 0 & 0 & 0 & 0 & 0 & -\alpha_2 \\ \beta_0 & 0 & 0 & \gamma_0 & 0 & 0 \\ \kappa_1 & \beta_1 & 0 & 0 & \gamma_1 & 0 \\ \kappa_2 & 0 & \beta_2 & 0 & 0 & \gamma_2 \end{bmatrix} x_t + \begin{bmatrix} 0 & 0 & 0 \\ 0 & \alpha_1 & 0 \\ 0 & 0 & \alpha_2 \\ \kappa_0 & 0 & 0 \\ 0 & 0 & 0 \\ 0 & 0 & 0 \end{bmatrix} u_t$$

$$y_t = \begin{bmatrix} 0 & 1 & 0 & 0 & 0 & 0 \\ 0 & 0 & 1 & 0 & 0 & 0 \\ 0 & 0 & 0 & 1 & 0 & 0 \end{bmatrix} x_t,$$

with coefficients $\alpha_i, \kappa_i, \beta_i$ for pipe P_i, $i = \{0,1,2\}$, as defined in B.1, and state $x_t = \begin{bmatrix} p_{0,r} & p_{1,r} & p_{2,r} & q_{0.\ell} & q_{1,\ell} & q_{2,\ell} \end{bmatrix}^\top$, input $u_t = \begin{bmatrix} p_{0,\ell} & q_{1,r} & q_{2,r} \end{bmatrix}^\top$ and output $y_t = \begin{bmatrix} p_{1,r} & p_{2,r} & q_{0,\ell} \end{bmatrix}^\top$.

B.2.1 Derivation

Building on (B.2), consider Assumption B.2 and suppose that additional losses at the intersection are accommodated by appropriately adjusting the friction factor for all pipes. Continuity at the boundary of pressure and mass flow means

$$p_{0,r} = p_{1,\ell} = p_{2,\ell},$$

$$q_{0,r} = q_{1,\ell} + q_{2,\ell},$$

which sets the input signal of the single pipe model of pipe P_0 as the sum of two other state variables. The related matrices for a branch model immediately follow. The extension to a split into more than two pipes is direct and hence for brevity not presented.

B.2.2 Conservation of mass

The state-space realization above satisfies conservation of mass, which follows from the first row of the steady state equation $\mathbf{0} = Ax + Bu$ and conservation of mass of the single pipe model.

B.3 Joint

We present models first for the case of two joining pipes and then consider the more complex case of multiple pipes joining.

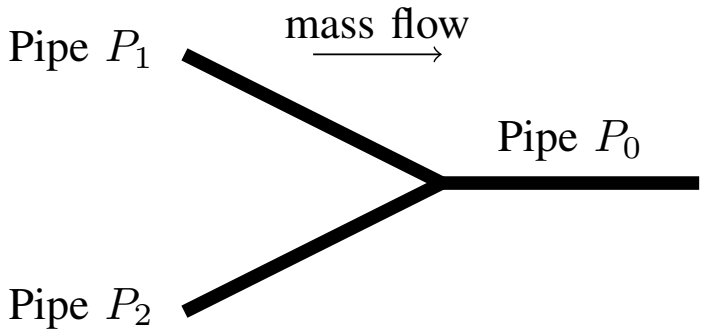

Figure B.2. Joint of 2 pipes merging into one

B.3.1 Two joining pipes

Simple joint model

Under the assumptions in Section B.1.1 and boundary conditions

$$p_{1,r} = p_{2,r} = p_{0,\ell},$$

$$q_{1,r} + q_{2,r} = q_{0,\ell},$$

two pipes merging into a single pipe are described by the following state-space model:

$$\dot{x}_t = \begin{bmatrix} 0 & -\alpha_0 & 0 & 0 & 0 \\ \beta_0 & \gamma_0 & \kappa_0 & 0 & 0 \\ 0 & \frac{\alpha_1\alpha_2}{\alpha_1+\alpha_2} & 0 & \frac{\alpha_1^2}{\alpha_1+\alpha_2} - \alpha_1 & -\frac{\alpha_1\alpha_2}{\alpha_1+\alpha_2} \\ 0 & 0 & \beta_1 & \gamma_1 & 0 \\ 0 & 0 & \beta_2 & 0 & \gamma_2 \end{bmatrix} x_t + \begin{bmatrix} 0 & 0 & \alpha_0 \\ 0 & 0 & 0 \\ 0 & 0 & 0 \\ \kappa_1 & 0 & 0 \\ 0 & \kappa_2 & 0 \end{bmatrix} u_t,$$

$$y_t = \begin{bmatrix} 1 & 0 & 0 & 0 & 0 \\ 0 & 0 & 0 & 1 & 0 \\ 0 & 0 & 0 & 0 & 1 \end{bmatrix} x_t,$$

with $y_t = \begin{bmatrix} p_{0,r} & q_{1,\ell} & q_{2,\ell} \end{bmatrix}$, $x_t = \begin{bmatrix} p_{0,r} & q_{0,\ell} & p_{1,r} & q_{1,\ell} & q_{2,\ell} \end{bmatrix}^\top$, and $u_t = \begin{bmatrix} p_{1,\ell} & p_{2,\ell} & q_{0,r} \end{bmatrix}^\top$.

Derivation

Building on (B.2), each joining pipe can be described by

$$\dot{p}_{j,r} = \alpha_j(q_{j,r} - q_{j,\ell}), \tag{B.6a}$$

$$\dot{q}_{j,\ell} = \beta_j p_{j,r} + \kappa_j p_{j,\ell} + \gamma_j q_{j,\ell}, \tag{B.6b}$$

where the subscript j corresponds to pipe P_j, with coefficients as defined above and $j \in \{0,1,\ldots,n\}$. Every $p_{j,r}$ and $q_{j,\ell}$ are state variables and every $p_{j,\ell}$ and $q_{j,r}$ are input variables related to pipe P_j.

Consider Assumption B.2 and algebraic constraints

$$p_{1,r} = p_{2,r} = p_{0,\ell}, \tag{B.7a}$$

$$q_{1,r} + q_{2,r} = q_{0,\ell}, \tag{B.7b}$$

which express continuity of the pressure and mass flow. Assume further that additional losses at the intersection are accommodated by appropriately adjusting the friction factor for all pipes.

Note that (B.7b) cannot directly be incorporated into the state-space formulation since it is not immediate how the signal $q_{0,\ell}$ is split between the flow of pipes 1 and 2. To eliminate variables $q_{1,r}, q_{r,2}$, consider (B.7a), take the derivative and use (B.6a) to obtain

$$(\alpha_1 + \alpha_2)q_{1,r} = \alpha_1 q_{1,\ell} + \alpha_2(q_{0,\ell} - q_{2,\ell}), \tag{B.8a}$$

$$(\alpha_1 + \alpha_2)q_{2,r} = \alpha_2 q_{2,\ell} + \alpha_1(q_{0,\ell} - q_{1,\ell}), \tag{B.8b}$$

which yields the state-space description above.

Conservation of mass

The state-space realization above satisfies conservation of mass, which follows from the third row of the steady state equation $\mathbf{0} = Ax + Bu$ and conservation of mass of the single pipe model.

B.3.2 Multiple joining pipes

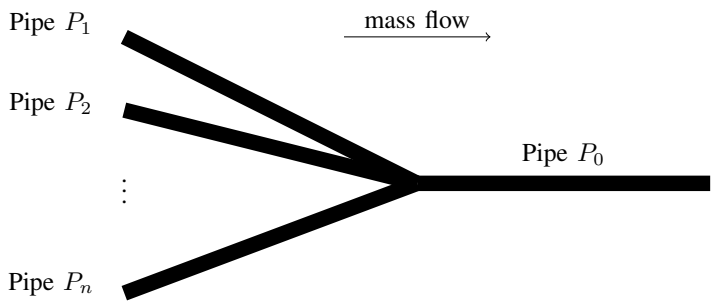

Figure B.3. Joint of n pipes merging into one

Joint model

Consider the assumptions in Section B.1.1 and matching conditions at the junction

$$p_{1,r} = p_{2,r} = \cdots = p_{n+1,r} = p_{0,\ell},$$

$$q_{1,r} + q_{2,3} + \cdots + q_{r,n} + q_{r,n+1} = q_{0,\ell}.$$

A joint of n pipes with dynamics (B.6) can be described by the state-space model,

$$\dot{x} = \begin{bmatrix} \mathbf{0}_{2,2} & A_{12} \\ A_{21} & A_{22} \end{bmatrix} x + \begin{bmatrix} B_1 \\ B_2 \end{bmatrix} u, \qquad y = \begin{bmatrix} 1 & 0 & 0 & 0 & \\ 0 & 0 & 0 & 1 & \mathbf{0}_{2,n-1} \\ & \mathbf{0}_{n-1,4} & & & I_{n-1} \end{bmatrix} x,$$

where

$$u = \begin{bmatrix} p_{1,\ell} & p_{2,\ell} & \dots & p_{n,\ell} & q_{0,r} \end{bmatrix}^\top, \qquad x = \begin{bmatrix} p_{0,r} & p_{1,r} & q_{0,\ell} & q_{1,\ell} & q_{2,\ell} & \dots & q_{n,\ell} \end{bmatrix}^\top,$$
$$y = \begin{bmatrix} p_{0,r} & q_{1,\ell} & q_{2,\ell} & \dots & q_{n,\ell} \end{bmatrix}^\top \in \mathbb{R}^{n+1},$$

$$A_{12} = \begin{bmatrix} -\alpha_0 & \mathbf{0}_n \\ a & -a\mathbf{1}_n \end{bmatrix}, \quad A_{21} = \begin{bmatrix} \beta_0 & 0 & 0 & \dots & 0 \\ \kappa_0 & \beta_1 & \beta_2 & \dots & \beta_n \end{bmatrix}^\top, \quad A_{22} = \operatorname{diag}(\gamma_0, \dots, \gamma_n)$$

$$B_1 = \begin{bmatrix} \mathbf{0}_n & \alpha_0 \\ \mathbf{0}_n & 0 \end{bmatrix}, \quad B_2 = \begin{bmatrix} & \mathbf{0}_{n+1} & \\ \kappa_1 & & \\ & \ddots & \mathbf{0}_n^\top \\ & & \\ & \kappa_n & \end{bmatrix},$$

with

$$a = \alpha_1 \left(\sum_{j=1}^{n} \prod_{\substack{i=1 \\ i \neq j}}^{n} \alpha_i \right)^{-1} \prod_{i=2}^{n} \alpha_i.$$

Derivation

We wish to extend the model for $n = 2$ joining pipes to any finite number of joining pipes. In particular, first we would like to obtain an expression for $q_{j,r}$ only depending on state variables and sources, as in (B.8).

Definition B.1. *We say* sources *for inputs into the joint model that are not related to states of any other pipes via algebraic constraints. We say* internal variables *for input variables that are not sources.*

We derive the model by induction. Consider the algebraic constraints for $n = 3$,

$$p_{1,r} = p_{2,r} = p_{3,r} = p_{0,\ell},$$
$$q_{1,r} + q_{2,r} + q_{3,r} = q_{0,\ell}.$$

Then,

$$\begin{aligned}
\dot{p}_{1,r} &= \dot{p}_{2,r},\\
(\alpha_1+\alpha_2)q_{1,r} &= \alpha_1 q_{1,\ell} + \alpha_2(q_{0,\ell} - q_{2,\ell} - q_{3,r}),
\end{aligned}$$

$$\begin{aligned}
\dot{p}_{3,r} &= \dot{p}_{2,r},\\
(\alpha_2+\alpha_3)q_{3,r} &= \alpha_3 q_{3,\ell} + \alpha_2(q_{0,\ell} - q_{2,\ell} - q_{1,r})\\
&= \alpha_3 q_{3,\ell} + \alpha_2\Big(q_{0,\ell} - q_{2,\ell} - (\alpha_1+\alpha_2)^{-1}[\alpha_1 q_{1,\ell} + \alpha_2(q_{0,\ell} - q_{2,\ell} - q_{3,r})]\Big).
\end{aligned}$$

so that

$$(\alpha_1\alpha_2 + \alpha_1\alpha_3 + \alpha_2\alpha_3)q_{3,r} = \alpha_1\alpha_2(q_{0,\ell} - q_{1,\ell} - q_{2,\ell}) + (\alpha_1\alpha_3 + \alpha_2\alpha_3)q_{3,\ell}. \tag{B.9}$$

Similarly,

$$(\alpha_1\alpha_2 + \alpha_1\alpha_3 + \alpha_2\alpha_3)q_{1,r} = \alpha_2\alpha_3(q_{0,\ell} - q_{2,\ell} - q_{3,\ell}) + (\alpha_1\alpha_2 + \alpha_1\alpha_3)q_{1,\ell}, \tag{B.10}$$

$$(\alpha_1\alpha_2 + \alpha_1\alpha_3 + \alpha_2\alpha_3)q_{2,r} = \alpha_1\alpha_3(q_{0,\ell} - q_{1,\ell} - q_{3,\ell}) + (\alpha_1\alpha_2 + \alpha_2\alpha_3)q_{2,\ell}. \tag{B.11}$$

Comparing equations (B.9)–(B.11) with (B.8) we recognize a certain pattern, which we explore next. Facilitated by observations above we derive a general statement.

Proposition B.1. *Consider n joining pipes with individual dynamics* (B.6a) - (B.6b). *Let* $q_{j,\ell}$, $j \in \{0,1,\ldots,n\}$, *be state variables. The internal variables* $q_{k,r}$, $k \in \{1,2,\ldots,n\}$, *can be described*

by state variables,

$$\left(\sum_{j=1}^{n}\prod_{\substack{i=1\\i\neq j}}^{n}\alpha_i\right)q_{k,r}=\prod_{\substack{i=1\\i\neq k}}^{n}\alpha_i\left(q_{0,\ell}-\sum_{\substack{i=1\\i\neq k}}^{n}q_{i,\ell}\right)+\left(\sum_{j=1}^{n}\prod_{\substack{i=1\\i\neq j}}^{n}\alpha_i-\prod_{\substack{i=1\\i\neq k}}^{n}\alpha_i\right)q_{k,\ell} \tag{B.12}$$

Proof. We prove the theorem by induction. We observe that (B.12) holds for $n\in\{2,3\}$. Hence, assume it holds for some n and for $n+1$ note that interconnections dictate the algebraic constraints

$$p_{1,r}=p_{2,r}=\cdots=p_{n+1,r}=p_{0,\ell}, \tag{B.13a}$$

$$q_{1,r}+q_{2,3}+\cdots+q_{r,n}+q_{r,n+1}\doteq q_{0,\ell}^{n}+q_{r,n+1}=q_{0,\ell}. \tag{B.13b}$$

Hence, by the algebraic constraints on the pressure and the pipe dynamics,

$$\begin{aligned}q_{n+1,r}&=\frac{1}{\alpha_{n+1}}(\dot{p}_{k,r}-\dot{p}_{n+1,r})+q_{n+1,r}\\&=\frac{1}{\alpha_{n+1}}\left(\alpha_k(q_{k,r}-q_{k,\ell})-\dot{p}_{n+1,r}\right)+q_{n+1,\ell}+\frac{\dot{p}_{n+1,r}}{\alpha_{n+1}}\\&=\frac{1}{\alpha_{n+1}}\alpha_k(q_{k,r}-q_{k,\ell})+q_{n+1,\ell},\end{aligned}$$

where without loss of generality $k \in \{1,2\ldots,n-1\}$. Then (B.12) yields

$$\begin{aligned}
\left(\sum_{j=1}^{n}\prod_{\substack{i=1\\ i\neq j}}^{n}\alpha_i\right) q_{k,r} &= \prod_{\substack{i=1\\ i\neq k}}^{n}\alpha_i\left(q_{0,\ell}^{n}-\sum_{\substack{i=1\\ i\neq k}}^{n}q_{i,\ell}\right)+\left(\sum_{j=1}^{n}\prod_{\substack{i=1\\ i\neq j}}^{n}\alpha_i-\prod_{\substack{i=1\\ i\neq k}}^{n}\alpha_i\right)q_{k,\ell}\\
&= \prod_{\substack{i=1\\ i\neq k}}^{n}\alpha_i\left(q_{0,\ell}-q_{n+1,r}-\sum_{\substack{i=1\\ i\neq k}}^{n}q_{i,\ell}\right)+\left(\sum_{j=1}^{n}\prod_{\substack{i=1\\ i\neq j}}^{n}\alpha_i-\prod_{\substack{i=1\\ i\neq k}}^{n}\alpha_i\right)q_{k,\ell}\\
&= -\prod_{i=1}^{n}\alpha_i\frac{1}{\alpha_{n+1}}(q_{k,r}-q_{k,\ell})+\prod_{\substack{i=1\\ i\neq k}}^{n}\alpha_i\left(q_{0,\ell}-q_{n+1,\ell}-\sum_{\substack{i=1\\ i\neq k}}^{n}q_{i,\ell}\right)\\
&\qquad +\left(\sum_{j=1}^{n}\prod_{\substack{i=1\\ i\neq j}}^{n}\alpha_i-\prod_{\substack{i=1\\ i\neq k}}^{n}\alpha_i\right)q_{k,\ell}\\
&= -\frac{1}{\alpha_{n+1}}\prod_{i=1}^{n}\alpha_i q_{k,r}+\prod_{\substack{i=1\\ i\neq k}}^{n}\alpha_i\left(q_{0,\ell}-\sum_{\substack{i=1\\ i\neq k}}^{n+1}q_{i,\ell}\right) \quad .\\
&\qquad +\left(\sum_{j=1}^{n}\prod_{\substack{i=1\\ i\neq j}}^{n}\alpha_i-\prod_{\substack{i=1\\ i\neq k}}^{n}\alpha_i+\frac{1}{\alpha_{n+1}}\prod_{i=1}^{n}\alpha_i\right)q_{k,\ell}
\end{aligned}$$

Move the first term of the right-hand side to the left, multiply the equation by α_{n+1} and observe that the left-hand side is

$$\sum_{j=1}^{n}\prod_{\substack{i=1\\ i\neq j}}^{n}\alpha_i\alpha_{n+1}+\prod_{i=1}^{n}\alpha_i=\sum_{j=1}^{n}\prod_{\substack{i=1\\ i\neq j}}^{n+1}\alpha_i+\prod_{i=1}^{n}\alpha_i=\sum_{j=1}^{n+1}\prod_{\substack{i=1\\ i\neq j}}^{n+1}\alpha_i.$$

This identity can also be used for the last term on the right-hand side. Then,

$$\left(\sum_{j=1}^{n+1}\prod_{\substack{i=1\\ i\neq j}}^{n+1}\alpha_i\right)q_{k,r}=\prod_{\substack{i=1\\ i\neq k}}^{n+1}\alpha_i\left(q_{0,\ell}-\sum_{\substack{i=1\\ i\neq k}}^{n+1}q_{i,\ell}\right)+\left(\sum_{j=1}^{n+1}\prod_{\substack{i=1\\ i\neq j}}^{n+1}\alpha_i-\prod_{\substack{i=1\\ i\neq k}}^{n+1}\alpha_i\right)q_{k,\ell},$$

which is equivalent to our induction hypothesis and thus concludes the proof. □

The state-space realization above is a direct consequence of Proposition B.1, the pipe

dynamics in (B.6), the algebraic constraint of equal pressure at the intersection in (B.13a), and the observation that for the ODE of $p_{1,r}$,

$$\alpha_1 \left(\sum_{j=1}^{n} \prod_{\substack{i=1 \\ i \neq j}}^{n} \alpha_i \right)^{-1} \left(\sum_{j=1}^{n} \prod_{\substack{i=1 \\ i \neq j}}^{n} \alpha_i - \prod_{i=2}^{n} \alpha_i \right) - \alpha_1 = -\alpha_1 \left(\sum_{j=1}^{n} \prod_{\substack{i=1 \\ i \neq j}}^{n} \alpha_i \right)^{-1} \prod_{i=2}^{n} \alpha_i.$$

Conservation of mass

As for $n = 2$ joining pipes, the state-space realization above satisfies conservation of mass, which follows from the third row of the steady state equation $\mathbf{0} = Ax + Bu$ and conservation of mass of the single pipe model.

B.4 Star junction

Consider the pipe geometry illustrated in Figure B.4, combining the branch and joint model to so called star junction.

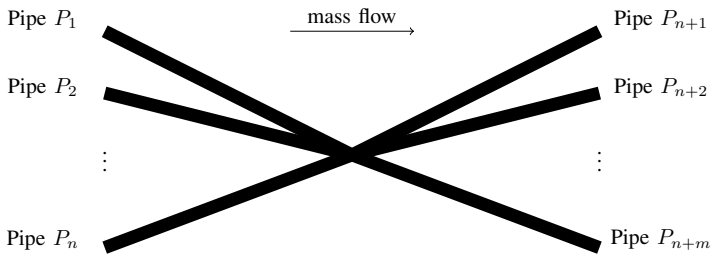

Figure B.4. Star junction of $n+m$ pipes

Star junction model

Consider the assumptions in Section B.1.1 and matching conditions at the junction

$$p_{1,r} = \cdots = p_{n,r} = p_{n+1,\ell} = \cdots = p_{n+m,\ell},$$

$$q_{1,r} + \cdots + q_{r,n} = q_{n+1,\ell} + \cdots + q_{n+m,\ell}.$$

A star junction of n pipes connecting to m pipes with individual dynamics (B.6a) - (B.6b) can be represented by the state-space model,

$$\begin{aligned}
\dot{x}_{t,1} &= A_1 x_{t,1} + B_1 u_t, \\
\dot{x}_{t,2} &= A_1 x_{t,2} + B_2 u_t, \\
\dot{x}_{t,3} &= A_1 x_{t,3} + B_3 u_t, \\
\dot{x}_{t,4} &= A_1 x_{t,4} + B_4 u_t, \\
y_t &= C(x_{t,1} + x_{t,2} + x_{t,3} + x_{t,4}),
\end{aligned}$$

where

$$\begin{aligned}
x_{t,1} &= x_{t,2} = x_{t,3} = x_{t,4} \\
&= [p_{1,r} \quad p_{n+1,r} \quad p_{n+2,r} \quad \cdots \quad p_{n+m,r} \quad q_{1,\ell} \quad q_{2,\ell} \quad \cdots \quad q_{n+m,\ell}]^\top \in \mathbb{R}^{n+2m+1}, \\
u_t &= [p_{1,\ell} \quad p_{2,\ell} \quad \cdots \quad p_{n,\ell} \quad q_{n+1,r} \quad q_{n+2,r} \cdots \quad q_{n+m,r}]^\top \in \mathbb{R}^{n+m}, \\
y_t &= [p_{n+1,r} \quad p_{n+2,r} \quad \cdots \quad p_{n+m,r} \quad q_{1,\ell} \quad q_{2,\ell} \cdots \quad q_{n,\ell}]^\top \in \mathbb{R}^{n+m},
\end{aligned}$$

$$A_1 = \left[\begin{array}{cccc} \mathbf{0}_{m+1} & -a & -a\mathbf{1}_{n-1} & a\mathbf{1}_m \\ \hline \multicolumn{4}{c}{\mathbf{0}_{n+2m,n+2m+1}} \end{array}\right], \quad B_1 = \mathbf{0}_{n+2m+1,n+m},$$

$$A_2 = \left[\begin{array}{c|c} & \begin{array}{cc} \multicolumn{2}{c}{\mathbf{0}_m} \\ \hline -\alpha_{n+1} & \mathbf{0} \\ & \ddots \\ \mathbf{0} & -\alpha_{n+m} \\ \hline \multicolumn{2}{c}{\mathbf{0}_{n+m}} \end{array} \end{array}\right],$$

$$B_2 = \left[\begin{array}{c|cc} \multicolumn{3}{c}{\mathbf{0}_{n+m}} \\ \hline & \alpha_{n+1} & \mathbf{0} \\ \mathbf{0}_{m,n} & \ddots & \\ & \mathbf{0} & \alpha_{n+m} \\ \hline \multicolumn{3}{c}{\mathbf{0}_{n+m,n+m}} \end{array}\right],$$

$$A_3 = \left[\begin{array}{c|c|c|c} \multicolumn{4}{c}{\mathbf{0}_{m+1,n+2m+1}} \\ \hline \beta_1 & & \gamma_1 \quad \mathbf{0} & \\ \vdots & \mathbf{0}_{n,m} & \ddots & \mathbf{0}_{n,m} \\ \beta_n & & \mathbf{0} \quad \gamma_n & \\ \hline \multicolumn{4}{c}{\mathbf{0}_{m,n+2m+1}} \end{array}\right], \quad B_3 = \left[\begin{array}{cc|c} \multicolumn{3}{c}{\mathbf{0}_{m+1,n+m}} \\ \hline \kappa_1 & \mathbf{0} & \\ \ddots & & \mathbf{0}_{n,m} \\ \mathbf{0} & \kappa_n & \\ \hline \multicolumn{3}{c}{\mathbf{0}_{m,n+m}} \end{array}\right],$$

$$A_4 = \left[\begin{array}{ccc|c|cc} \multicolumn{6}{c}{\mathbf{0}_{n+m+1,n+2m+1}} \\ \hline \kappa_{n+1} & \beta_{n+1} & \mathbf{0} & & \gamma_{n+1} & \mathbf{0} \\ \vdots & \ddots & & \mathbf{0}_{m,n} & \ddots & \\ \kappa_{n+m} & \mathbf{0} & \beta_{n+m} & & \mathbf{0} & \gamma_{n+m} \end{array}\right],$$

$$B_4 = \mathbf{0}_{n+2m+1,n+m},$$

$$C = \begin{bmatrix} \mathbf{0}_{n+m} & I_{n+m} & \mathbf{0}_{n+m,m} \end{bmatrix},$$

Derivation

Proposition B.1 also facilitates a statement about a general star junction, which consists of n pipes connecting to m pipes, as illustrated in Figure B.4. Towards a state-space realization and akin to the case of a joint, we wish to express internal variables in terms of state variables.

Corollary B.1. *Consider a star junction with n joining pipes connecting to m branching pipes with individual dynamics* (B.6a) - (B.6b). *Let* $q_{i,\ell}$, $i \in \{1,2,\ldots,n+m\}$, *and* $p_{1,r}$ *be state variables. The internal variables* $q_{k,r}$, $k \in \{1,2,\ldots,n\}$ *and* $p_{j,\ell}$, $j \in \{n+1,n+2,\ldots,n+m\}$, *can be described by state variables through*

$$\left(\sum_{j=1}^{n}\prod_{\substack{i=1\\ i\neq j}}^{n}\alpha_i\right)q_{k,r} = \prod_{\substack{i=1\\ i\neq k}}^{n}\alpha_i\left(\sum_{i=n+1}^{n+m}q_{i,\ell}-\sum_{\substack{i=1\\ i\neq k}}^{n}q_{i,\ell}\right)+\left(\sum_{j=1}^{n}\prod_{\substack{i=1\\ i\neq j}}^{n}\alpha_i-\prod_{\substack{i=1\\ i\neq k}}^{n}\alpha_i\right)q_{k,\ell}, \tag{B.14}$$

$$p_{j,\ell} = p_{1,r}. \tag{B.15}$$

Proof. Consider (B.12) from Proposition B.1 and note that therein that $q_{0,\ell} = \sum_{j=n+1}^{n+m} q_{j,\ell}$. The result for the first equation follows immediately. The second equation is a direct consequence of the algebraic constraint of all pressures being equal at the intersection. □

The state-space realization above follows directly: the system related to x_1 describes the solution to $\dot{p}_{1,r}$ and directly follows from (B.14). The system corresponding to x_2 describes $p_{j,r}$, $j \in \{n+1,n+2,\ldots,n+m\}$ and is immediately obtained by the dynamics (B.6a). The systems for x_3 and x_4 relate to $q_{j,\ell}$, $j \in \{1,2,\ldots,n+m\}$ and are a consequence of the dynamics (B.6b) and the algebraic constraint (B.15).

Conservation of mass

Conservation of mass can be established from the branch and joint above and is omitted for brevity.

B.5 Control valve

We present two models for control valves: firstly, we use a static gain (less or equal than 1) on the pressure and unity gain on mass flow; secondly, we provide a more complex model with the mass flow varying with in- and outlet pressure and cross-sectional area.

B.5.1 Static model

Static valve model

For the static gain model let the states and inputs be:

$$x_t = \begin{bmatrix} p_r & q_\ell \end{bmatrix}^\top, \quad u_t = \begin{bmatrix} p_\ell & q_r \end{bmatrix}^\top, \tag{B.16}$$

and define the static relationship

$$x_t = \begin{bmatrix} k_v & 0 \\ 0 & 1 \end{bmatrix} u,$$

where $k_v \in (0,1)$.

Conservation of mass is immediate.

B.5.2 Dynamic model

Here we develop a model based on a static relationship commonly used for orifices combined with a first order low pass filter approximating the dynamics between command and actuation.

Dynamic valve model [1]

Assume an isentropic expansion and approximate the command-to-actuation relationship by a first order model. Define the state, about and input signals as

$$x_t = \begin{bmatrix} A_o \end{bmatrix}, \quad y_t = \begin{bmatrix} q_v \end{bmatrix}, \quad u_t = \begin{bmatrix} u_v & p_\ell & p_r \end{bmatrix}^\top.$$

The dynamics are

$$\dot{x}_t = \begin{bmatrix} -1/\tau \end{bmatrix} x_t + \begin{bmatrix} K/\tau & 0 & 0 \end{bmatrix} u_t, \tag{B.17a}$$

$$y_t = \begin{bmatrix} g_o(A_o, \bar{p}_\ell, \bar{p}_r)/A_o \end{bmatrix} x_t + \begin{bmatrix} 0 & \zeta_o(A_o, \bar{p}_\ell, \bar{p}_r) & \xi_o(A_o, \bar{p}_\ell, \bar{p}_r) \end{bmatrix} u_t, \tag{B.17b}$$

where g_0 is the orifice equation from (B.18), τ and K the time constant and gain from transfer function (B.20) between the control command and actual actuation, q_v the mass flow through the valve, $u_v \in (0,1)$ the control input, A_o the cross-sectional area of the valve, and ξ_o and ζ_o the linearization terms from (B.21) and (B.22).

Conservation of mass as defined in Definition 2.2 does not apply here, since there are no mass flows as model inputs.

Derivation

The static mapping is justified by pipe time constants and the usual sampling time, which both vastly exceed the low time constants of the valve [18].

In [32, Equ. (3-34)], assuming an isentropic expansion the mass flow through an orifice is approximated by

$$q_o = C p_{o,\ell} A_o \sqrt{\frac{2}{R_s T_0 z_0} \frac{\mu}{\mu - 1} \left[\left(\frac{p_{o,r}}{p_{o,\ell}} \right)^{2/\mu} - \left(\frac{p_{o,r}}{p_{o,\ell}} \right)^{(\mu+1)/\mu} \right]}, \tag{B.18}$$

$$\doteq g_o(A_o, p_r, p_\ell) \tag{B.19}$$

where $C \doteq C_d / \sqrt{1 - (D_o/D)^4}$ corrects for the head loss, with C_d being the discharge coefficient, μ the ratio of specific heat, $\mu = c_p/c_v$ and $D_o(D)$ the orifice (pipe) diameter.

For the control valve let the cross-sectional area, A_o, from (B.18) represent the manipulated variable. To approximate the dynamics of the actuator itself, i.e., the relationship between

[1] The dynamic valve model has not been fully tested in operational models.

the control command and actual actuation, consider a first-order low pas filter with transfer function,

$$K\frac{1}{\tau s+1}, \tag{B.20}$$

where $\tau > 0$ is the time constant, $K = A_{o,max}$ is the gain. The control input is constrained, i.e., $u_v \in (0,1)$, where 0 is closed and 1 is open. Towards a linear model:

$$\frac{\partial g_o(A_o, p_\ell, p_r)}{\partial p_r} \doteq \xi_o(A_o, p_\ell, p_r), \tag{B.21}$$

$$\frac{\partial g_o(A_o, p_\ell, p_r)}{\partial p_\ell} \doteq \zeta_o(A_o, p_\ell, p_r). \tag{B.22}$$

Combining these equations with (B.20) yields the state-space model above.

B.6 Tank

We next introduce two tank models: the first model approximates pressure changes while assuming a constant temperature; the second model additionally admits temperature changes.

B.6.1 Isothermal tank

Isothermal tank model

Assume there are multiple in- and outlets at the tank and the temperature is constant. Under the assumptions below, for the pressure as the single state, $x = p$, and input vector

$$u_t = \begin{bmatrix} q_{1,\ell} \dots & q_{n_\ell,\ell} & q_{1,r} & \dots & q_{n_r,r} \end{bmatrix},$$

with $n_\ell \in \mathbb{N}$ as the number of inlets and $n_r \in \mathbb{N}$ as the number of outlets, the linear state-space model is

$$\dot{x}_t = \frac{R_s z_0 T_0}{V} \begin{bmatrix} \mathbf{1}_{n_\ell} & -\mathbf{1}_{n_r} \end{bmatrix} u,$$

with V as the constant volume.

Conservation of mass as defined in Definition 2.2 does not apply here, as all mass flows are model inputs. However, we observe that bounded pressure implies equalizing mass flows.

Assumptions

Assumption B.3. *Suppose:*

B.3(i) *there is perfect mixing inside the volume;*

B.3(ii) *the compressibility factor, z, changes negligibly or if necessary can be represented by a time-varying parameter;*

B.3(iii) *the gas is described by the ideal gas equation;*

Derivation

For the pressure inside the constant volume, we have

$$\begin{aligned} p &= \rho R_s T_0 z_0, \\ \dot{p} &= R_s z_0 T_0 \dot{\rho} = R_s z_0 T_0 \frac{q}{V} = \frac{R_s z_0 T_0}{V} \left(\sum_{j=1}^{n_\ell} q_{j,\ell} - \sum_{k=1}^{n_r} q_{k,r} \right) \end{aligned} \tag{B.23}$$

where the first equation is the ideal gas equation. The derivative uses Assumption B.3(ii) and the last line conservation of mass: change in mass equals mass flow in minus mass flow out. The variables are: ρ density; $\Sigma_j q_{j,\ell}$ ($\Sigma_k q_{k,r}$) sum of mass flowing in (out). The state-space model above follows directly.

B.6.2 Non-isothermal tank

We now drop the isothermal assumption and incorporate temperature dynamics. This also has an effect on the pressure dynamics themselves.

Non-isothermal tank model

Consider Assumptions B.3 and B.4. We obtain a nonlinear representation relating the entering mass flows and temperatures, $q_{i,\ell}$ and $T_{i,\ell}, i = \{1,\dots,n_\ell\}$, and exiting mass flows, $q_{i,r}, i = \{1,\dots,n_r\}$, to the pressure and temperature inside the tank, p and T:

$$\dot{p} = \frac{R_s z_0 \mu}{V}\left(\sum_{j=1}^{n_\ell} q_{j,\ell} T_{j,\ell} - \sum_{k=1}^{n_r} q_{k,r} T\right),$$
$$\dot{T} = \frac{R_s T z_0}{p V c_v}\left(\sum_{j=1}^{n_\ell} q_{i,j}\left(c_{p,j} T_j - c_v T\right) - R_s T \sum_{k=1}^{n_r} q_{o,k}\right).$$

Therefore, with $x_t = \begin{bmatrix} p & T \end{bmatrix}^\top$ and

$$u_t = \begin{bmatrix} q_{1,\ell} & T_{1,\ell} & \dots & q_{n_\ell,\ell} & T_{n_i,\ell} & & q_{1,r} & \dots & q_{n_r,r} \end{bmatrix},$$

we can use the linearized dynamics for pressure and temperature to generate a linear state-space model.

As for the isothermal case, conservation of mass does not apply here, as all mass flows are model inputs.

Assumptions

Assumption B.4. *Suppose:*

B.4(i) potential and kinetic energy are negligible;

B.4(ii) the reference states for internal energy and enthalpy are set to zero at zero degree Kelvin;

B.4(iii) specific heats are constant;

B.4(iv) the heat flux to the environment is negligible.

Derivation

The pressure dynamics are akin to the isothermal case but differ as the temperature is not a constant anymore:

$$\begin{aligned}\dot{p} &= R_s z_0 \left(\frac{\sum_{j=1}^{n_\ell} q_{j,\ell} - \sum_{k=1}^{n_r} q_{k,r}}{V} T + \rho \dot{T} \right) \\ &= R_s z_0 \left(\frac{\sum_{j=1}^{n_\ell} q_{j,\ell} - \sum_{k=1}^{n_r} q_{k,r}}{V} T + \frac{p}{R_s T z_0} \dot{T} \right) \end{aligned} \tag{B.24}$$

We next derive an expression for $\dot{T}$, which we will plug back in.

Temperature dynamics

As mentioned in Assumptions B.3(iii) and B.4(ii) we assume ideal gas and select the reference states for the internal energy and enthalpy to be zero at zero degree Kelvin: $T_{\text{ref}} = 0 \implies U_{\text{ref}}, H_{\text{ref}} = 0$ (see for example [34, Ch. 3.6.3]). Then, the derivative of the total energy of a system, E, is [34, Equ. (2.27)]:

$$\frac{d}{dt}E \overset{Ass.B.4(i)}{=} \frac{d}{dt}U \tag{B.25}$$

$$\overset{Ass.B.3(i),B.4(ii)}{=} \frac{d}{dt}(mc_v T)$$

$$\overset{Ass.B.4(iii)}{=} \left(\sum_{j=1}^{n_\ell} q_{j,\ell} - \sum_{k=1}^{n_r} q_{k,r} \right) c_v T + m c_v \dot{T} \tag{B.26}$$

with U being the internal energy. Moreover, conservation of energy implies [34, Equ. (4.9)-(4.12)]

$$\begin{aligned}\frac{d}{dt}U &\overset{Ass.B.4(i)}{=} \dot{Q} + \sum_{j=1}^{n_\ell} q_{j,\ell} h_j - \sum_{k=1}^{n_r} q_{k,r} h_k \\ &\overset{Ass.B.3(i)}{=} \dot{Q} + c_p \sum_{j=1}^{n_\ell} q_{j,\ell} T_j - c_p T \sum_{k=1}^{n_r} q_{k,r}, \end{aligned} \tag{B.27}$$

where h is the specific enthalpy, and $\dot{Q}$ is the rate of heat transfer to the environment, which is a function of the temperature (deviations) inside and outside the volume. Usually, empirical formulations are used for conduction, convection and radiation (see [34, Ch. 2]). Here for brevity we assume it is negligible (cf. Assumption B.4(iv)). Combining (B.26) and (B.27) yields

$$\begin{aligned}\dot{T} &= \frac{1}{mc_v}\left[c_vT\left(\sum_{k=1}^{n_r} q_{k,r} - \sum_{j=1}^{n_\ell} q_{j,\ell}\right) + \sum_{j=1}^{n_\ell} q_{j,\ell}c_pT_j \; - c_pT\sum_{k=1}^{n_r} q_{k,r}\right] \\ &= \frac{1}{mc_v}\left[\sum_{j=1}^{n_\ell} q_{j,\ell}\left(c_pT_j - c_vT\right) \; - R_sT\sum_{k=1}^{n_r} q_{k,r}\right] \\ &= \frac{R_sTz_0}{pVc_v}\left[\sum_{j=1}^{n_\ell} q_{j,\ell}\left(c_pT_j - c_vT\right) - R_sT\sum_{k=1}^{n_r} q_{k,r}\right], \end{aligned} \tag{B.28}$$

which represents the nonlinear temperature dynamics from the model. Note that (B.28) also coincides with that in [16, Ch. 13.4.5]. Using this equation in (B.24) yields the stated nonlinear dynamics for the pressure.

B.7 Valve manifold

Consider a valve manifold as illustrated in Figure B.5. The following model is derived by

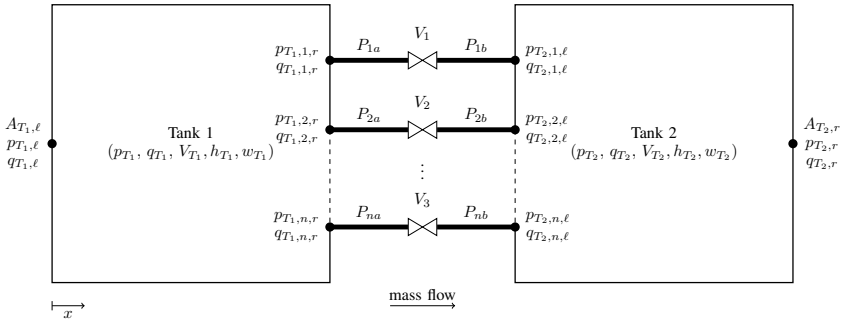

Figure B.5. Valve manifold

using the tank models from above for Tanks 1 and 2, the single pipe model for each pipe-valve-pipe connection with adjusted friction factor, and the orifice equation for the entrances of the tanks. We provide more details in the derivation subsequently.

Valve manifold model

Consider Assumptions B.2–B.3 (for isothermal pipes and tanks) and approximate the entering mass flow into Tanks 1 and 2 as an isentropic expansion described by orifice equation (B.18). Further, let each pipe-valve-pipe connection be approximated by single pipe models with adjusted friction factors. Let the state, output and input vectors be defined as

$$
\begin{aligned}
x_t &= \begin{bmatrix} p_{T_1} & p_{1,r} & q_{1,\ell} & p_{2,r} & q_{2,\ell} & p_{T_2} \end{bmatrix}^\top, \\
y_t &= \begin{bmatrix} p_{T_2} & q_{T_1,\ell} \end{bmatrix}^\top, \\
u_t &= \begin{bmatrix} p_{T_1,\ell} & q_{T_2,r} \end{bmatrix}^\top,
\end{aligned}
$$

where subscript $i = \{1,2\}$ refers to middle section $P_{ia} - V_i - P_{ib}$ and other terms as shown in Figure B.5. Then the overall dynamics are described by

$$
\begin{aligned}
\dot{x}_t = &\begin{bmatrix}
\alpha_{T_1}\xi_{T_1} & 0 & -\alpha_{T_1} & 0 & -\alpha_{T_1} & 0 \\
0 & \alpha_1\zeta_{T_2} & -\alpha_1 & 0 & 0 & \alpha_1\xi_{T_2} \\
\kappa_1 & \beta_1 & \gamma_1 & 0 & 0 & 0 \\
0 & 0 & 0 & \alpha_2\zeta_{T_2} & -\alpha_2 & \alpha_2\xi_{T_2} \\
\kappa_2 & 0 & 0 & \beta_2 & \gamma_2 & 0 \\
0 & \alpha_{T_2}\zeta_{T_2} & 0 & \alpha_{T_2}\zeta_{T_2} & 0 & 2\alpha_{T_2}\xi_{T_2}
\end{bmatrix} x_t \\
&+ \begin{bmatrix}
\alpha_{T_1}\zeta_{T_1} & 0 & 0 & 0 & 0 & 0 \\
0 & 0 & 0 & 0 & 0 & -\alpha_{T_2}
\end{bmatrix}^\top u_t, \\
y_t = &\begin{bmatrix}
0 & 0 & 0 & 0 & 0 & 1 \\
\xi_{T_1} & 0 & 0 & 0 & 0 & 0
\end{bmatrix} x_t + \begin{bmatrix}
0 & 0 \\
\zeta_{T_1} & 0
\end{bmatrix} u_t,
\end{aligned}
$$

where $\xi_{T_1} = \xi_{T_1}(\bar{p}_{T_1,\ell}, \bar{p}_{T_1})$ from (B.21) and $\zeta_{T_1} = \zeta_{T_1}(\bar{p}_{T_1,\ell}, \bar{p}_{T_1})$ from (B.22) are related to the linearized orifice equation for the entrance into Tank 1, and accordingly for Tank 2. The parameters $\alpha_i, \beta_i, \kappa_i$ and $\gamma_i, i = \{1,2,3\}$ are as defined in (B.1) for pipes, whereas $\alpha_{T_i} = \frac{R_s z_0 T_0}{V_{T_i}}, i = \{1,2\}$.

Conservation of mass (as a steady state property) follows from B.30 applied to Tank 1 and 2, and conservation of mass of the single pipe model from Section B.1.3.

B.7.1 Derivation

The model is based on the assumptions of each component, stated in the corresponding sections above. The primary motivation for including the orifice model for the entrance but not the exit is to obtain compatible boundary conditions. Our focus here is application and control orientation; an experimental validation is out of the scope of this work. Without loss of generality, we assume a positive flow, two middle sections, and that all outlets of Tank 1 and inlets of Tank 2 are of identical geometry, resp.

Tanks

For Tank 1, (B.23) from the tank model above yields

$$\dot{p}_{T_1} = \alpha_{T_1}(q_{T_1,\ell} - q_{T_1,1,r} - q_{T_1,2,r}), \tag{B.30}$$

where $q_{T_1,\ell}$ is the mass flow at the inlet of Tank 1 and $q_{T_1,i,r}$ is the mass flow at its i^{th} outlet. We interpret the tank entrance as an orifice, and as in (B.21) and (B.22) define

$$\frac{\partial g_o(p_{T_1}, p_{T_1,\ell})}{\partial p_{T_1}} \doteq \xi_{T_1}, \quad \frac{\partial g_o(p_{T_1}, p_{T_1,\ell})}{\partial p_{T_1,\ell}} \doteq \zeta_{T_1}. \tag{B.31}$$

Therefore, with (B.30) – (B.31), we obtain a model for Tank 1:

$$
\begin{aligned}
x_t &= \begin{bmatrix} p_{T_1} \end{bmatrix}, \\
y_t &= \begin{bmatrix} p_{T_1} & q_{T_1,\ell} \end{bmatrix}^\top, \\
u_t &= \begin{bmatrix} p_{T_1,\ell} & q_{T_1,1,r} & q_{T_1,2,r}, \end{bmatrix}^\top
\end{aligned}
$$

with dynamics

$$\dot{x}_t = \begin{bmatrix} \alpha_{T_1}\xi_{T_1} \end{bmatrix} x_t + \begin{bmatrix} \alpha_{T_1}\zeta_{T_1} & -\alpha_{T_1} & -\alpha_{T_1} \end{bmatrix} u_t, \tag{B.32a}$$

$$y = \begin{bmatrix} 1 \\ \xi_{T_1} \end{bmatrix} x_t + \begin{bmatrix} 0 & 0 & 0 \\ \zeta_{T_1} & 0 & 0 \end{bmatrix} u_t. \tag{B.32b}$$

Similarly, for Tank 2 we have:

$$
\begin{aligned}
x_t &= \begin{bmatrix} p_{T_2} \end{bmatrix}, \\
y_t &= \begin{bmatrix} p_{T_2} & q_{T_2,1,\ell} & q_{T_2,2,\ell} \end{bmatrix}^\top \\
u_t &= \begin{bmatrix} p_{T_2,1,\ell} & p_{T_2,2,\ell} & q_{T_2,r} \end{bmatrix}^\top,
\end{aligned}
$$

with dynamics

$$\dot{x}_t = \alpha_{T_2}(\xi_{T_2} + \xi_{T_2})x_t + \begin{bmatrix} \alpha_{T_2}\zeta_{T_2} & \alpha_{T_2}\zeta_{T_2} & -\alpha_{T_2} \end{bmatrix} u_t, \tag{B.33a}$$

$$y_t = \begin{bmatrix} 1 \\ \xi_{T_2} \\ \xi_{T_2} \end{bmatrix} x_t + \begin{bmatrix} 0 & 0 & 0 \\ \zeta_{T_2} & 0 & 0 \\ 0 & \zeta_{T_2} & 0 \end{bmatrix} u_t. \tag{B.33b}$$

Composite valve manifold model

The state-space models for Tanks 1 and 2 in (B.32) and (B.33) as well as the single pipe model from (B.2) for each connection, $P_{1a} - V_1 - P_{1b}$ and $P_{2a} - V_2 - P_{2b}$, resp., share the following boundary conditions,

$$p_{T_1,i,r} = p_{ia,\ell}, \quad p_{T_2,i,\ell} = p_{ib,\ell}$$

$$q_{T_1,i,r} = q_{ia,\ell}, \quad q_{T_2,i,\ell} = q_{ib,\ell},$$

for $i = \{1,2\}$. Connecting tank and pipe models accordingly generates the model stated above.

B.8 Compressor

Similar to the valve modeling, we present a static gain model as well as a more complex dynamic model for the compressor.

B.8.1 Static model

Static compressor model

For the static gain model let the states and inputs be :

$$x_t = \begin{bmatrix} p_r & q_\ell \end{bmatrix}^\top, \quad u_t = \begin{bmatrix} p_\ell & q_r \end{bmatrix}^\top, \tag{B.34}$$

where the suction side corresponds to subscript ℓ and discharge side to subscript r. We define the static relationship

$$x_t = \begin{bmatrix} k_c & 0 \\ 0 & 1 \end{bmatrix} u_t,$$

where $k_c > 1$.

Conservation of mass is immediate.

B.8.2 Dynamic model

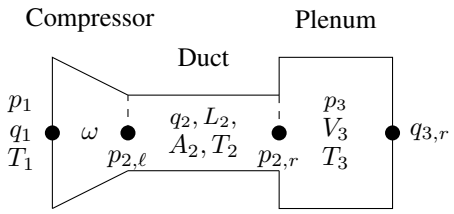

Figure B.6. Compressor system consisting of compressor, duct and plenum. The compression is isentropic, whereas duct and plenum are isothermal. We consider boundary conditions $p_1, q_{3,r}$ and T_1 as known. Variables at internal boundaries are continuous.

Consider a compressor system as shown in Figure B.6, which consists of a compressor, a duct and a plenum. Similar to [22] and [16], we model each of these elements separately and then connect them via boundary conditions, akin to the valve manifold model above.

Dynamic compressor model

Consider Assumptions B.2 (for duct), B.3 (for isothermal plenum) and B.5 (for compression) below. Define state, input and output vectors as

$$x_t = \begin{bmatrix} p_3 & q_2 \end{bmatrix}^\top, \tag{B.35}$$

$$u_t = \begin{bmatrix} p_1 & q_{3,r} & T_1 & \omega \end{bmatrix}^\top, \tag{B.36}$$

$$y_t = \begin{bmatrix} p_3 & q_2 & T_3 \end{bmatrix}^\top, \tag{B.37}$$

with terms as shown in Figure B.6, and ω the compressor speed. The the nonlinear dynamics are

$$\dot{x}_t = \begin{bmatrix} \frac{R_s T_2 z_0}{V_3}(q_2 - q_{3,r}) \\ \frac{A_2}{L_2}(\Phi(q_2, \omega) - p_3) \end{bmatrix} \tag{B.38}$$

$$y_t = \begin{bmatrix} x_t \\ T_1 \left(\frac{\Phi(q_2,\omega)}{p_1}\right)^{(\eta-1)/\eta} \end{bmatrix}, \tag{B.39}$$

where $\Phi(q_2, \omega) = p_{2,\ell}$ is the suction pressure after the isentropic compression modeled as a static map. A linear state-space model can be derived by linearization.

Conservation of mass directly follows from setting (B.38) to zero and the fact that $q_2 = q_1$.

Assumptions

Assumption B.5. *Suppose:*

B.5(i) The compression is isentropic.

B.5(ii) The discharge pressure of the compressor, $p_{2,\ell}$, is defined by a static relation between speed, ω, suction pressure, p_1, and mass flow, q_2: $\Phi(q_2, \omega) : \mathbb{R}_{>0} \times \mathbb{R}_{>0} \to \mathbb{R}_{>0}$.

B.5(iii) The friction in the duct is negligible.

B.5(iv) The temperature change in the duct is negligible.

B.5(v) The gas in the duct and plenum is perfectly mixed.

Derivation

For the plenum we obtain from the isothermal tank model in (B.23),

$$\dot{p}_3 = \frac{R_s T_2 z_0}{V_3}(q_2 - q_{3,r}). \tag{B.40}$$

For the duct, by (B.2b) and boundary condition $p_{2,r} = p_3$,

$$\dot{q}_2 = \frac{A_2}{L_2}(p_{2,\ell} - p_3). \tag{B.41}$$

The suction pressure after the isentropic compression is modeled as a static map, $p_{2.\ell} = \Phi(q_2, \omega)$, with compressor speed ω. The mapping is usually based on empirical formulas [41], or compres-

sor geometry [16, Ch. 13]. It follows that

$$\dot{q}_2 = \frac{A_2}{L_2}(\Phi(q_2, \omega) - p_3). \tag{B.42}$$

By the hypothesis of isentropic compression and isothermal duct and plenum,

$$T_3 = T_1 \left(\frac{p_{2,\ell}}{p_1} \right)^{(\eta-1)/\eta} = T_1 \left(\frac{\Phi(q_2, \omega)}{p_1} \right)^{(\eta-1)/\eta}, \tag{B.43}$$

with isentropic coefficient η. The model above immediately follows. Note that conservation of mass is immediate: by hypothesis and (B.40), $\bar{q}_1 = \bar{q}_2 = \bar{q}_{3,r}$.

B.9 Heat exchanger

We provide a heat exhanger model based on the non-isothermal one-dimensional pipe model presented in Chapter 1. The assumptions are therefore similar to those for the pipe in Section B.1.1. Given the fact that under usual operating conditions no phase change occurs within the gas our model is similar to that in [40] in the context of air conditioning systems. While we provide a nonlinear formulation, linearization around the nominal operating point directly leads to a linear state-space realization.

Our rudimentary model replaces the heat exchanger with a single pipe, with the geometric and conductivity properties accommodated by adjusting the heat transfer coefficient, k_{rad}, and friction factor, λ, to parametrize the exchanger design and nominal operating point. The temperature output of the model can be used to set the temperature parameter for subsequent downstream isothermal (or other) pipe models.

Heat exchanger

Considering Assumption B.2, if the heat flux is dominated by radial conduction we define the state and input vectors to be

$$x_t = \begin{bmatrix} p_r & q_\ell & T_r \end{bmatrix},$$
$$u_t = \begin{bmatrix} p_\ell & q_r & T_\ell \end{bmatrix}.$$

Then, the nonlinear dynamics of the heat exchanger are governed by

$$\dot{p}_r = \frac{R_s z_0}{A c_v}\left[k_{\text{rad}}\pi D_o(T_{\text{amb}} - T_r) - \frac{q_r - q_\ell}{L}T_r(c_v + R_s z_0) + \frac{p_r - p_\ell}{L}\frac{R_s z_0 T_r q_r}{p_r} - \frac{T_r - T_\ell}{L}q_r(c_v + R_s z_0) + \frac{\lambda R_s^2 z_0^2 T_r^2 q_r^2 |q_r|}{2DA^2 p_r^2}\right] \tag{B.44a}$$

$$\dot{q}_\ell = -A\frac{p_r - p_\ell}{L} - \frac{\lambda R_s T_\ell z_0}{2DA}\frac{q_\ell |q_\ell|}{p_\ell} - \frac{Ag}{R_s T_\ell z_0}\frac{dh}{dx}p_\ell \tag{B.44b}$$

$$\dot{T}_r = \frac{R_s z_0 T_r}{A c_v p_r}\left[k_{\text{rad}}\pi D_o(T_{\text{amb}} - T_r) - \frac{q_r - q_\ell}{L}T_r R_s z_0 + \frac{p_r - p_\ell}{L}\frac{R_s z_0 T_r q_r}{p_r} - \frac{T_r - T_\ell}{L}q_r(c_v + R_s z_0) + \frac{\lambda R_s^2 z_0^2 T_r^2 q_r^2 |q_r|}{2DA^2 p_r^2}\right] \tag{B.44c}$$

Conservation of mass as defined in Definition 2.2 only applies to isothermal models.

B.9.1 Derivation

This is the spatially discretized model of non-isothermal pipe flow developed in Chapter 1. As remarked above, the heat transfer coefficient, k_{rad}, is deliberately non-negligible and the friction factor, λ, can be significant depending on exchanger geometry.

B.10 Interconnections

Suppose each component is described by a state-space model with signals describing pressures, p, and mass flows, q. In this section we show how these component models can be

interconnected to build an entire network model. Towards this goal, we recall interconnection rules from Chapter 2, which translate allowable boundary conditions to signal flows.

B.10.1 Directed pipe connections and 'ports'

The signal flow graph models derived later have directions associated with each signal. Thus, p_ℓ and q_r are input signals, indicating that they are specified from outside the component, and p_r and q_ℓ are output signals, meaning that they are determined by the component itself and the input signals. The spatially localized connection sites, however, possess one input signal and one output signal, namely (p_ℓ, q_ℓ) at the left end and (p_r, q_r) at the right. We further appropriate circuit terminology and identify two distinct location types, which we term *ports*. As in [5], every element in our interconnected system presents signal interfaces to other elements and to the outside world.

Definition B.2 (Ports)**.**

***p*-port** *of a component possesses two signals: an input pressure signal p_ℓ and an output flow signal q_ℓ.*

***q*-port** *of a component possesses two signals: an input flow signal q_r and an output pressure signal p_r.*

Internal series connection of two components, 1 and 2, will involve the cascading of signals $p_{2,\ell} = p_{1,r}$ and $q_{1,r} = q_{2,\ell}$ at the junction point. This describes a p-port to q-port connection. Likewise, connection to the outside of the network must respect the type and causality of the signals. These rules are specified below.

B.10.2 Interconnection rules

Interconnection rules

I. Connections are permitted only between:

   i. a p-port and a q-port, or

   ii. a p-port and an external pressure source/input signal plus an external flow sink/output signal, or

   iii. a q-port and an external flow source/input signal plus an external pressure sink/output signal.

II. Pressure input signals must connect to pressure output signals, and flow input signals must connect to flow output signals.

III. Connection of one variable of a port requires connection of the other.

IV. All ports must be connected and algebraic loops avoided.

These rules conform to the connections examined in Chapter 1 to formulate the systematic interconnection of state-space models. Each component model possesses input and output signals and, in Proposition 1.3, it is shown how a (possibly non-minimal) state-space realization of the interconnection of gas system elements can be directly constructed with the above rules. This construction replaces and extends the graph-theoretic DAE methods of [5] and yields a new input-output transfer function satisfying Mason's Gain Formula, see Proposition 1.4.

B.10.3 Matrix methodology

Recalling Section 1.8, we begin by stacking the state-space models of the individual network components:

$$\dot{x}_t = Ax_t + Bw_t, \quad y = Cx_t + Dw_t \tag{B.45}$$

where

$$A = \text{blkdiag}(A^{(1)}, A^{(2)}, \ldots, A^{(N)}), \tag{B.46a}$$

$$B = \text{blkdiag}(B^{(1)}, B^{(2)}, \ldots, B^{(N)}), \tag{B.46b}$$

$$C = \text{blkdiag}(C^{(1)}, C^{(2)}, \ldots, C^{(N)}), \tag{B.46c}$$

$$D = \text{blkdiag}(D^{(1)}, D^{(2)}, \ldots, D^{(N)}), \tag{B.46d}$$

with superscript $(i), i = \{1, \ldots, N\}$, denoting the respective matrix of component i, and $x_t \in \mathbb{R}^{n_x}, w \in \mathbb{R}^{n_w}$ and $y_t \in \mathbb{R}^{n_y}$. Interconnections and external sources $u_t \in \mathbb{R}^{n_u}$ and sinks $z_t \in \mathbb{R}^{n_z}$ are described by

$$w_t = F y_t + G u_t, \quad z_t = H x_t + J u_t, \tag{B.47}$$

with structured matrices $[F, G, H, J]$ with 0-1 elements:

$$[F]_{i,j} = \begin{cases} 1, & \text{if } [y]_j = [w]_i, \\ 0, & \text{otherwise.} \end{cases} \tag{B.48}$$

Matrix interconnection methodology

A (perhaps non-minimal) state-space realization of (B.45) and (B.47) is given by

$$x_t = \bar{A} x + \bar{B} u_t, \quad y = \bar{C} x_t + \bar{D} u_t, \tag{B.49}$$

where

$$\bar{A} = A + BF(I - DF)^{-1}C, \quad \bar{C} = (I - DF)^{-1}C,$$
$$\bar{B} = B\left[I + F(I - DF)^{-1}D\right]G, \quad \bar{D} = (I - DF)^{-1}DG.$$

We next show an example applying the methodology.

Example: two pipes in series

Consider two pipes in series, 1 and 2, with aggregated input and state/output vectors,

$$x_t = y_t = \begin{bmatrix} p_{1,r} \\ q_{1,\ell} \\ p_{2,r} \\ q_{2,\ell} \end{bmatrix}, \quad w_t = \begin{bmatrix} p_{1,\ell} \\ q_{1,r} \\ p_{2,\ell} \\ q_{2,r} \end{bmatrix}, \tag{B.50}$$

We further define the sources and sinks:

$$u_t = \begin{bmatrix} p_{1,\ell} \\ q_{2,r} \end{bmatrix}, \quad z_t = \begin{bmatrix} p_{2,r} \\ q_{1,\ell} \end{bmatrix}. \tag{B.51}$$

As $p_{1,r} = p_{2,\ell}$ and $q_{1,r} = q_{2,\ell}$, this leads to the following matrices:

$$F = \begin{bmatrix} 0 & 0 & 0 & 0 \\ 0 & 0 & 0 & 1 \\ 1 & 0 & 0 & 0 \\ 0 & 0 & 0 & 0 \end{bmatrix}, \quad G = \begin{bmatrix} 1 & 0 \\ 0 & 0 \\ 0 & 0 \\ 0 & 1 \end{bmatrix}, \tag{B.52}$$

$$H = \begin{bmatrix} 0 & 0 & 1 & 0 \\ 0 & 1 & 0 & 0 \end{bmatrix}, \quad J = \mathbf{0}. \tag{B.53}$$

The aggregate system can directly be implemented in MATLAB using (B.49).

MATLAB example: vented gas loop

We recall a similar example to Section 1.9 in Figure B.7.

The gas flows clockwise, entering through pipe P_1 and exiting through pipes P_6 and P_9.

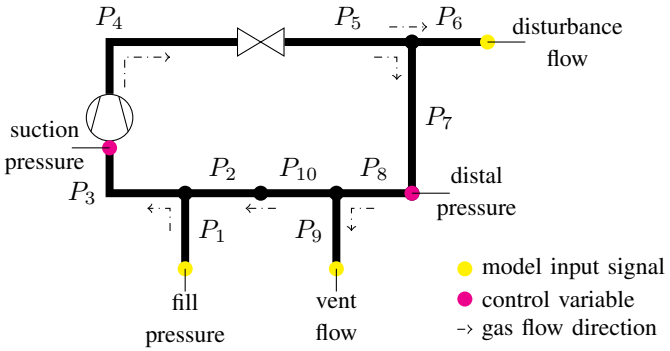

Figure B.7. Pipe network with compressor and valve $\bowtie$. In process control parlance, the fill pressure and vent flow are manipulated variables, the suction and distal pressures are controlled variables, and the flow from P_6 is a disturbance signal.

The compressor and valve, whose corresponding variables are respectively labeled by subscripts c and v, are modeled as static gains as in Sections B.5 and B.8,

$$D_c = \begin{bmatrix} k_c & 0 \\ 0 & 1 \end{bmatrix}, \quad D_v = \begin{bmatrix} k_v & 0 \\ 0 & 1 \end{bmatrix},$$

where $k_c = 4$ and $k_v = 0.8$. Further, pipes (P_1, P_2, P_3) are modeled as a joint, as in Subsection B.3.1, and (P_5, P_6, P_7) and (P_8, P_9, P_{10}) as branches, as in Section B.2. Composing the system according to (B.46), results in the component input vector,

$$w_t = \begin{bmatrix} p_{1,\ell} & p_{2,\ell} & q_{3,r} & p_{c,\ell} & q_{c,r} & p_{4,\ell} & q_{4,r} & p_{v,\ell} & q_{v,r} & p_{5,\ell} & q_{6,r} & q_{7,r} & p_{8,\ell} q_{9,r} & q_{10,r} \end{bmatrix}^\top,$$

and the total output vector,

$$y_t = \begin{bmatrix} p_{3,r} & q_{1,\ell} & q_{2,\ell} & p_{c,r} & q_{c,\ell} & p_{4,r} & q_{4,\ell} & p_{v,r} & q_{v,\ell} & p_{6,r} & p_{7,r} & q_{5,\ell} & p_{9,r} & p_{10,r} & q_{8,\ell} \end{bmatrix}^\top.$$

The external sources are

$$u_t = \begin{bmatrix} p_{1,\ell} & q_{6,r} & q_{9,r} \end{bmatrix}^\top.$$

MATLAB code

```
%% Parameters
clear all
close all

pbar = 2.54e6; % nominal pressure Pa
qbar = 15.44; % nominal flow Kg/s
Re = 1.0901e7; % Reynolds number
T = 300; % nominal temperature K
z = 1; % gas compression factor
Rs = 518.28; % specific gas constant JK^{-1}mol^{-1} methane
lambda = 0.0113; % friction factor
gamma = Rs*T; % constant gas state
mu = 1.31; % from https://www.engineeringtoolbox.com/methane
   -d_1420.html

%% System J123 join of three 10m pipes
La = 10; % m
Da = 27.25*2.54/100; % m
Aa = pi*Da*Da/4;

alfa = gamma*z/Aa/La;
beta = Aa/La;
kappa = lambda*gamma*z*qbar/Da/Aa/pbar;
```

```
23
24 Lb = 10; % m
25 Db = 17.25*2.54/100; % m
26 Ab = pi*Db*Db/4;
27
28 alfb = gamma*z/Ab/Lb;
29 betb = Ab/Lb;
30 kappb = lambda*gamma*z*qbar/Db/Ab/pbar;
31
32 Lc = 10; % m
33 Dc = 27.25*2.54/100; % m
34 Ac = pi*Dc*Dc/4;
35
36 alfc = gamma*z/Ac/Lc;
37 betc = Ac/Lc;
38 kappc = lambda*gamma*z*qbar/Dc/Ac/pbar;
39
40 gammab = alfa/(alfa+alfb); % splitting ratio for joining
      problem
41
42 F123 = [0 alfa*(1-gammab) alfa*(1-gammab) 0 -alfa*(1-gammab)
      ;
43     -beta -kappa 0 0 0;
44     -betb 0 -kappb 0 0;
45     0 0 0 0 alfc;
46     betc 0 0 -betc -kappc];
```

```
G123 = [0 0 0;beta 0 0;0 betb 0;0 0 -alfc;0 0 0];
H123 = [0 0 0 1 0;0 1 0 0 0;0 0 1 0 0];
J123 = zeros(3,3);

%% Systems Br567 and Br8910 identical branching systems
F567 = [0 alfa 0 -alfa 0 -alfa;
    -beta -kappa 0 0 0 0;
    0 0 0 alfb 0 0;
    betb 0 -betb -kappb 0 0;
    0 0 0 0 0 alfc;
    betc 0 0 0 -betc -kappc];
G567 = [0 0 0; beta 0 0; 0 -alfb 0;0 0 0;0 0 -alfc;0 0 0];
H567 = [0 0 1 0 0 0;0 0 0 0 1 0;0 1 0 0 0 0];
J567 = zeros(3,3);
F8910=F567; G8910=G567; H8910=H567; J8910=J567;

%% Single pipe 4
F4 = [0 alfa;-beta -kappa];
G4 = [0 -alfa;beta 0];
H4 = eye(2);
J4 = zeros(2,2);

%% System C compressor
kC = 4;
FC = zeros(0);
GC = zeros(0,2);
```

```
HC = zeros(2,0);
JC = diag([kC,1]);

%% System resistor
kR = 0.8;
FR = zeros(0);
GR = zeros(0,2);
HR = zeros(2,0);
JR = diag([kR,1]);

%% Compose interconnected system

% stack up components
A = blkdiag(F123,FC,F4,FR,F567,F8910);
B = blkdiag(G123,GC,G4,GR,G567,G8910);
C = blkdiag(H123,HC,H4,HR,H567,H8910);
D = blkdiag(J123,JC,J4,JR,J567,J8910);

% Internal connections
F = zeros(15,15);
F(2,14)=1; F(3,5)=1; F(4,1)=1; F(5,7)=1; F(6,4)=1; F(7,9)=1;
F(8,6)=1; F(9,12)=1; F(10,8)=1; F(12,15)=1; F(13,11)=1; F
   (15,3)=1;

% External sources
G = zeros(15,3);
```

```
G(1,1)=1; G(11,3)=1; G(14,2)=1;

% Interconnected systems
Abar = A+B*F/(eye(15)-D*F)*C;
Bbar = B*(eye(15)+F/(eye(15)-D*F)*D)*G;
Cbar = (eye(15)-D*F)\C;
Dbar = (eye(15)-D*F)\D*G;

%% State space model
complete_sys = ss(Abar, Bbar, Cbar, Dbar);
```

B.10.4 MATLAB's connect function

As an alternative to the matrix methodology we can use the `connect` function in MATLAB. This is best explained by the example below. For each component we name the input and output signals, respecting the boundary conditions. We then define the input and output signal names of the aggregate system and call the `connect` function.

MATLAB example: two pipes in series

```
% sys1 - Pipe 1
% sys2 - Pipe 2

% Pipe 1
sys1.InputName = {'p1l', 'q2l'};  % q1r = q2l
sys1.OutputName = {'p1r', 'q1l'};

% Pipe 2
```

```
sys2.InputName = {'p1r', 'q2r'};  % p1r = p2l
sys2.OutputName = {'p2r', 'q2l'};

% Connect pipes
sys_inputs = {'p1l', 'q2r'};
sys_outputs = {'p2r', 'q1l'};
sys = connect(sys1,sys2, sys_inputs, sys_outputs);
```

MATLAB example: vented gas loop

```
%% Parameters
clear all
close all

pbar = 2.54e6; % nominal pressure Pa
qbar = 15.44; % nominal flow Kg/s
Re = 1.0901e7; % Reynolds number
T = 300; % nominal temperature K
z = 1; % gas compression factor
Rs = 518.28; % specific gas constant JK^{-1}mol^{-1} methane
lambda = 0.0113; % friction factor
gamma = Rs*T; % constant gas state
mu = 1.31; % from https://www.engineeringtoolbox.com/methane
   -d_1420.html

%% System J123 join of three 10m pipes
La = 10; % m
```

```
17 Da = 27.25*2.54/100; % m
18 Aa = pi*Da*Da/4;
19
20 alfa = gamma*z/Aa/La;
21 beta = Aa/La;
22 kappa = lambda*gamma*z*qbar/Da/Aa/pbar;
23
24 Lb = 10; % m
25 Db = 17.25*2.54/100; % m
26 Ab = pi*Db*Db/4;
27
28 alfb = gamma*z/Ab/Lb;
29 betb = Ab/Lb;
30 kappb = lambda*gamma*z*qbar/Db/Ab/pbar;
31
32 Lc = 10; % m
33 Dc = 27.25*2.54/100; % m
34 Ac = pi*Dc*Dc/4;
35
36 alfc = gamma*z/Ac/Lc;
37 betc = Ac/Lc;
38 kappc = lambda*gamma*z*qbar/Dc/Ac/pbar;
39
40 gammab = alfa/(alfa+alfb); % splitting ratio for joining
      problem
41
```

```
F123 = [0 alfa*(1-gammab) alfa*(1-gammab) 0 -alfa*(1-gammab)
   ;
    -beta -kappa 0 0 0;
    -betb 0 -kappb 0 0;
    0 0 0 0 alfc;
    betc 0 0 -betc -kappc];
G123 = [0 0 0;beta 0 0;0 betb 0;0 0 -alfc;0 0 0];
H123 = [0 0 0 1 0;0 1 0 0 0;0 0 1 0 0];
J123 = zeros(3,3);
sys123 = ss(F123,G123,H123,J123);
sys123.InputName = {'p1l','p10r','qCl'};
sys123.OutputName = {'p3r','q1l','q2l'};


%% Systems Br567 and Br8910 identical branching systems
F567 = [0 alfa 0 -alfa 0 -alfa;
    -beta -kappa 0 0 0 0;
    0 0 0 alfb 0 0;
    betb 0 -betb -kappb 0 0;
    0 0 0 0 0 alfc;
    betc 0 0 0 -betc -kappc];
G567 = [0 0 0; beta 0 0; 0 -alfb 0;0 0 0;0 0 -alfc;0 0 0];
H567 = [0 0 1 0 0 0;0 0 0 0 1 0;0 1 0 0 0 0];
J567 = zeros(3,3);
sys567 = ss(F567,G567,H567,J567);
sys567.InputName = {'pVr','q6r','q8l'};
```

```
67 sys567.OutputName = {'p6r','p7r','q5l'};
68 sys8910 = sys567;
69 sys8910.InputName = {'p7r', 'q9r', 'q2l'};
70 sys8910.OutputName = {'p9r', 'p10r', 'q8l'};
71
72 %% Single pipe 4
73 F4 = [0 alfa;-beta -kappa];
74 G4 = [0 -alfa;beta 0];
75 H4 = eye(2);
76 J4 = zeros(2,2);
77 sys4 = ss(F4,G4,H4,J4);
78 sys4.InputName = {'pCr', 'qVl'};
79 sys4.OutputName = {'p4r', 'q4l'};
80
81 %% System C compressor
82 kC = 4;
83 FC = zeros(0);
84 GC = zeros(0,2);
85 HC = zeros(2,0);
86 JC = diag([kC,1]);
87 sysC = ss(FC,GC,HC,JC);
88 sysC.InputName = {'p3r', 'q4l'};
89 sysC.OutputName = {'pCr', 'qCl'};
90
91 %% System resistor
92 kR = 0.8;
```

```
FR = zeros(0);
GR = zeros(0,2);
HR = zeros(2,0);
JR = diag([kR,1]);
sysR = ss(FR,GR,HR,JR);
sysR.InputName = {'p4r', 'q5l'};
sysR.OutputName = {'pVr', 'qVl'};

%% Compose interconnected system
inputs = {'p1l', 'q6r', 'q9r'};
outputs = {'p3r','q1l','q2l','p6r','p7r','q5l','p9r','p10r',
   'q8l','p4r','q4l','pVr', 'qVl'};
complete_sys = connect(sysR,sysC,sys4,sys123,sys567,sys8910,
    inputs, outputs);
```

B.11 Conclusion

We derived composite state-space models for the transient dynamics of gas flow through intersecting pipe geometries, valves, compressors, and valve manifolds that are well-suited candidates for model-based control design. They also capture conservation of mass at steady state by subsuming algebraic constraints that would otherwise appear as part of a system of DAEs. Additionally, we provide examples of how to use the matrix methodology introduced in Section 1.9 in MATLAB and alternatively show how to use MATLAB's `connect` function.

Appendix B, in full, is a reprint of the material as it appears in: Sven Brüggemann, Robert H. Moroto, and Robert R. Bitmead. " Compendium of Control-Oriented Models of Gas Processing Equipment Components." ArXiv e-prints, November 2022.

Bibliography

[1] R. Alamian, M. Behbahani-Nejad, and A. Ghanbarzadeh. A state space model for transient flow simulation in natural gas pipelines. *Journal of Natural Gas Science and Engineering*, 9:51 – 59, 2012.

[2] B.D.O. Anderson and S. Vongpanitlerd. *Network Analysis and Synthesis*. Prentice-Hall, Englewood-Cliffs, NJ, 1973.

[3] M. Behbahani-Nejad and A. Bagheri. A MATLAB Simulink Library for Transient Flow Simulation of Gas Networks. *World Academy of Science, Engineering and Technology, International Journal of Mechanical, Aerospace, Industrial, Mechatronic and Manufacturing Engineering*, 2:873–879, 2008.

[4] O. Beker, C.V. Hollot, and Y. Chait. Plant with integrator: an example of reset control overcoming limitations of linear feedback. *IEEE Transactions on Automatic Control*, 46(11):1797–1799, 2001.

[5] P. Benner, S. Grundel, C. Himpe, C. Huck, T. Streubel, and C. Tischendorf. Gas Network Benchmark Models. In S. Campbell, A. Ilchmann, V. Mehrmann, and T. Reis, editors, *Applications of Differential-Algebraic Equations: Examples and Benchmarks. Differential-Algebraic Equations Forum*. Springer, Cham., 2018.

[6] P. Benner, S. Grundel, C. Himpe, C. Huck, T. Struble, and C. Tischendorf. Gas network benchmark models. In S. Campbell, A. Ilchmann, V. Mehrmann, and T. Reis, editors, *Applications of Differential-Algebraic Equations: Examples and Benchmarks*, pages 171–197. Springer Nature, 2018.

[7] H. S. Black. Stabilized feedback amplifiers. *The Bell System Technical Journal*, 13(1):1–18, 1934.

[8] W. Borutzky. *Bond Graph Methodology: Development and Analysis of Multidisciplinary Dynamic System Models*. Springer London, 2010.

[9] Sven Brüggemann and Robert R. Bitmead. Control-Oriented Modeling of Pipe Flow through Intersecting Pipe Geometries. *ArXiv e-prints*, 2021.

[10] Y.A. Çengel and J.M. Cimbala. *Fluid Mechanics: Fundamentals and Applications*. College Ie Overruns. McGraw-Hill Education, 2018.

[11] Huaichen Chen. The matrix expression of signal flow graph and its application in system analysis software. *Chinese Journal of Electronics*, 11(3):361–364, 2002.

[12] M.C. de Oliveira. *Fundamentals of Linear Control: A Concise Approach*. Cambridge University Press, 2017.

[13] Hector Delgado-Garibay, Nathan Poerner, Donghui Zhang, Rainer Kurz, and Greg Phillippi. Chapter 12 - compressor testing. In Klaus Brun and Rainer Kurz, editors, *Compression Machinery for Oil and Gas*, pages 449–461. Gulf Professional Publishing, 2019.

[14] Oxford English Dictionary. acknowledge. https://www.oed.com/view/Entry/1607rskey=URF4wG&result=2&isAdvanced=false#eid. [Online; accessed October 20, 2022].

[15] Olav Egeland and Jan Gravdahl. *Modeling and Simulation for Automatic Control*. Marine Cybernetics AS, 2 edition, 06 2003.

[16] Olav Egeland and Jan T. Gravdahl. *Modeling and Simulation for Automatic Control*. Marine Cybernetics AS, 2nd edition, 06 2003.

[17] Rolf Findeisen and Frank Allgöwer. Nonlinear model predictive control for index–one dae systems. In F. Allgöwer and A. Zheng, editors, *Nonlinear Model Predictive Control. Progress in Systems and Control Theory*, volume 26, pages 145–161. Birkhäuser, Basel, 2000.

[18] J. E. Funk, D. J. Wood, and S. P. Chao. The Transient Response of Orifices and Very Short Lines. *Journal of Basic Engineering*, 94(2):483–489, 06 1972.

[19] P. Garabedian. *Partial Differential Equations*. AMS Chelsea Publishing Series. Chelsea Publishing Company, 1986.

[20] P.J. Gawthrop and G.P. Bevan. Bond-graph modeling. *IEEE Control Systems*, 27(2):24–45, April 2007.

[21] Anurag Goyal, Marcel A. Staedter, and Srinivas Garimella. A review of control methodologies for vapor compression and absorption heat pumps. *International Journal of Refrigeration*, 97:1–20, 2019.

[22] E. M. Greitzer. Surge and Rotating Stall in Axial Flow Compressors—Part II: Experimental Results and Comparison With Theory. *Journal of Engineering for Power*, 98(2):199–211, 04 1976.

[23] S. E. Haaland. Simple and Explicit Formulas for the Friction Factor in Turbulent Pipe Flow. *Journal of Fluids Engineering*, 105(1):89–90, 03 1983.

[24] J.P. Holman. *Heat Transfer*. McGraw-Hill Education, 2009.

[25] Christoph Huck and Caren Tischendorf. Topology motivated discretization of hyperbolic PDAEs describing flow networks. Technical report, Humboldt-Universität zu Berlin, 2017.

[26] J Králik, P Stiegler, Z Vostrý, and J Závorka. *Dynamic modeling of large-scale networks with application to gas distribution*. Elsevier, 1988.

[27] Decision Lab. How do our sentimental feelings for the past influence our actions in the present? https://thedecisionlab.com/biases/nostalgia-effect. [Online; accessed October 20, 2022].

[28] Larry Laudan. *Beyond Positivism and Relativism: Theory, Method, and Evidence*. Westview Press, Oxford and New York, 1996.

[29] Michael V. Lurie. *Modeling of Oil Product and Gas Pipeline Transportation*. John Wiley & Sons, Ltd, 2008.

[30] S. J. Mason. Feedback theory-further properties of signal flow graphs. *Proceedings of the IRE*, 44(7):920–926, 1956.

[31] Samuel J. Mason. Feedback theory – some properties of signal flow graphs. *Proceedings of the IRE*, 41(9):1144–1156, 1953.

[32] Jack. D. Mattingly. *Elements of Gas Turbine Propulsion*. Tata McGraw Hill, New Delhi, Inida, 2005.

[33] R.H. Middleton. Trade-offs in linear control system design. *Automatica*, 27(2):281–292, 1991.

[34] M.J. Moran, H.N. Shapiro, D.D. Boettner, and B.B. Margaret. *Fundamentals of Engineering Thermodynamics*. Wiley, 8$^{\text{th}}$ edition, 2014.

[35] R.W. Newcomb. *Linear Multiport Synthesis*. McGraw Hill, Boston MA, 1966.

[36] Goro Obinata and Brian D.O. Anderson. *Model Reduction for Control System Design*. Springer-Verlag, London, 1981.

[37] Andrzej J. Osiadacz and Maciej Chaczykowski. Comparison of isothermal and non-isothermal pipeline gas flow models. *Chemical Engineering Journal*, 81(1):41–51, 2001.

[38] Venugopal Pichai, Mesut E. Sezer, and Dragoslav D. Šiljak. A Graph-Theoretic Algorithm for Hierarchical Decomposition of Dynamic Systems with Applications to Estimation and Control. *IEEE Transactions on Systems, Man, and Cybernetics*, SMC-13(2):197–207, 1983.

[39] K. R. Popper. *The Logic of Scientific Discovery*. Hutchinson, London, 1934.

[40] Bryan P Rasmussen and Andrew G Alleyne. Control-Oriented Modeling of Transcritical Vapor Compression Systems. *Journal of Dynamic Systems, Measurement, and Control*, 126(1):54–64, Apr 2004.

[41] D.C. Rennels and H.M. Hudson. *Pipe Flow: A Practical and Comprehensive Guide*. Wiley, 2012.

[42] Claude E. Shannon. The theory and design of linear differential equation machines (Jan. 1942). In N.J.A. Sloane and A.D. Wyner, editors, *Claude E. Shannon: Collected Papers*, chapter 33, pages 514–559. Wiley IEEE Press, 1993.

[43] Ascher H. Shapiro. *The Dynamics and Thermodynamics of Compressible Fluid Flow*, volume I. John Wiley & Sons, 1953.

[44] Dragoslav D. Šiljak. Stability of large-scale systems. *IFAC Proceedings Volumes*, 5(1, Part 4):75–85, 1972. IFAC 5th World Congress: Part 4, Paris, France, June 12-17, 1972.

[45] Dragoslav D. Šiljak. *Large-Scale Dynamic Systems*. Dover Publications, 1978.

[46] Jan C. Willems. The behavioral approach to open and interconnected systems: Modeling by tearing, zooming, and linking. *IEEE Control Systems*, 24:46–99, December 2007.

[47] Jan C. Willems. Terminals and ports. *IEEE Circuits & Systems Magazine*, pages 8–26, December 2010.

[48] Jan C. Willems. Power and energy as systemic properties – Part I: Electrical circuits. In *52nd IEEE Conference on Decision and Control*, pages 168–174, Florence Italy, 2013.

[49] Jan C. Willems. Power and energy as systemic properties – Part II: Mechanical circuits. In *52nd IEEE Conference on Decision and Control*, pages 175–181, Florence Italy, 2013.

[50] Matthew A. Williams, Justin P. Koeln, Herschel C. Pangborn, and Andrew G. Alleyne. Dynamical Graph Models of Aircraft Electrical, Thermal, and Turbomachinery Components. *Journal of Dynamic Systems, Measurement, and Control*, 140(4), 12 2017. 041013.

[51] Zou Xi. To take more risks, try a dose of nostalgia. https://www.todayonline.com/commentary/take-more-risks-try-dose-nostalgia, August 2019. [Online; accessed October 20, 2022].

[52] J. G. Ziegler and Nathaniel B. Nichols. Optimum Settings for Automatic Controllers. *Journal of Dynamic Systems Measurement and Control-transactions of The Asme*, 115:220–222, 1942.